Summer 2007

Static evaluation of the out-of-plane behavior of URM infill walls utilizing modern blast retrofit systems

Trevor D. Hrynyk

STATIC EVALUATION OF THE OUT-OF-PLANE BEHAVIOR

OF URM INFILL WALLS UTILIZING MODERN BLAST RETROFIT SYSTEMS

by

TREVOR D. HRYNYK

A THESIS

Presented to the Faculty of the Graduate School of the

UNIVERSITY OF MISSOURI-ROLLA

In Partial Fulfillment of the Requirements for the Degree

MASTER OF SCIENCE IN CIVIL ENGINEERING

2007

Approved by

_____   _____
John J. Myers, Advisor   Abdeldjelil Belarbi

_____
Jason Baird

ABSTRACT

The use of unreinforced masonry (URM) infill walls continues to be common practice in building construction throughout the United States. URM walls typically have very low flexural capacities and possess brittle failure modes making them highly susceptible to failure when exposed to out-of-plane loadings such as a blast load. Therefore, it is critical that high-threat-level URM facilities undergo some type of retrofit to increase their abilities to withstand blast loads from potential attacks and to limit the amount of damage that occurs within these structures as a result of debris scatter.

Due to the brittle nature of URM walls, emphasis has been placed on utilizing retrofit systems that increase energy absorption capabilities and reduce the debris scatter of the masonry upon failure. Based upon the aforementioned criteria, two different retrofit materials were selected for investigation: a glass fiber reinforced polymer (GFRP) grid and an elastomeric polyurea. The research program was divided into two phases of study. Phase 1 focused on the behavior of partially framed, non-slender infill walls. In this phase, the effect of framing elements on wall behavior and their influence on the governing mode of failure of the retrofitted URM walls was investigated. Additionally, the use of an alternative base masonry material for URM construction was investigated to evaluate its applicability for the use of framed infills. The experimental data were used to develop an analytical model for determining the out-of-plane load capacity at the ultimate limit state for framed infills. Phase 2 of the research program investigated the behavior of slender infill walls and was specifically focused on the bond behavior of the materials used in the retrofit system. The Phase 2 walls were also evaluated on the basis of their out-of-plane load capacities and deformation capabilities.

ACKNOWLEDGMENTS

I would like to thank my advisor Dr. John J. Myers for his guidance and support throughout this project. I would also like to thank my committee members Dr. Abdeldjelil Belarbi and Dr. Jason Baird for their involvement and input aiding in the completion of this research. Additionally, I would like to express my gratitude to Dr. Nestore Galati for his guidance and assistance in the development of the analytical model presented in this thesis.

I would like to acknowledge Robert Sinclair of Encore Building Solutions, Inc. for providing funds for this research as well as materials that were used in the construction of the URM walls. Additionally, I would like to thank the National Science Foundation's University Cooperative Research Center, the Repair of Buildings and Bridges with Composites (RB^{2}C) for providing funding for this research project. I also thank BASF Building Systems, TechFab LLC., and International Paper for donating materials which were vital to the execution of this research program.

The experimental program could not have been completed without the assistance of the technical staff of the UMR Civil Engineering Department and, therefore, special thanks to Jason Cox, Travis Hernandez, Jeff Bradshaw, Steve Gabel, and Gary Abbott. I would also like to thank Harold Martin of Rolla Technical Institute (RTI) for his assistance in the construction of the URM walls. Also, I would like to thank all of my friends and peers in the Center for Infrastructure Engineering Studies (CIES) for their efforts in the laboratory; their contributions to this research were very much appreciated.

Lastly, I would like to thank my family for their undying support throughout my entire academic career.

TABLE OF CONTENTS

LIST OF ILLUSTRATIONS

LIST OF TABLES

NOMENCLATURE

Symbol	Description
a	distance from the support to the applied load, in. (mm)
A	location of the hinge at the wall boundary
A_{frp}	area of FRP strengthening material, in.^{2} (mm^2)
A_n	net cross-sectional area of URM wall, in.^{2} (mm^2)
b_m	width of infill wall, in. (mm)
B	location of the hinge at mid-height
c	depth to neutral axis location, in. (mm)
C	compression force in the masonry at the mid-height hinge location, lb (N)
d_v	depth of masonry in direction of shear considered, in. (mm)
D	term in equation
e	the eccentricity of the arching thrust, in. (mm)
E_{frp}	modulus of elasticity of FRP, psi (MPa)
E_m	modulus of elasticity of masonry assemblage, psi (MPa)
f_{fe}	stress determined from the limiting strain in the FRP, psi (MPa)
f_{fu}	ultimate achievable stress in the FRP, psi (MPa)
f'_m	specified compressive strength of masonry, psi (MPa)
$f'_{m,n}$	net compressive strength of masonry, psi (MPa)
g_1, g_2	initial gaps between the ends of the wall and the framing abutments, in. (mm)
h	overall height of infill wall, in. (mm)
h_{g1}, h_{g2}	gaps in airbag coverage at each side of the wall, in. (mm)
k	parameter related to the eccentricity of the arching thrust, $k = e/t$
k_m	efficiency factor used to limit strain in the FRP
K_1, K_2	abutment stiffnesses per unit height of the wall, lb/in. (N/mm)
K_3	stiffness contribution from the FRP strengthening material, lb/in. (N/mm)
l_b	unbonded length of FRP strengthening material, in. (mm)
L	free-span length of Phase 2 URM walls, in. (mm)
m	term in equation

M	theoretical mid-height moment acting on URM wall, lb-in. (N-mm)
M_{cr}	the cracking moment, lb-in. (N-mm)
M_n	nominal moment capacity, lb-in. (N-mm)
M_a	maximum moment at section of URM wall under consideration, lb-in. (N-mm)
M_u	the ultimate moment, lb-in. (N-mm)
M_{udl}	theoretical mid-height moment due to uniformly distributed load, lb-in. (N-mm)
p	pressure, psi (MPa)
$p_{applied}$	pressure applied by the airbag loading system, psi (MPa)
$p_{uniform}$	equivalent uniform pressure, psi (MPa)
P	arching membrane force, also referred to as the arch-thrust, lb (N)
(PAF)	pressure adjustment factor
q	uniform load applied to half-wall segment, lb/in. (N/mm)
q_u	out-of-plane load resistance, lb/in. (N/mm)
t	thickness of infill wall, in. (mm)
t'	effective width of masonry compression core, in. (mm)
T	tension force in the FRP, lb (N)
V	shear force acting on the URM wall, lb (N)
V_a	shear force in URM wall at section under consideration, lb (N)
v_{g1}, v_{g2}	gaps in airbag coverage area at the ends of the wall, in. (mm)
w	partial uniformly distributed load due to airbag coverage area, lb/in. (N/mm)
w_f	reinforcement index
w_{udl}	uniformly distributed load, lb/in. (N/mm)
W	resultant force from uniform load, lb (N)
x_{uc}	theoretical uncracked length of the URM wall, in. (mm)
z	notation for the lateral deflection at mid-height used in analytical derivations, in. (mm)
β_1	factor relating depth of rectangular stress block to neutral axis
δ_a	average movement of the abutments, in. (mm)

δ_t	movement of the wall due to initial gaps, moisture movements, temperature strains, in. (mm)
δ_s	shortening of masonry due to the arch-thrust, in. (mm)
δ_{frp}	deformation of FRP strengthening material, in. (mm)
Δ	mid-height/midspan deflection, in. (mm)
Δ_{cr}	midspan deflection at the state of masonry cracking, in. (mm)
Δ_u	midspan deflection at the ultimate limit state, in. (mm)
ε_{fe}	limiting strain in the FRP
ε_{frp}	effective strain in the FRP
ε_{fu}	ultimate achievable strain in the FRP
ε_s	moisture movements and temperature strains
ε_{mu}	maximum usable strain at extreme compression fibers of masonry
ε'_m	strain in masonry relating to peak compressive stress
γ	factor relating distribution of stress to uniform value
ρ_{frp}	reinforcement ratio for FRP material; ratio of A_{frp} to $b_m \cdot t$
ϕ_{cr}	midspan curvature in the URM wall at cracking, rad/in. (rad/mm)
ϕ_u	midspan curvature in the URM wall at ultimate, rad/in. (rad/mm)

1. INTRODUCTION

1.1. BACKGROUND

In light of recent events, it is evident that much of the current infrastructure throughout the United States is vulnerable to acts of terrorism. Attacks are commonly directed toward highly populated or diplomatic structures and often involve some form of explosive device. Experience has shown that in many cases, the load from the explosive device is not large enough to result in the collapse of a structure, but still results in significant damages and fatalities due to the inward projected debris and fragmentation of the building envelope.

The Federal Emergency Management Agency (FEMA) classifies the damage to a structure as a result of blast into three different levels, the most critical being structural collapse (FEMA, 2003). The collapse of a structure due to blast is most likely to occur from large explosions at small standoff distances and results in the largest amount of injuries and loss of human life. The 1995 Oklahoma City bombing of the Alfred P. Murrah Federal Building (see Figure 1.1) resulted in a significant portion of the structure collapsing due to the detonation of a large explosion immediately outside of the building. The majority of the fatalities occurred within the collapsed region of the structure; however, several of the deaths and many serious injuries were attributed to the projected debris from the infill wall system.

In cases where an explosion does not ultimately result in the collapse of a structure, only a minor portion of the damages and injuries that occur can be directly attributed to the shock from the explosive device. In this case, the major damage

Figure 1.1. Damage to Alfred P. Murrah Building (FEMA, 2003)

contributor, and the major threat to the building occupants, is the fragmentation and

debris scatter of the building envelope. In 1998, the damage sustained to the U.S.

Embassy in Dar El Salaam, Tanzania, as a result of a terrorist attack is an example of

such a case when an explosive device did not result in the collapse of the structure; but

still resulted in significant damage. The damage to the embassy building is presented in

Figure 1.2. Although there were no fatalities as a result of the attack, several injuries and

significant damages were attributed to the scatter of debris from the exterior unreinforced

masonry (URM) infill wall system (FEMA, 2003).

The lowest classification of damage that can occur to a structure as a result of a

blast load is that which involves no actual structural damage. This type of damage often

occurs in nearby structures surrounding the targeted area of attack. Although no

structural damage occurs, injuries and possibly even fatalities can still occur as a result of

glass and other types of non-structural debris being projected within the structure.

Figure 1.2. Failure of Exterior URM Infill Walls

The use of URM infill walls has been and continues to be common practice in building construction throughout the United States. Typically, infill walls are constructed within the structural framing of a building making up the external building envelope, or they are used as partitions within the building. URM walls have low flexural capacities and possess brittle failure modes making them highly susceptible to failure when exposed to out-of-plane loadings such as a blast load. Therefore, in the case of high-threat-level facilities in which URM wall systems have been implemented, it is critical that these structures undergo some type of retrofit to increase their abilities to not only withstand the blast loads from potential attacks, but to also limit the amount of damage that occurs within these structures as a result of debris scatter and fragmentation.

There are several different retrofit methods that can be employed to increase the out-of-plane load resistance and improve the behavior of URM infill wall systems. Conventional masonry retrofitting methods, which typically involve the use of additional concrete and steel reinforcement, tend to not only add significant mass to a structure, but

in many cases the methods result in a reduction of available space for building occupants. In addition to the effects on the building, conventional retrofit methods also tend to be both time consuming and expensive. The use of modern retrofit systems, which involve the use of fiber reinforced polymers (FRP) or elastomeric coatings, are aimed to address and improve upon the negative traits associated with conventional techniques of retrofitting masonry structures.

FRP has successfully been used to reinforce concrete structures for several decades, and as a result of extensive investigation, its applicability in the construction industry continues to grow. The initial attraction of using FRP in construction was because it did not experience the common durability problems that are typically associated with conventional steel reinforcement. Additionally, FRP reinforcement is lightweight and is available in multiple forms, many of which could easily be manipulated to match variable structural shapes and geometries (ACI 440.2R, 2002).

Today significant research is still being carried out to assess the use of FRP as an alternative for steel reinforcement. However, in recent years, the focus of much of the research has shifted to the use of FRP as a means of retrofitting current infrastructure. As a result, the use of various externally bonded FRP systems continues to be studied extensively not only in concrete structures but also in masonry, steel, and timber structures. The benefits of using FRP as opposed to conventional steel in structural retrofits are the same as those in new construction and in most cases externally bonded FRP systems are less intrusive to building occupants. This benefit is primarily because externally bonded FRP systems are typically easy to install and are less time consuming than conventional retrofit methods.

1.2. SCOPE AND OBJECTIVES

Previous investigations have shown that the use of modern retrofit systems can significantly improve the behavior of URM infill walls subjected to variable out-of-plane loads. It has also been shown that the use of externally bonded retrofit systems can greatly reduce the amount of fragmentation and debris scatter that is found to occur in URM walls subjected to high intensity blast loads. The methodology and key findings from these previous works are presented in Section 2.

The main objective of this study is to investigate, through static testing, the use of modern materials for the purpose of improving the behavior of URM walls subjected to blast loads. This study implemented externally bonded FRP grids and an elastomeric polyurea coating as strengthening materials. The resulting retrofit methods were evaluated based on their ability to improve the out-of-plane behavior of URM infill walls. Additionally, the use of an alternative base masonry material was also investigated to determine the advantages and applicability of its use in the construction of new infill wall systems. The behavior of the URM walls was studied under quasi-static loading conditions and was evaluated using several criteria:

- out-of-plane load resistance
- out-of-plane deflection capability
- energy absorption
- reduction in fragmentation and debris scatter at failure

The evaluation of the URM walls under static loading conditions does not serve as a direct relation to walls subjected to actual blast events, but the behavior observed

from this testing is intended to be used as an indicator of potential performance for URM walls subjected to actual blast loading.

The experimental program consisted of testing both slender and non-slender URM wall systems to address the applicability of the retrofit strategies in each case. In the case of the non-slender strengthened wall systems, the findings from the experimental data were used to develop and calibrate an analytical model used to determine the load capacity of URM walls at the ultimate limit state. For the slender wall systems, the experimental data were compared to theoretical predictions determined using a traditional analytical approach.

1.3. THESIS LAYOUT

The purpose, execution, and findings from this study have been presented in the following manner. Section 1 provides a brief introduction addressing attacks on U.S. infrastructure carried out in the past and shows the significant role that URM masonry walls can play in the overall damage to a structure and its occupants. This section also explains the possible advantages of retrofitting high-threat-level infrastructure, and more specifically, explains the benefits of using modern construction materials to retrofit URM masonry wall systems. Lastly, Section 1 outlines the objectives of this research program and their significance in modern retrofitting techniques. The second section of this thesis presents the findings from previous research programs encompassing various techniques of strengthening URM walls subject to out-of-plane loads. The presentation of the results and methodologies from previous studies is intended to provide the reader with some basis for the need of the research program presented in this paper.

In Section 3 of this thesis, the material properties and test methods used to characterize the various materials have been presented for both the retrofit strengthening materials and the base masonry materials. The experimental program, test results, discussion, and analytical approaches have been subdivided into two separate sections corresponding to the two phases of study performed in this program. For clarification, Section 4 briefly presents the methodology and purpose of the two phased approach to the research study. Section 5 presents material related to the non-slender wall systems, and Section 6 presents information regarding the slender wall systems. A general discussion encompassing the entire research program has been presented in Section 7. In Section 8, the main findings from the study are summarized, and recommendations for future research programs are presented.

2. REVIEW OF LITERATURE

The following section of the thesis is intended to provide the reader with background information regarding concepts and past research programs that are closely related to the study presented in this thesis. Literature pertaining to the use of traditional and alternative materials in masonry construction, the behavior of URM infill walls subject to out-of-plane loads, and modern retrofit strategies for URM walls will be presented as an aid to further clarify the significance of the results from this study.

2.1. MASONRY CONSTRUCTION MATERIALS

From centuries of past experiences and continual research, it has been proven that masonry can be used effectively as a construction material. The use of masonry over other alternatives can significantly improve the aesthetics and the durability, and in many cases can reduce a structure's cost (Hendry et al., 1997).   However, the quality and performance of a masonry structure greatly depends on the materials that are used in construction.

2.1.1. Traditional Masonry Materials. The basic materials that are used in masonry construction are brick, block, and mortar. Bricks and blocks are typically made of fired clay, calcium silicate, or concrete (Hendry et al., 1997). They are available in various shapes, sizes, and colors and are typically categorized based upon their material properties or performance characteristics. Because of the wide range of readily available bricks and blocks, brickwork is often a viable option in many construction projects.

Clay bricks are made from clay or shale and are hardened with heat by way of a firing process. The units are typically manufactured to be small and rectangular making

them easy to handle and work with. The manufacturing process involves either crushing or grinding a clay or shale material and mixing it with water until the material reaches a plastic state. Once in the plastic state, the material can be molded, textured, and dried to meet the needs of the manufacturer. The coloring of the brick can be manipulated through the selection of the original base material and the heat at which the bricks are fired. Typical firing temperatures for clay bricks range from 1650°F to 2200°F (900°C to 1200°C). It should be noted that the fabrication of clay units requires a significant amount of energy due to the required material processing and the methods used to produce clay units. Clay bricks are regularly used in the construction of both load bearing and non-load bearing elements. In addition to their aesthetic appeal, the use of clay bricks is often desirable due to their durability characteristics. Clay bricks have a high resistance to fire and extreme heat, have moderate insulating properties, and usually require little or no maintenance. Clay units are graded in accordance to their durability characteristics, such as compressive strength and weather resistance. The most important property in determining the applicable usage for clay brick is the compressive strength of the unit, which is dependant upon the composition of the base material, the manufacturing process, and the degree of firing (Mamlouk and Zaniewski, 1999).

Concrete units, often referred to as concrete masonry units (CMU), are either manufactured as small, solid units called bricks, or larger hollow units called blocks. The units are classified into three categories determined by their densities: lightweight units, medium-weight units, and normal-weight units (Mamlouk and Zaniewski, 1999). Concrete masonry units are made primarily from Portland cement, graded aggregates, and water. However, additional ingredients such as air-entraining agents, coloring

materials, and siliceous and pozzolanic materials are often included in the composition. The manufacturing process used to create these units involves the use of very dry, no-slump concrete, which is vibrated, compacted, and consolidated into molds by way of machines. Similar to that of the clay units, concrete units are manufactured in many different sizes, shapes, and geometries making them a suitable option for many different types of construction projects; they are also applicable for both load bearing and non-load bearing construction (Randall and Panarese, 1976). In terms of the ease of which concrete masonry units can be produced, the physical fabrication of concrete units is not as intensive as that of clay unit fabrication but still requires significant energy for the production of the Portland cement.

2.1.2. Alternative Masonry Materials. To date, significant research has been performed in an effort to investigate possible uses for the overwhelming and ever increasing production of by-products in the United States. Today, the use of by-products in construction materials is quite common. Fly ash, a by-product created from the burning of coal, possesses pozzolanic characteristics, allowing it to act as a mineral admixture or replacement material for Portland cement. When used in the proper proportion, the addition of fly ash in concrete can result in a number of beneficial characteristics including increased workability, decreased water requirements, and increased strength. Blast furnace slag, a by-product of the steel manufacturing industry, is also commonly used as an admixture in concrete. Slag reacts naturally with the hydration process of concrete and sets when exposed to NaOH and CaOH, both of which are produced as Portland cement hydrates (Mamlouk and Zaniewski, 1999). As a result of the success that the construction industry has had with the use of by-products in

various types of materials, significant research has been performed to investigate the use of by-products explicitly to create modern materials, many of which are potentially suitable for use in masonry construction.

A previous study performed by Joshi and Myers (2006) investigated the use of an energy efficient, alternative wood-fiber fly ash material for the purpose of creating masonry units for the construction of infill masonry walls. The study consisted of evaluating the mechanical properties as well as the durability characteristics for various mixture designs of the wood-fiber fly ash composite material. In all, 36 different material designs were investigated to determine the optimum proportions of wood-fiber, fly ash, and water. Of the 36 designs, 18 of the mix designs also consisted of some percentage of Portland cement for comparative purposes. As an additional constraint in this study, only mixture designs that reached compressive strength values of 1,000psi (6.89MPa) or greater were considered in the selection of the optimum design to be consistent with that of low-strength clay units and aerated autoclave concrete (AAC).

Based on the aforementioned 'optimum design,' an additional phase of study explicitly focused on the behavior of the composite material was performed. The behavioral areas investigated focused on the freeze-thaw resistance, the shrinkage behavior, and the load-deformation response of the material. The key findings from this phase of the study have been summarized:

- The freeze-thaw resistance of the wood-fiber fly ash material was very much comparable with that of other cementitious-based materials. There was no mass loss after 300 freeze-thaw cycles, and only minor surface damage was observed.

- ▪ The shrinkage levels of the wood-fiber fly ash material obtained from testing were of the same order of conventional concretes.

- ▪ Based upon the load-deformation behavior of the wood-fiber fly ash material, it would appear that the material could have desirable damping and energy-absorbing characteristics.

The load-deformation behavior from one of the test specimens has been presented in Figure 2.1 to illustrate the energy-absorption potential referred to by the investigators of this study.
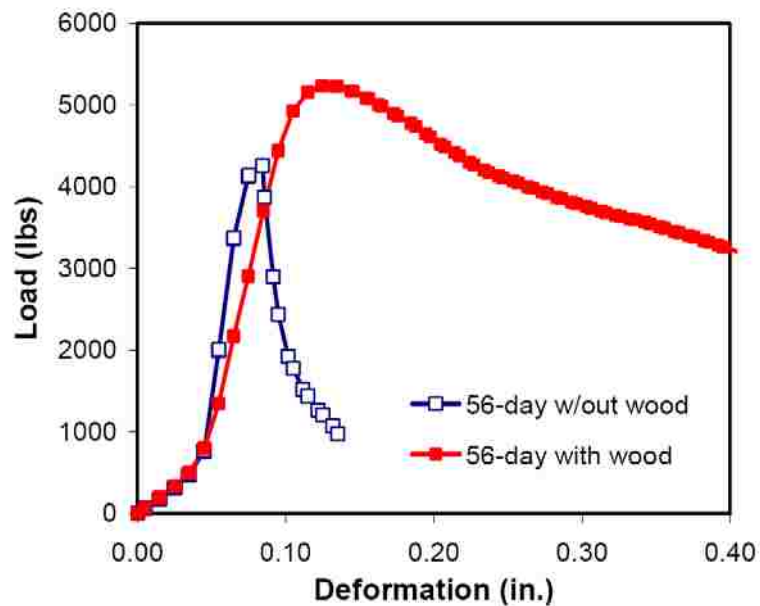
Figure 2.1. Load-Deformation Behavior of Wood-Fiber Fly Ash (Joshi and Myers, 2006)

Another research study carried out at the University of Missouri-Columbia has shown that through the use of high-pressure compaction technology, fly ash can be created into building materials that upon curing have similar strength characteristics with

that of fired clay brick and concrete blocks. In this study, fly ash logs were created through the use of high-pressure compaction and were evaluated in an effort to determine the applicability of their use as a modern building material. Several different factors were found to be influential on the performance of the compacted fly ash: the fly ash to water (F/W) ratio, the curing conditions, the curing time, and the compaction pressure used to create the logs. In the majority of the cases, as the F/W ratio increased, the strength also increased. It was also found that curing the logs was necessary to increase their strength, and that higher compaction pressure resulted in higher compressive strength. Two types of Class-C fly ash, high-grade and low-grade fly ash, were studied in this program to evaluate the effectiveness of each material. The compressive strength of the logs was evaluated at 60 days for the optimal mix designs and was found to be 10,000psi (68.9MPa) for the logs created from the high-grade fly ash and 3,300psi (22.8MPa) for logs created from the low-grade fly ash (Hu et al., 2001). On the basis of compressive strength, material created from both grades of fly ash would be applicable for the use of masonry construction.

2.2. OUT-OF-PLANE BEHAVIOR OF URM WALL SYSTEMS

The behavioral mechanism of a URM wall subjected to out-of-plane loading, also referred to as transverse loading, depends upon several different factors, the most important being the support conditions at the wall boundaries and the height-to-thickness ratio of the wall. These are the factors that govern whether the out-of-plane load carrying capacity of the wall is controlled by the tensile strength of the masonry or by the in-plane compressive strength of masonry.

The behavior of URM infill walls can be greatly affected by the presence of the surrounding frame. When a wall is built between rigid supports, which is often the case for walls with relatively stiff surrounding frames or for panels that have continuity with adjacent infills, the wall can become effectively restrained along the in-plane direction. Due to this restraint condition at edges of the wall, membrane compressive forces in the plane of the wall and shear forces at the supports are induced as the wall bends. This membrane force development is referred to as arching action (Angel et al., 1994; Tumialan and Nanni, 2001). The arching action mechanism is illustrated in Figure 2.2.
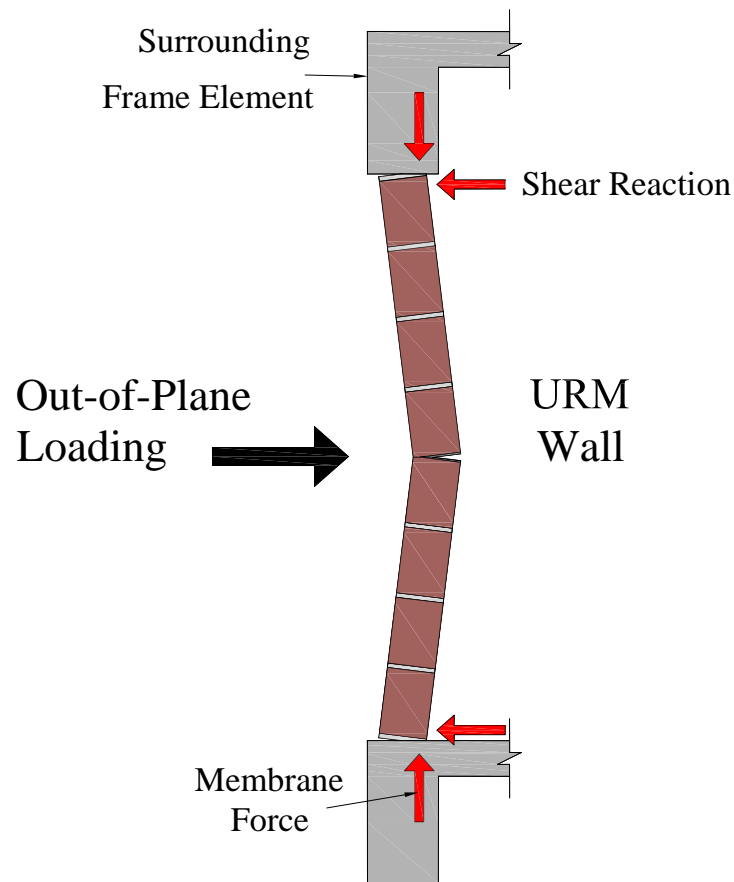
Figure 2.2. Arching Action Mechanism

The out-of-plane capacity of URM walls is often assumed to be controlled, or highly dependent upon the tensile strength of the masonry. However, when an arching action is present, the tensile strength of the masonry plays only a minor role, and the wall capacity is predominantly governed by the in-plane compressive properties of the masonry. From previous studies investigating the behavior of framed infill walls, the contribution of the membrane forces developed due to arching action has been found inversely proportional to the height-to-thickness *(h/t)* ratio, often referred to as the slenderness ratio, of a wall panel. That is, as the slenderness ratio increases, the contribution from the arching effect decreases. For walls with a height-to-thickness ratio greater than a value of 30, the arching effect is essentially negligible (Angel et al., 1994).

Several different models have been developed in an effort to predict the load resistance of unstrengthened URM infills. Typically, these models are primarily based on the stiffness of the surrounding frame, the height-to-thickness ratio of the wall, and the material properties of the masonry. However, consideration of the deformation of the surrounding frame can result in a complex interaction between the frame and the URM wall. Therefore, to simplify the problem, the frame is often treated as a rigid element. A codified version of this type of model is presented in the European Building Code (Eurocode 6, 2005). In this model, the wall is assumed to develop into a three-hinged arch as illustrated in Figure 2.2, and it is assumed that the bearing width at each of the hinge locations is equal to a value of 0.10 times the thickness of the wall. This methodology provides a basis for determining the maximum arch-thrust that can be developed prior to crushing of masonry. Based upon these assumptions, the following

equation has been developed to determine the out-of-plane load resistance, q_u, for a given width of wall, b_m (Garbin et al., 2005):

$$q_u = 0.58 f'_m b_m \left(\frac{t}{h} \right)^2 \tag{1}$$

where f'_m is the gross compressive strength of the masonry, t is the thickness of the wall, and h is the overall height of the URM wall.

2.3. RETROFITTING MASONRY WALLS FOR OUT-OF-PLANE LOADS

To date, significant research has focused on improving the out-of-plane behavior of URM wall systems. Much of this research was carried out in an effort to investigate various methods of increasing the load carrying capacity and ductility of these systems. However, many studies have solely focused on improving the brittle failure modes of URM walls subjected to out-of-plane loads.

2.3.1. Catcher Systems. One method of retrofitting a structure to improve its performance under blast loading is to implement what is known as a catcher system. The design of a catcher system is focused on preventing debris from entering the internal structure, and the system may or may not increase the capacity of the retrofitted element. The use of catcher systems in the retrofitting of URM infill walls serves as an applicable example of where such a system would be feasible. Because URM infill walls often carry little or none of the load from the surrounding structure, it is not necessary that infill walls maintain the ability to carry structural loads after being subjected to a blast

event. However, debris from the URM infill wall system as a result of a blast event must be prevented from entering the structure.

A case study performed by Bogosian and Crawford (2000) presented an aesthetically acceptable, non-intrusive retrofit method to improve the performance of URM wall systems subjected to extreme blast loads. The URM retrofit implemented in this study was designed as a catcher system and consisted of a 1/8in. (3.2mm) thick steel plate spanning from floor to ceiling on the interior face of the wall, high density polyurethane foam, and a stiffened steel anchorage system. This type of steel plate catcher system is highly attractive because the system subtracts little space from the floor plan of the building, and the surface of the steel plate on the interior face of the wall can be easily covered. The retrofit was highly effective in preventing debris and fragmentation from projecting inward into the structure. As a result of the blast, the plate deformed plastically and bent into a membrane to accommodate the impulsive load from the wall debris. The deformation due to the blast load can be seen from the interior face of the strengthened wall and the anchorage system presented in Figure 2.3.

Figure 2.3. Steel Plate Catcher System (Bogosian and Crawford, 2000)

2.3.2. Strengthening with FRP. A previous study performed at the University of Missouri-Rolla (UMR) investigated the use of near surface mounted (NSM) FRP bars to increase the out-of-plane load capacity of slender URM walls (Galati et al., 2006). The use of NSM bars is an attractive retrofit technique to increase the flexural and shear capacity of URM wall systems because, with the exception of the slots that are cut to place the bars, the system does not require surface preparation and requires only minimal installation time. In this study, 15 strengthened masonry walls were tested, 3 of which were constructed using clay bricks, while the remaining 12 walls were constructed using concrete blocks. Four different FRP bars varying in size, geometry, and composition were investigated for the applicability of their use in the strengthening of URM walls. All of the walls were tested under four-point bending, and the load-deformation behavior of the walls was observed. Figure 2.4 presents the load-deformation behavior for a single series of tested walls from the experimental program.
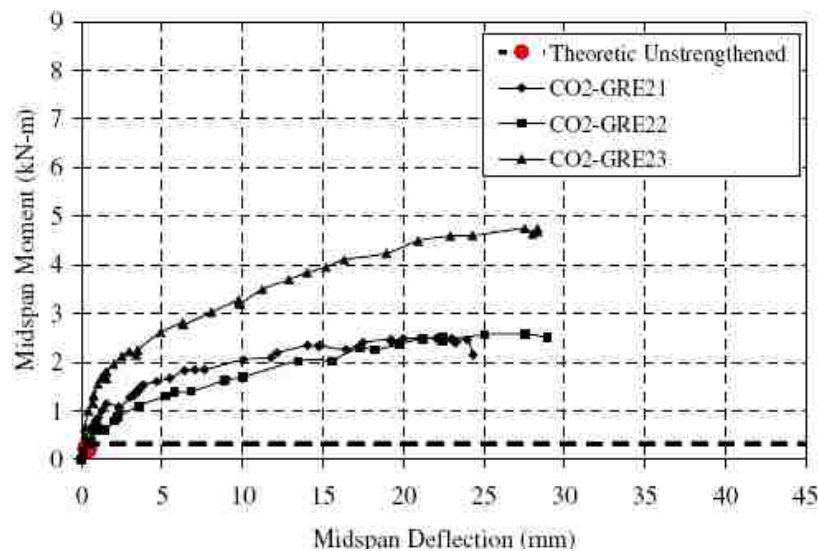
Figure 2.4. Load-Deformation Behavior NSM Strengthened URM (Galati et al., 2006)

The walls in this series of the program were strengthened using rectangular glass FRP (GFRP) bars that were embedded within the surface of the wall using an epoxy paste. As shown in the figure, the NSM bars were highly effective in increasing both the capacity and deformation ability of the URM walls. When the results of the strengthened walls are compared to the theoretical value of an unstrengthened wall (represented in the figure by the circular data point), the significance of the improvement in the behavior of the walls becomes apparent.

In addition to the experimental program performed, Galati et al. (2006) also presented a conservative design approach to determine the capacity of simply-supported FRP strengthened URM walls. The design approach was initially developed based on the ultimate limit states of crushing of the masonry or rupture of the FRP strengthening material. However, based on experimental results from this study as well as other studies, it was necessary to modify the design approach to account for premature failure modes, primarily bond failures. Rather than attempting to predict bond failures between the FRP and the base masonry material, the ultimate achievable strain in the FRP was conservatively limited by incorporating an additional multiplier, k_m, which ranged from 0.35 to 0.65 depending on the type of FRP bars and installation technique used. The design equations developed from this study are as follows:

The nominal moment capacity, M_n, of a simply-supported FRP strengthened wall is obtained from the equilibrium of internal forces and is determined using Equations (2) and (3):

$$M_n = A_{frp} f_{fe} \left(t - \frac{\beta_1 c}{2} \right) \tag{2}$$

$$(\gamma f_m')(\beta_1 c)b_m = A_{frp} f_{fe} \tag{3}$$

where A_{frp} is the area of FRP strengthening material, and $\beta_1 c$ is the depth of the

rectangular stress-block. The variable f_{fe} represents the stress determined from the

limiting strain in the FRP and is calculated using the k_m factor, the ultimate strain in the

FRP, ε_{fu}, and the modulus of elasticity of the FRP, E_{frp}, using Equation (4); (Galati et al.,

2006):

$$f_{fe} \leq \varepsilon_{fe} E_{frp} = (k_m \varepsilon_{fu}) E_{frp} \tag{4}$$

The ultimate moment capacity for the strengthened walls is taken as the minimum of that

determined using Equation (1) or the evaluated theoretical shear capacity.

Overall, the moment capacities determined using the aforementioned analytical

model agreed well with the results from the experimental program. A comparison of the

experimental and theoretical values is presented in Figure 2.5. The comparative results

have been presented in terms of the respective reinforcement index, w_f, for each of the

FRP strengthened walls, determined using Equation (5):

$$w_f = \frac{\rho_{frp} E_{frp}}{f'_m (h/t)} \tag{5}$$

where ρ_{frp} represents the flexural reinforcement ratio.
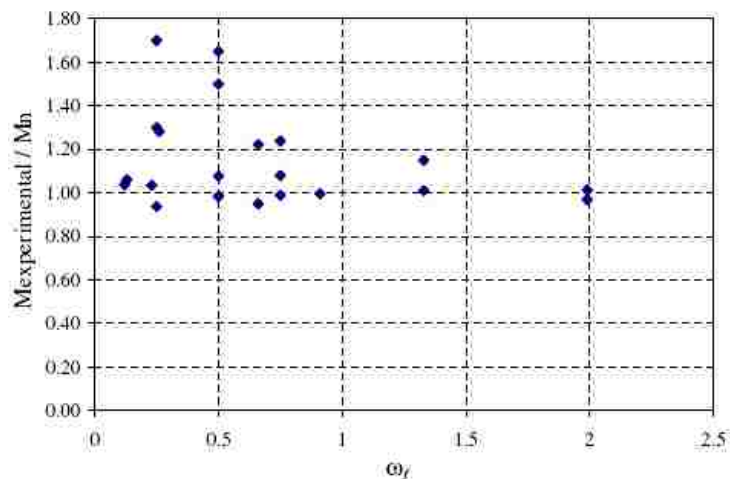
Fig. 7. Ratio between experimental and nominal moments.

Figure 2.5. Ratio Between Experimental and Nominal Moments (Galati et al., 2006)

Velazquez-Dimas et al., (2000) studied the behavior of URM walls subjected to cyclic out-of-plane loading. The walls in this study had a height-to-thickness ratio equal to 28 and were reinforced using surface laminate GFRP strips. The walls were constructed within a steel frame that simulated simply-supported conditions at the top and bottom boundaries and free conditions along the side edges of the walls. The walls were loaded with a uniform pressure through use of an airbag system that was moved from one face of the wall to the other to accommodate the cyclic loading. Both single wythe and double wythe wall construction were investigated. Tension failure, delamination, or combinations of both were found to be the controlling failure modes. It was found that the use of the surface laminate GFRP strips resulted in large increases in the out-of-plane load capacity of the walls as well as the ability to undergo deflection. Pressure values up to 25 times the self weight and deflection values of 1/20 times the wall height were achieved.

Another study carried out at UMR implemented the use of two different FRP retrofit techniques resulting in significant increases in the flexural capacity of partially framed URM infill walls. The walls in this study were tested in the laboratory under static loading using an airbag system. A second phase of study tested strengthened walls in the field under actual blast loads (Carney and Myers, 2003). The walls in this study were restrained between two rigid boundary elements at the upper and lower boundaries of the wall, had a slenderness ratio of 12, and were constructed using CMUs. Due to the low slenderness ratio and the restraint at the member-ends imposed by the surrounding frame, one-way arching action was observed in all of the strengthened and unstrengthened URM walls. The use of both NSM GFRP rods and surface laminate GFRP strips was investigated, and both were found to significantly increase the out-of-plane load carrying capacity as well as the ductility of URM infills. The ductility results from testing have been presented in Figure 2.6.
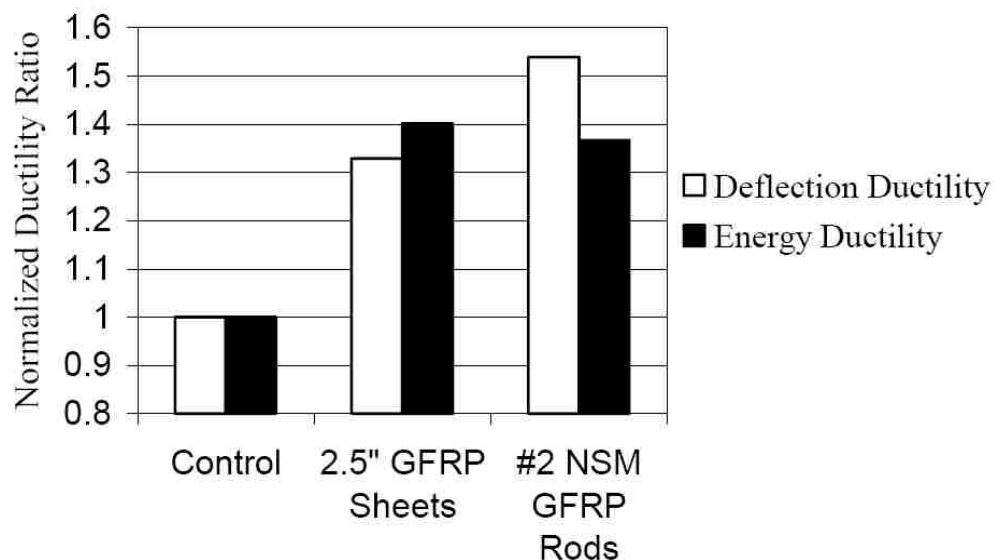
Figure 2.6. Normalized Ductility Results (Carney and Myers, 2003)

In addition to the increased load carrying capacity and ductility that resulted from the FRP retrofits implemented in this program, the effect of the retrofit schemes on the debris scatter at failure was also investigated. It was also found that the use of the NSM FRP rods resulted in essentially no improvement in the scatter of debris of base masonry material at failure. The use of the FRP surface laminates in this program was found to result in modest improvements in reducing the amount of debris and fragmentation at failure. The failure behavior of each type of retrofitted wall is presented in Figure 2.7.

(a) Surface Laminate Retrofit   (b) NSM Retrofit

Figure 2.7. Debris Scatter of Masonry Substrate Material (Carney and Myers, 2003)

2.3.3. Strengthening with Elastomeric Polymers. The use of elastomeric polymers for the purpose of retrofitting URM walls to mitigate damage due to blast has been investigated in previous experimental programs. In 2002, an experimental study performed by Connell was aimed at evaluating the effectiveness of inexpensive, lightweight polymer retrofits for protection against blast loads. Initially a total of 21

prospective polymers were evaluated to determine their applicability for use in the experimental study. Of the 21 polymers, 13 of them were spray-on polymers made up of polyurethanes, polyurea, and what can be classified as polyurea/urethanes. Ultimately, the pure polyurea spray-on material was selected for use in the study due to its low stiffness and ability to elongate without rupture.

Three blast tests were performed in this research study. Each of the blast tests consisted of 2 wall panels constructed within a rigid reaction structure. Of the 6 URM walls tested, 4 of them were retrofitted by spraying polyurea on the interior surfaces the wall panels and overlapping the polyurea by approximately 6in. (152mm) onto the surrounding frame. Three of the retrofitted wall panels had a 1/8in. (3.2mm) thick application of polyurea, and 1 of the wall panels had a 1/4in. (6.4mm) thick application of polyurea. For each of the 3 blast tests, the wall panels were framed at the top and bottom boundaries and were free to move along the sides to force a one-way response. The boundary conditions were varied for each of the 3 tests by providing additional external cladding systems, which were used to provide anchorage and to vary the rigidity of the boundary conditions.

In each of the blast tests, it was clear that the polyurea retrofit was highly effective in limiting fragmentation and preventing debris from entering within the structure. The study successfully showed that an elastomeric polyurea retrofit system could be used to strengthen URM walls both rapidly and effectively. In comparison to other studies that have implemented the use of much stiffer retrofit materials, the experimental program also showed that the ability of the retrofit material to absorb strain energy is a key factor in the effectiveness towards preventing projectiles from entering

the structure. For the retrofitted walls in this study, peak response pressures greater than 60psi (414kPa) were easily achieved, whereas the unstrengthened URM walls failed at response pressure values of less than 10psi (69kPa).

Lastly, a previous study performed by Yu et al. (2004) investigated the use of an elastomeric polyurea for the purpose of improving the in-plane load resistance of URM infill walls and the flexural capacity of reinforced concrete (RC) beams. The study also investigated the effectiveness of embedding FRP grids within polyurea to strengthen URM walls and RC beams. The results from the study showed that the application of polyurea material to retrofit RC beams resulted in no increase in flexural capacity. However, the addition of the polyurea did result in a modest increase in the cracking load and decreased flexural crack widths. The use of the FRP embedded within the polyurea yielded increases in the flexural capacity of the section and resulted in significant increases in the stiffness. Most importantly, the FRP grid ultimately ruptured at midspan, and no debonding or delamination was found to occur between the polyurea and the concrete or the polyurea and FRP grid.

3. MATERIAL CHARACTERIZATION

The research program presented in this paper consisted of retrofitting URM walls with the use of GFRP grids and an elastomeric polyurea surface coating. To effectively determine the properties of the strengthened URM walls, it was necessary to determine the mechanical properties of both strengthening materials that were used in the masonry retrofit. It was also necessary to determine the mechanical properties of the base masonry materials used in the wall construction.

3.1. GLASS FIBER REINFORCED POLYMER

The GFRP reinforcement used in this research program was classified as a high strength, unidirectional reinforcement manufactured for the purpose of seismic strengthening of masonry structures and infrastructure repair and retrofit (TechFab, 2003). The mechanical properties of the GFRP grid material was determined by performing a series of uni-axial tension tests in accordance with the ACI 440R-04 guidelines. In all, five GFRP coupons were prepared and tested. Each of the specimens had a gage length of 6.5in. (165mm) and an approximate width of 1.75in. (44.5mm), consisting of 4 longitudinal grid chords. Due to slight variances in the dimensions of each individual chord, an average value of $0.0066in.^2$ ($4.29mm^2$) was taken as the cross-sectional area of a single chord (Yu et al., 2004). Figure 3.1 presents the testing of a GFRP coupon.

The GFRP coupons were tested at a constant displacement rate of 0.10in./min (2.54mm/min). Strain data were recorded through the use of a 1in. (25.4mm) extensometer placed at the midpoint of the gage length and sampled at a rate of 10Hz.
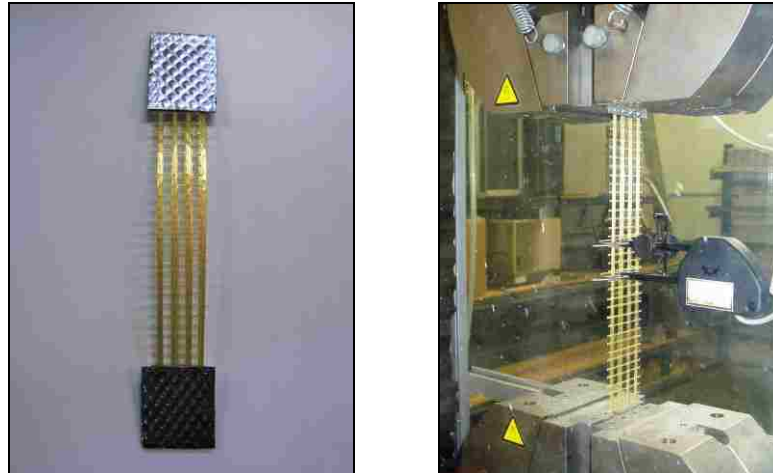
Figure 3.1. Testing of GFRP Coupon

The resulting stress-strain behavior from the coupon tests is presented in Figure 3.2. The results from each of the five tests performed are presented in Table 3.1. The mechanical properties determined for the GFRP material were calculated by averaging the values in Table 3.1 and resulted in the properties presented in Table 3.2.
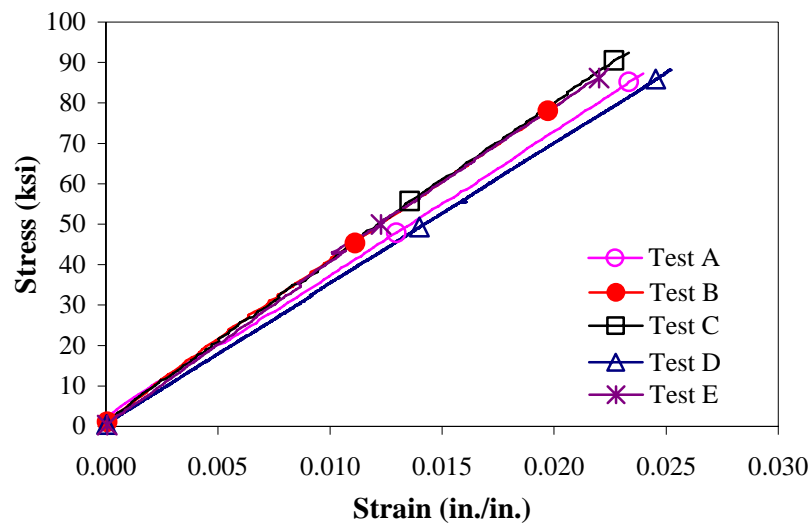
Conversions: 1 ksi = 6.895 MPa; 1 in./in. = 1 mm/mm

Figure 3.2. Stress-Strain Behavior of GFRP

Table 3.1. Results from GFRP Coupon Tests

Test	Max Load kips (kN)	Max Stress ksi (MPa)	Ultimate Strain	Modulus of Elasticity ksi (GPa)
A	2.30 (10.2)	87.2 (601)	0.024	3669 (25.3)
B	2.13 (9.5)	80.8 (557)	0.020	4038 (27.8)
C	2.44 (10.9)	92.4 (637)	0.023	4037 (27.8)
D	2.33 (10.4)	88.1 (607)	0.025	3552 (24.5)
E	2.29 (10.2)	86.7 (598)	0.022	4002 (27.6)

Table 3.2. Mechanical Properties of GFRP Grid

Tensile Strength ksi (MPa)	Modulus of Elasticity ksi (GPa)	Ultimate Strain	Strength per Unit Width kips/in. (kN/mm)
87.0 (600)	3860 (26.6)	0.023	1.28 (224)

3.2. POLYUREA

The mechanical properties of the polyurea strengthening material were determined in a similar fashion to that of the GFRP reinforcement. A series of four coupons of polyurea material were tested under uni-axial tension to determine the stress-strain behavior of the material. The polyurea coupons varied in cross-sectional geometry, but had a uniform gage length of 5in. (127mm) satisfying the minimum allowable gage length specified by the ACI 440R-04 testing guidelines. Figure 3.3 presents the testing of a polyurea coupon.

The coupons were tested at a rate of 0.50in./min (12.7mm/min). The strain data were recorded using a 1in. (25.4mm) extensometer placed at the midpoint of the gage

Figure 3.3. Testing of Polyurea Coupon

length. In all of the tests performed on the polyurea coupons, the extensometer was
removed after reaching the apparent yield of the material, but prior to ultimate, to prevent
damaging the testing machine. It should also be noted that the tensile testing machine
reached its displacement limit prior to rupturing the polyurea material. In all four tests
performed, the limiting displacement of the testing machine corresponded to a cross-head
displacement greater than three times the original gage length. The results from the
polyurea coupon tests are presented in Figure 3.4 and summarized in Table 3.3. The
mechanical properties determined for the polyurea material were found by averaging the
results in Table 3.3 and resulted in the values presented in Table 3.4.

The application of the elastomeric polyurea material, which is later discussed in
Sections 5 and 6, involved the use of an epoxy primer. The provided manufacturer's
properties of the epoxy primer used in this study are presented in Table 3.5.
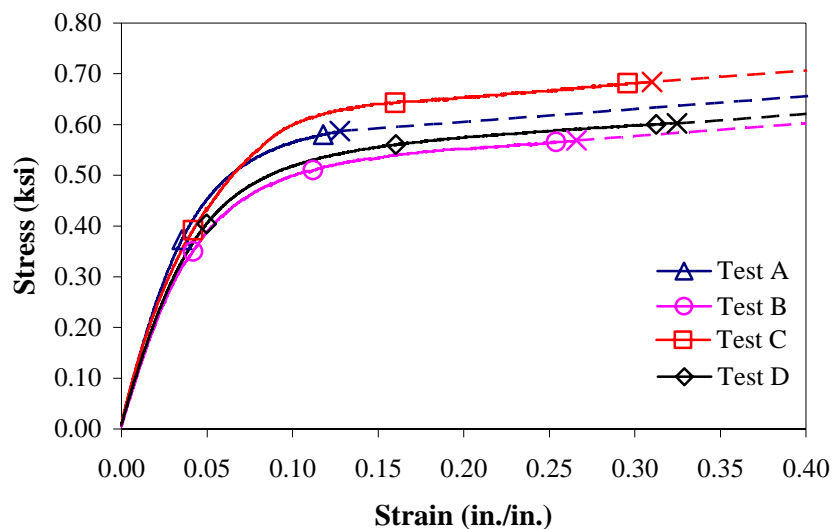
Note: X indicates the point at which the extensometer was removed

Conversions: 1 ksi = 6.895 MPa; 1 in./in. = 1 mm/mm

Figure 3.4. Stress-Strain Behavior of Polyurea

Table 3.3. Results from Polyurea Coupon Tests

Test	Cross-Sectional Area in.^{2} (mm^2)	Full Yield Stress ksi (MPa)	Full Yield Strain	Modulus of Elasticity ksi (GPa)	Max Stress Recorded ksi (MPa)
A	0.627 (404.5)	0.59 (4.07)	0.128	13.3 (0.092)	1.06 (7.31)
B	0.642 (414.2)	0.53 (3.65)	0.147	10.7 (0.074)	1.06 (7.31)
C	0.404 (260.6)	0.64 (4.41)	0.156	13.2 (0.091)	0.88 (6.07)
D	0.731 (471.6)	0.56 (3.86)	0.148	11.3 (0.078)	1.21 (8.34)

Table 3.4. Mechanical Properties of Polyurea

Stress at Full Yield ksi (MPa)	Modulus of Elasticity ksi (GPa)	Strain at Full Yield	Ultimate Stress ksi (MPa)
0.58 (4.00)	12.1 (0.083)	0.145	> 1.0 (6.89)

Table 3.5. Mechanical Properties of Epoxy Primer (Watson, 2002)

Tensile Strength ksi (MPa)	Tensile Modulus ksi (MPa)	Tensile Rupture Strain	Compressive Strength ksi (MPa)	Compressive Modulus ksi (MPa)	Compressive Rupture Strain
2.1 (14.5)	105.0 (717)	0.40	4.1 (28.3)	97.0 (670)	0.10

3.3. MASONRY MORTAR

The mortar used for construction of the URM walls was a readily available premixed product classified as Type-S defined by ASTM C270. The compressive strength of the mortar was verified by testing 2in. (50mm) mortar cubes in accordance with ASTM C109. A set of 3 mortar cubes were cast, moist-cured, and tested at 28 days for verification of the mortar type. Additional sets of mortar cubes were prepared and match cured for each URM wall constructed. The match cured mortar cubes were tested at the same time as the wall specimens. The casting and testing of the mortar cubes is illustrated in Figures 3.5 and 3.6, respectively. The results from the cube testing have been summarized in Table 3.6.
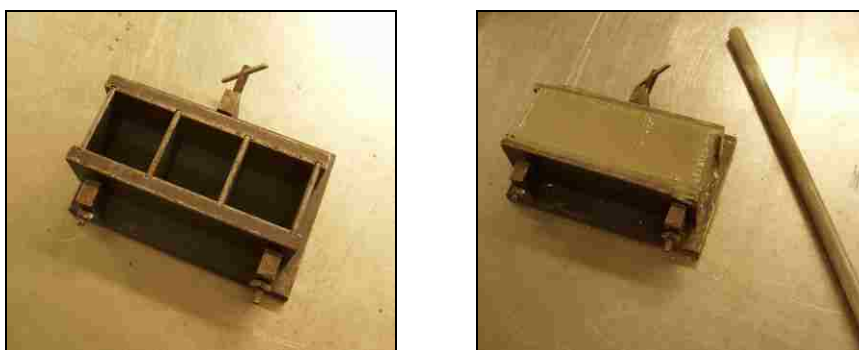
Figure 3.5. Mortar Cube Casting

Figure 3.6. Mortar Cube Testing

Table 3.6. Mortar Cube Strength

Research Phase	Series	28 Day Strength (moist cured) psi (MPa)	Experimental Strength At Test Age of Wall (match cured) psi (MPa)
Phase 1	Series 1	1700 (11.7)	1850 (12.8)
	Series 2	1750 (12.1)	1750 (12.1)
Phase 2	Series 1	1700 (11.7)	1750 (12.1)
	Series 2	1800 (12.8)	2000 (13.8)

3.4. BASE MASONRY MATERIAL

Three different types of base masonry material were investigated in this research program. For the purpose of characterizing the walls built from these materials, it was necessary to determine the mechanical properties of the masonry units, as well as the mechanical properties of the masonry assemblages constructed from these units.

3.4.1. Masonry Units. For the purpose of characterizing the mechanical properties of the individual masonry units, testing was performed on each of the three

base masonry materials to determine the compressive strength of the units in their intended orientation of loading.

3.4.1.1. Clay brick. The individual clay brick units used in this research program had gross nominal dimensions of 2 ¾ x 2 ½ x 9 ½ in. (70x64x241mm) resulting in a gross cross-sectional area of 26.0in.^{2} (16,770mm^2). The net area of each unit was determined to be 21.3in.^{2} (13,740mm^2). In order to determine the compressive strength of the clay units, testing was performed on uncapped individual half-length units in accordance with ASTM C67. The gross compressive strength of the clay units was found to be 2,400psi (16.5MPa), and the net strength was determined to be 2,900psi (20.0MPa). The individual clay bricks and testing of the half-length units is illustrated in Figure 3.7.
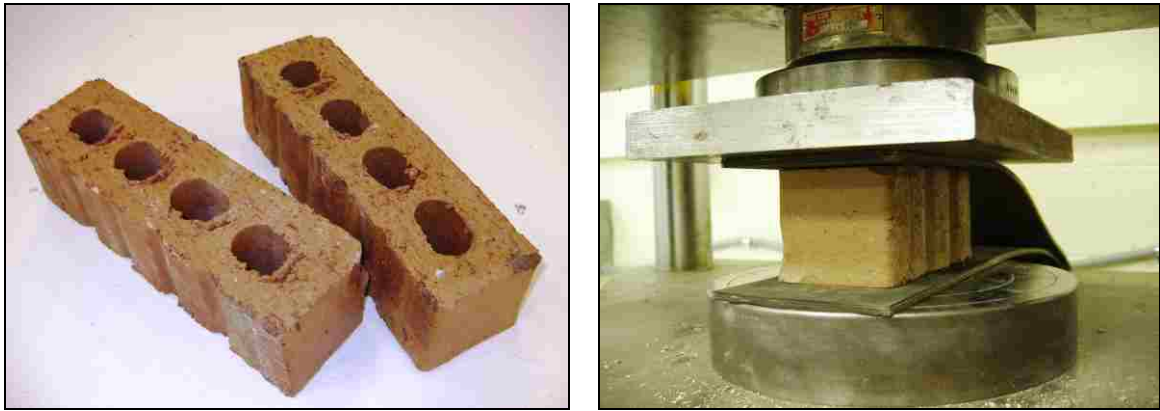
Figure 3.7. Testing of Individual Clay Brick Units

3.4.1.2. Concrete masonry units. The concrete block, or CMUs, had gross dimensions of 3 ⅝ x 7 ⅝ x 15 ⅝ in. (92x194x397mm), resulting in a gross cross-sectional area of 56.6in.^{2} (36,520mm^2). The net cross-sectional area of the individual CMU units was found to be 45.1in.^{2} (29,100mm^2). The compressive strength of the concrete block

was determined by testing full-length uncapped units in accordance with ASTM C140-05a. The gross compressive strength of the CMU units was found to be 1,700psi (11.7MPa), and the net compressive strength was determined to be 2,100psi (14.5MPa). The testing of the individual concrete blocks is illustrated in Figure 3.8.

Figure 3.8. Testing of Individual Concrete Masonry Units

3.4.1.3. Wood-fiber fly ash masonry. The wood-fiber fly ash masonry units (WF-FA) used in this research were made from a composite mixture consisting of primarily white oak wood-fibers and a Class-C fly ash. The raw materials are presented in Figure 3.9.

The mix design used to create the composite material was established in a previous study focusing on evaluating the performance of the composite material (Joshi and Myers, 2006) and has been discussed in Section 2 of this thesis. The mix design selected for construction of the WF-FA masonry units is based on the optimum design determined from this previous study and is presented in Table 3.7.

(a) Wood-Fiber   (b) Fly Ash

Figure 3.9. WF-FA Primary Materials

Table 3.7. Wood-Fiber Fly Ash Mix Design

Material	Mixture Design lb/yd^3 (kg/m^3)
Fly Ash (FA-C-1)	1861 (1104)
Wood-Fibers	278 (165)
Water	513 (304)

Admixtures: 2 fl.oz high-range water reducer (HRWR)/100lb fly ash (1.30 mL/kg)

The WF-FA material was mixed in 2ft^3 (0.057m^3) batches using a rotating drum mixer with a volumetric capacity of 4ft^3 (0.113m^3). As shown in Figure 3.10, after adequately mixing, the material was placed into wooden forms, which were subdivided into a series of brick sized units. The material was placed in two layers, and voids were removed by way of rodding the material with a standard tamping rod.

Figure 3.10. WF-FA Material Placement

The dimensions of the individual brick units were made to match that of the clay bricks used in this study with nominal dimensions of 2¾ x 2½ x 9½ in. (70x64x241mm). The bricks were constructed as solid units with no holes, resulting in a cross-sectional area of 26.0in.^{2} (16,770mm^2). The bricks were allowed to cure for a period of 24 hours under ambient conditions before stripping the forms and placing the bricks into a moist curing chamber. After moist curing for an additional 7 days, the bricks were removed from the curing chamber, and the remainder of the curing process took place in the laboratory under ambient conditions. The dry density of the material was determined after 60 days of ambient condition curing and was found to be approximately 90lb/ft^3 (1442kg/m^3).

For the purpose of strength characterization, 2in. (50mm) cubes, 4 x 8in. (102 x 203mm) cylinders, and 6 x 12in. (152 x 305mm) cylinders were cast throughout the material batching process to determine the compressive strength and stiffness of the WF-FA material. The compressive strength values obtained from the testing of the cubes were found to be much higher than that of the cylinders. Therefore, the average 28-day

compressive strength from each of the batches of material was based solely on cylinder

testing and was found to be 450psi (3.1MPa). The stiffness of the material was

determined in accordance with the ASTM C469 test method. The 6 x 12in. (152 x

305mm) cylinders were loaded at a rate of 500lb/sec (2.22kN/sec), and longitudinal strain

data were acquired using a compressometer. The testing resulted in relatively low

stiffness values with an average modulus of elasticity value of 300ksi (2070MPa). The

compressive strength testing of the WF-FA material is presented in Figure 3.11.

Figure 3.11. WF-FA Compression Testing

The compressive strength for each type of masonry unit used in the research

program has been summarized in Table. 3.8. It should be noted that only the 28-day

strength has been reported for the strength of the WF-FA brick.

3.4.2. Masonry Compressive Strength. The strength of the masonry

assemblages was determined for each of the base masonry materials through pure

compression testing of masonry prisms. The prisms were constructed at the time of wall

Table 3.8. Compressive Strength of Individual Masonry Units

Masonry Substrate	Gross Compressive Strength psi (MPa)	Net Compressive Strength psi (MPa)
Clay Brick	2400 (16.5)	2900 (20.0)
Concrete Block (CMU)	1700 (11.7)	2100 (14.5)
Wood-Fiber Fly Ash Units (WF-FA)	*450 (3.1)	N/A

 *28-day strength.

construction by the same mason using the same mortar. The prisms were match-cured

and tested at the same time as the URM walls were tested. The prisms were tested

uncapped in accordance with ASTM C1314.

   The masonry prisms constructed from the clay units had gross overall dimensions

of 2¾ x 11½ x 9½ in. (70x292x241mm). The prisms consisted of four courses of single

full-length units. The gross compressive strength of the clay masonry was found to be

1,500psi (10.3MPa) and the net strength was determined to be 1,850psi (12.8MPa). The

testing of the clay prisms is illustrated in Figure 3.12.

   The prisms constructed from the concrete masonry units had overall dimensions

of $15\frac{5}{8}$ x $3\frac{5}{8}$ x 16in. (397x92x406mm). The prisms consisted of two courses of single

full-length units. The gross strength of the prisms constructed from the concrete masonry

units was found to range from 1,300psi (9.0MPa) to 1,500psi (10.3MPa), and the net

strength of the prism ranged from 1,650psi (11.4MPa) to 1,900psi (13.1MPa).

   Similar to the clay and concrete base materials, prisms were constructed from the

WF-FA composite material for the purpose of evaluating the strength of the masonry

Figure 3.12. Compression Testing of Clay Prism

assemblage. The WF-FA prisms had gross overall dimensions of 9½ x 2¾ x 11½in. (241x70x292mm). The prisms consisted of four courses of single full-length units. In addition to the determination of the compressive strength of the WF-FA prisms, the stiffness of the assemblage was also determined. Testing of the WF-FA prisms is illustrated in Figure 3.13.

Figure 3.13. Compression Testing of WF-FA Prism

During the testing of the WF-FA prisms, the load-deflection behavior was recorded through use of 1in. (25mm) potentiometers spanning the mortar joints of the prisms. The potentiometers measured displacements from the mid-height locations of the courses immediately above and below the mortar joints. The load data were recorded through use of a 25kip (111kN) load cell. From the data acquired for the WF-FA prism testing, the stress-strain behavior was developed for each of the tests performed. The stress-strain behavior from one of the three WF-FA prism tests is presented in Figure 3.14.

The stiffness of the WF-FA assemblage was found to be essentially the same at both potentiometer locations for each of the tests performed. The stiffness of the WF-FA prisms was determined by averaging the stiffness across the mortar joints from each of the three prism tests and resulted in an overall stiffness value of 585ksi (4.03GPa).
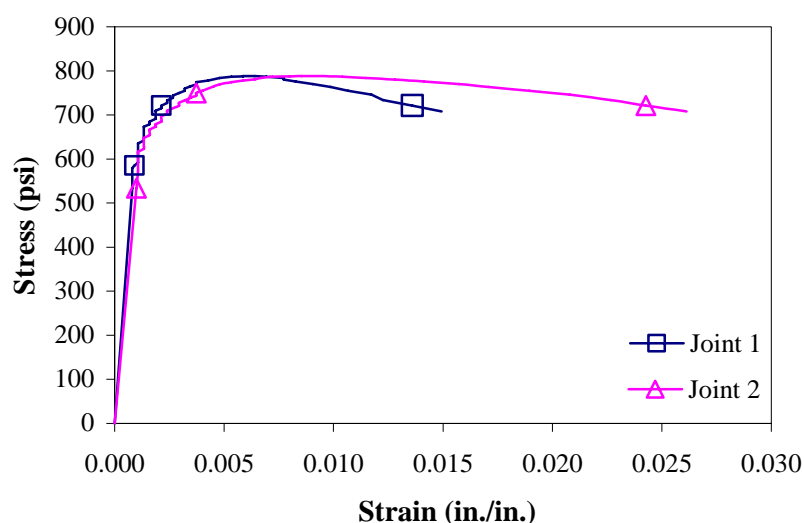
Conversions: 1 psi = 6.895 kPa; 1 in./in. = 1 mm/mm

Figure 3.14. Stress-Strain Behavior of WF-FA Prism

This value agrees well with Equation (6), which is the recommended equation used to determine the stiffness for clay masonry assemblages provided by the Building Code Requirements for Masonry Structures (ACI530-02/ASCE5-02/TMS402-02).

$$E_m = 700 f'_m \qquad (6)$$

It should be noted that the stiffness of the WF-FA prism was only evaluated for a single series of constructed prisms. Since the strength of the WF-FA prisms tested throughout the experimental program were found to vary significantly, unique stiffness values were considered for each of the walls constructed from WF-FA brick and were determined using Equation (6) exclusively.

As previously stated, the compressive strength of the WF-FA prisms was found to vary for each of the walls constructed from the WF-FA brick units. Therefore, compressive strength values specific to each WF-FA wall have been reported, as opposed to an average strength to be used for all walls constructed from the WF-FA brick. The compressive strength of the walls determined from prism testing ranged from 850psi (5.9MPa) to 1,000psi (6.9MPa).

The compressive strength values determined from the testing of the masonry prisms have been summarized in Table 3.9. It should be noted that strength values presented for the clay and concrete prisms represent average values, which are applicable for each phase of wall testing. Unique compressive strength values have been reported for the walls constructed from the WF-FA material due to the variance of strength for this material.

Table 3.9. Compressive Strength of Masonry Prisms

Base Masonry Material	Phase / Wall	Gross Compressive Strength psi (MPa)	Net Compressive Strength psi (MPa)
Clay Brick Masonry	Phase 1	1500 (10.3)	1850 (12.8)
	Phase 2	1500 (10.3)	1850 (12.8)
Concrete Block (CMU)	Phase 1	1300 (9.0)	1650 (11.4)
	Phase 2	1500 (10.3)	1900 (13.1)
Wood-Fiber Fly Ash Masonry (WF-FA)	Wall P1-6	1000 (6.9)	N/A
	Walls P1-7, P1-8	850 (5.9)	N/A

3.4.3. Masonry Flexural Bond. The flexural bond strength of masonry construction can be approximated using codified values based on the mechanical properties of the mortar and the masonry units used in the construction. However, because the use of WF-FA masonry units in construction is a relatively new idea, it was necessary to determine the flexural bond performance of the composite brick units to evaluate the applicability of using such units for infill wall systems.

Flexural bond testing was performed on each of the base masonry materials using a bond wrench testing apparatus in accordance with ASTM C1072. A total of eight tests were performed for each type of masonry. The results from the testing showed that the flexural bond strength of un-roughened, smooth faced WF-FA masonry units was approximately half of that determined for traditional masonry units. The masonry flexural bond testing and the apparatus used are illustrated in Figure 3.15. The results from the bond testing have been averaged and are summarized in Table 3.10.

(a) WF-FA Prism   (b) Clay Prism

Figure 3.15. Masonry Flexural Bond Test

Table 3.10. Masonry Flexural Bond Strength

Base Masonry Material	Flexural Bond Strength psi (kPa)
Clay Brick	60 (414)
Concrete Block (CMU)	55 (379)
Wood-Fiber Fly Ash Masonry Units (WF-FA)	35 (241)

4. TEST PROGRAM DEVELOPMENT

The following section presents the methodology behind the development of the research study presented in this paper. The selection of the materials used in the study, the two-phased approach to the research program, and the development of the test matrix are presented in this section of the paper.

The test program implemented for this study was developed from a previous study performed at UMR, which investigated the behavior of FRP strengthened arching walls subjected to blast loads (Carney and Myers, 2003). Carney and Myers found that the use of FRP retrofit systems can greatly enhance the out-of-plane capacity of non-slender partially framed infill walls, and more specifically, they found that the use of FRP surface laminates can reduce the amount of fragmentation of substrate material upon failure. Based upon these results, the experimental program presented in this paper was established.

This research program is specifically focused on the mitigation of damage to URM walls as a result of blast loads. Because of this, emphasis has been placed on increasing the energy absorption capability of URM walls and on reducing the debris scatter and fragmentation of the masonry material upon failure. Based upon the aforementioned criteria, two different strengthening materials were selected for investigation: a GFRP grid and a spray-on elastomeric polyurea. It was anticipated that when applied to the entire wall face, the use of the GFRP grid would not only significantly increase the load carrying capacity of the URM walls, but would also aid in the prevention of material fragmentation upon failure. The use of the grid over other forms of FRP was desirable because it allowed for a relatively small amount of

reinforcement material to be distributed over a large area both easily and efficiently. The use of elastomeric polyurea material to retrofit URM walls for the purpose of blast mitigation has been studied previously (Connell, 2002). Its use in blast applications seems desirable due to its proven ability to deform and absorb energy. However, additional benefits from the use of a spray-on polyurea system are that the URM walls require only minor surface preparation, and the polyurea material can be rapidly applied in a very short period of time.

The use of an alternative masonry material made primarily from wood-fibers and fly ash is also being investigated to evaluate the applicability of its use in new infill construction. Based upon previous research performed by Joshi and Myers (2006), the WF-FA material yielded promising results in terms of its energy absorption capabilities, which is a desirable trait when designing for blast. Additionally, because the material is made almost entirely from by-products, its use in modern construction could potentially be more cost effective than the use of traditional masonry materials for masonry construction.

The research program presented in this section has been divided into two phases of study. The first phase of the program, Phase 1, pertains to the investigation of retrofitting non-slender, partially framed URM infill walls to improve their out-of-plane behavior under blast loads. A total of eight walls constructed from three different substrate materials were tested in Phase 1. Five of the walls were constructed from clay brick units and concrete block to represent masonry that is typical of current infrastructure throughout the United States. The remaining three walls were constructed using units created from the WF-FA material. A single control wall constructed from

each type of masonry material was tested to establish a baseline to be used in evaluating the effectiveness of the retrofit strategies, as well as for comparison amongst the different masonry materials used to construct the URM walls. Two strengthening schemes were investigated in Phase 1 of the study: a spray-on polyurea retrofit that consisted of the polyurea material exclusively and a GFRP-polyurea retrofit system, which incorporated the use of the GFRP grid embedded within spray-on polyurea material. The walls in this phase of study were tested in the laboratory under quasi-static conditions by way of a uniformly distributed pressure. The uniform pressure was applied using an airbag system. Although blast loading cannot be replicated under static conditions, the use of the airbag loading system was selected because URM walls subjected to actual blast events would experience relatively uniform pressures acting on the wall face as a result of the blast. It should be noted that although this test methodology seems relevant when considering blast events, it in no way simulates the impulsive loading generated as a result of actual blast events.

The second phase of the experimental program, Phase 2, corresponds to the testing of what are often referred to as slender URM infill walls. The walls in this phase of the study had similar geometry to those in Phase 1, but were tested under four-point bending with no end restraints to represent infill walls whose behavior is unaffected by the presence of a surrounding frame. A total of seven walls were tested in Phase 2 of the experimental program. All of the walls in this phase of study were constructed from clay brick or concrete block. Although both previously mentioned retrofit schemes were investigated in Phase 2 of the experimental program, this phase of research was developed to focus primarily on the bond behavior between polyurea and base masonry

material. As a result, walls with and without the use of a simulated retrofit-anchored

condition were considered. No control walls were tested in Phase 2 of the program due

to their extremely low load capacities.

The developed test matrix for this research program incorporates both phases of

research and has been presented in Table 4.1. Walls corresponding to the first phase of

study have been characterized as Walls P1-1 to P1-8 where the prefix P1 pertains to

Phase 1. Walls pertaining to the second phase of the study have been characterized

Table 4.1. Test Matrix

Phase	Wall	Masonry	w_f	Anchorage	Retrofit Scheme		
					Control	Polyurea	GFRP
Phase 1	P1-1	Clay	-		√		
	P1-2	Clay	1.07			√	√
	P1-3	Concrete	-		√		
	P1-4	Concrete	0.04			√	
	P1-5	Concrete	0.93			√	√
	P1-6	WF-FA	-		√		
	P1-7	WF-FA	0.08			√	
	P1-8	WF-FA	1.89			√	√
Phase 2	P2-1	Clay	1.14	√		√	√
	P2-2	Clay	2.27	√		√	√
	P2-3	Concrete	0.05			√	
	P2-4	Concrete	1.01			√	√
	P2-5	Concrete	1.01	√		√	√
	P2-6	Concrete	2.02			√	√
	P2-7	Concrete	2.02	√		√	√

similarly from P2-1 to P2-7, where the prefix P2 corresponds to Phase 2. All of the walls

presented in Table 4.1 have been presented in terms of their respective reinforcement

indexes, w_f, which has been defined previously in Section 2 using Equation (5). It should

also be noted that the reinforcement index has been calculated using the gross

compressive strength of the masonry for the walls from both phases of study.

5. PHASE 1 – NON-SLENDER FRAMED INFILLS

The following section of the thesis presents the portion of the research study pertaining to non-slender, framed URM infill walls. A detailed presentation of the experimental program and test results are provided. The results from the testing are summarized, and the applicability of the URM wall strengthening methods and base masonry materials are discussed. Lastly, the development of an analytical model used to predict the load-capacity of non-slender URM infills at the ultimate limit-state is presented, and its validity is discussed.

5.1. EXPERIMENTAL PROGRAM

5.1.1. Wall Construction. The URM walls in Phase 1 of the experimental program were built by experienced masons from the Rolla Technical Institute (RTI) of Rolla, Missouri, and by the senior technical staff of the Center for Infrastructure and Engineering Studies (CIES) at UMR. The walls were constructed on top of RC beams, which would later serve as boundary elements during the testing of the Phase 1 walls. The concrete boundary elements were 7ft (2.13m) in length, had cross-sectional dimensions of 12 x 12in. (305 x 305mm), and were used to simulate the interaction of a concrete structural frame at the top and base of the wall. The RC boundary elements had square tubing inserts placed transversely in each end to coincide with a steel frame assembly that is used in the test setup for the walls in this phase of the program. The beams were reinforced with three #3 bars in the longitudinal direction at the top and bottom of the cross-section. Also, #3 stirrups were spaced at 14in. (356mm) on-center

(Carney, 2003). A schematic of the reinforcement layout for the beams is presented in

Figure 5.1.
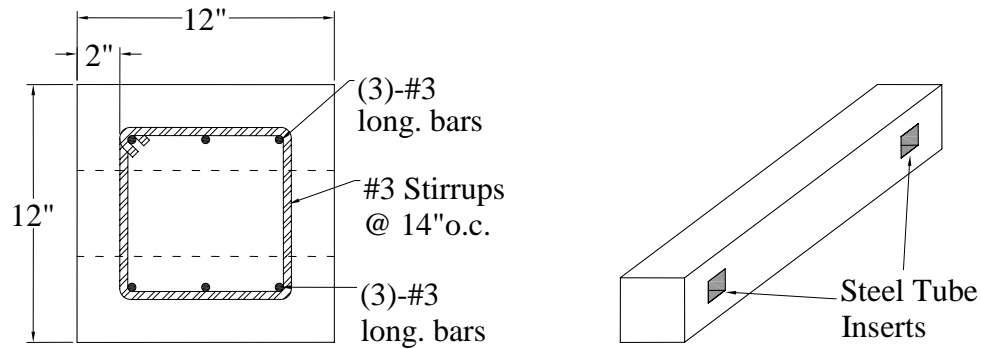
(a) Layout of Internal Reinforcement   (b) Isometric View of Boundary Element

Conversion: 1 in. = 25.4mm

Figure 5.1. Reinforced Concrete Boundary Elements

All of the walls in this phase of the program were constructed using a running

bond and had an approximate slenderness, or height-to-thickness ratio, equal to 13. The

walls were constructed using a Type-S mortar, and mortar joints were finished flush with

the surface of the masonry units. The walls were constructed with a uniform width of

36in. (914mm), but varied in height due to the variation in thickness of the masonry units.

Walls constructed from the clay brick or WF-FA brick units consisted of 12 courses and

were 36in. (914mm) in height. Walls constructed from the CMU block consisted of 6

courses and were 48in. (1219mm) in height. The construction of one of the WF-FA

masonry walls from Phase 1 of the experimental program is presented in Figure 5.2.

(a) Initial Bed Joint

(b) First Course

(c) Half Wall

(d) Completed Wall

Figure 5.2. Construction of WF-FA Phase 1 Wall

After wall construction was completed, a second RC beam was placed on top of

the wall using a 20ton (18,150kg) overhead crane to serve as the upper boundary element.

The walls were allowed to cure for a minimum of 14 days prior to placing the upper

boundary element. To ensure that the upper element was properly positioned during the

placement process, a steel frame assembly, which is used to anchor the boundary

elements during the wall testing, was semi-erected and used as a guide. The surrounding

steel frame assembly consisted of 3/8in. (9.5mm) structural steel tubing and #11 dywidag

rods. The steel tubing was small enough to slide inside of the inserts that were cast into

the RC beams during construction. The dywidag rods, along with a series of rigid steel plates, were used to join the upper and lower boundary elements and secure them into their final position. Once the upper boundary element was positioned, the gap between the top of the wall and the beam was adjusted to approximately 3/8in. (9.5mm). The process of lowering the upper boundary element into position is presented in Figure 5.3.
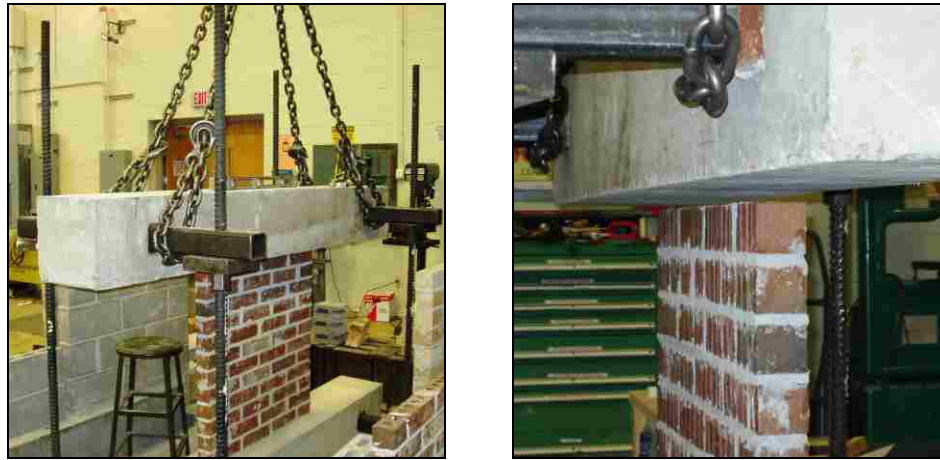
Figure 5.3. Placement of Upper Boundary Element

After the gap between the wall and the upper boundary element was properly adjusted, the beam was raised approximately 15in. (380mm), and mortar was placed on the top of the wall to form the final bed joint. The beam was lowered back into position and was left to cure. After 24 hours, wooden shoring was added to secure and stabilize the wall and beam assembly, and the steel frame was disassembled.

5.1.2. Strengthening Procedure. The strengthening procedure used for the walls in Phase 1 of the experimental program consisted of two different retrofit techniques. The walls were either retrofitted with the application of a GFRP grid embedded within and bonded to the wall surface using an elastomeric polyurea coating, or they were

retrofitted using only the spray-on polyurea material. The strengthening procedures used for both retrofit schemes were very similar.

Prior to the application of the strengthening material, the mortar joints of the walls were ground down smooth using a mason's stone, and all dust and debris was removed from the surface of the walls and boundary elements. The walls and surrounding frame elements were taped off, so only the front face of URM wall and a 2in. (51mm) strip on the upper and lower boundary elements would be exposed during the spray-on application of the polyurea elastomer. The overlap of material onto the boundary elements was done in an attempt to provide some level of wall anchorage to the surrounding frame by way of the polyurea. The taped off wall is shown in Figure 5.4.

(a) Face of URM Wall   (b) Lower Boundary Beam   (c) Upper Boundary Beam

Figure 5.4. Taped-off Wall

Before the walls were sprayed with the polyurea elastomer, an epoxy primer was applied to the wall surface as well as to the exposed portions of the concrete boundary elements. The use of the epoxy primer was done to prevent any reaction from occurring

between the applied polyurea and any free moisture within the base masonry material. The application of the primer material and the primed walls are shown in Figure 5.5.
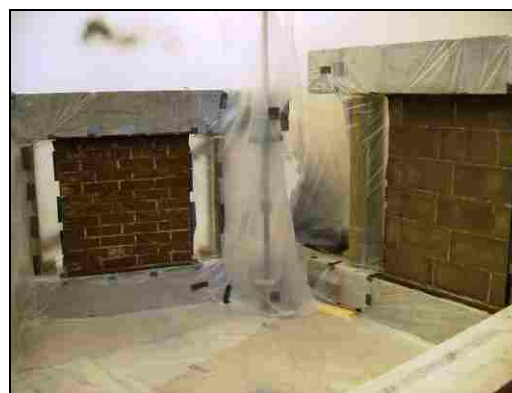
(a) Application of Primer   (b) Primed Walls

Figure 5.5. Primer Application of Phase 1 Walls

The primer was allowed to cure for approximately one hour prior to spraying the walls with the elastomeric polyurea material. For walls strictly undergoing the polyurea retrofit, a 1/8in. (3.2mm) layer of material was applied to face of the wall as well as to the exposed areas of the surrounding frame. For the walls that were retrofitted with the FRP grid embedded within the polyurea, a thin initial layer of polyurea was sprayed onto the walls prior to the application of the FRP grid. Immediately after the first layer of polyurea was sprayed onto the wall surface, the grid was embedded into the still-soft polyurea material using a heavy roller. The set-time for the polyurea was approximately 10 to 20 seconds; therefore, the application of the grids had to immediately follow the application of the polyurea. For the purpose of applying the FRP grids as quickly as possible, the grids were precut to match the width of the walls but were cut slightly

shorter than the wall height to avoid interference from the frame elements. Finally, a second application of polyurea was sprayed over the FRP until the surface became free of voids, and the FRP was fully embedded within the polyurea. The combination of the FRP and polyurea material resulted in an overall retrofit thickness of approximately 3/8in. (9.5mm). The spraying of the polyurea and the application of the FRP grids is presented in Figure 5.6. Additionally, a schematic of the two retrofit schemes used for the Phase 1 walls has peen provided for illustration in Figure 5.7.

(a) Primed URM Wall   (b) Application of Polyurea

(c) Embedding FRP Grid   (d) GFRP-Polyurea Retrofit

Figure 5.6. Strengthening Procedure for Phase 1 Walls

(a) Polyurea Retrofit   (b) FRP Grid - Polyurea Retrofit
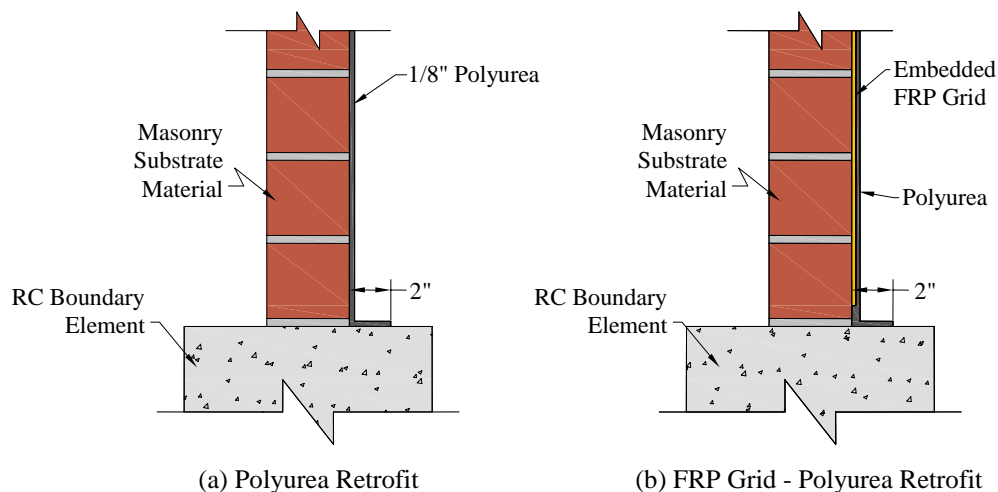
Figure 5.7. Retrofit Schemes for Phase 1 Walls

A test matrix for the Phase 1 walls has been provided in Table 5.1. The matrix provides a summary of the geometry and retrofit scheme used for each of the Phase 1 walls. The walls have been presented using the identification system established in Section 4.

Table 5.1. Test Matrix – Phase 1

Wall	Masonry	(h/t)	w_f	Retrofit Scheme		
				Control	Polyurea	GFRP
P1-1	Clay	13.1	-	√		
P1-2	Clay	13.1	1.07		√	√
P1-3	Concrete	13.2	-	√		
P1-4	Concrete	13.2	0.04		√	
P1-5	Concrete	13.2	0.93		√	√
P1-6	WF-FA	13.1	-	√		
P1-7	WF-FA	13.1	0.08		√	
P1-8	WF-FA	13.1	1.89		√	√

5.1.3. Test Setup and Testing Procedure. The wall tests for Phase 1 of the research program were performed in UMR's Structural Engineering Research Laboratory (SERL). The URM walls were constructed outside of the testing area and were later moved into place using a 20ton (18,150kg) overhead crane. To prevent any damage or cracking from occurring while moving the walls, the steel frame that was used during the placement of the upper boundary element was reassembled and used to apply a mild preload, causing the URM walls to be in a state of compression while being moved. After being transported to their final location, the applied compressive load was removed.

The test setup for this phase of the experimental program involved the bracing and anchoring of the upper and lower boundary elements in an effort to make them as rigid as possible throughout the duration of the test. In addition to the boundary element bracing, the airbag, which was used to apply the uniform load to URM walls, also required a stiff reaction structure that was capable of withstanding high pressure values and would undergo little or no deformation.

Once the URM wall was in its final position, the lower boundary element was anchored to a concrete strong floor through use of the threaded dywidag rods used in the steel frame assembly. A stiffened 1/2in. (13mm) steel plate was used as the reaction structure for the airbag system. The plate was stiffened using built-up WF-sections oriented in both the horizontal and vertical directions and is presented in Figure 5.8. The steel plate was lifted into position using the overhead crane and was supported at five locations, the four corners, and at center. The center of the plate was supported by an 8 x 8 x 3/8in. (203 x 203 x 10mm) structural steel tube that housed a dywidag rod assembly. The use of the dywidag assembly made the section adjustable in length. The center plate

support reacted directly against a 4ft (1.20m) thick concrete strong wall. The plate

supports used at each of the four corners were 6 x 6 x 1/4in. (152 x 152 x 6mm) built-up

rectangular sections. These members were shimmed into place using masonry units and

steel plates, which also reacted against the concrete strong wall.

Figure 5.8. Stiffened Plate Assembly

To effectively anchor the upper boundary element, restraints had to be provided in

both the vertical and horizontal directions. To prevent vertical translation from

occurring, 8 x 8 x 3/8in. (203 x 203 x 10mm) structural steel tubes were attached to the

steel frame assembly that was used to position the upper and lower boundary elements.

The horizontal translation was limited through the use of a pair of 12kip (53.4kN)

capacity chains. One end of the chains was wrapped around the upper boundary element

at each side of the URM wall, and the other end of each chain was wrapped around a

small steel beam built-up from stiffened C-sections. The steel beam was loosely attached

to a concrete strong wall using a dywidag rod assembly. This method of anchoring the chains allowed for the tension in the chains to be adjusted both prior to and during testing. The reaction system used for the chains is presented in Figure 5.9.

Figure 5.9. Chain Restraint System

The airbags used to apply the out-of-plane load to the URM walls were commercially available dunnage bags provided by International Paper's Ride Rite division. The airbags were capable of withstanding pressures greater than 20psi (138kPa) and were available in multiple sizes, allowing them to be matched to the face-dimensions of the walls tested in this study.

The airbag was placed between the stiffened reaction plate and the URM wall. The amount of space between the plate and the wall was not the same for each of the tests due to the variation in size of the masonry units that were used to construct the URM walls. However, it was found that a 2in. (51mm) gap between the wall and the reaction structure was optimal because it provided enough room to attach the airbag inflation

assembly, and it resulted in a relatively large coverage area of the URM wall when the airbag was inflated. In most cases, sheets of plywood were used to decrease the space between the reaction plate and the URM walls. The full test setup for the Phase 1 walls is illustrated in Figure 5.10 and Figure 5.11.
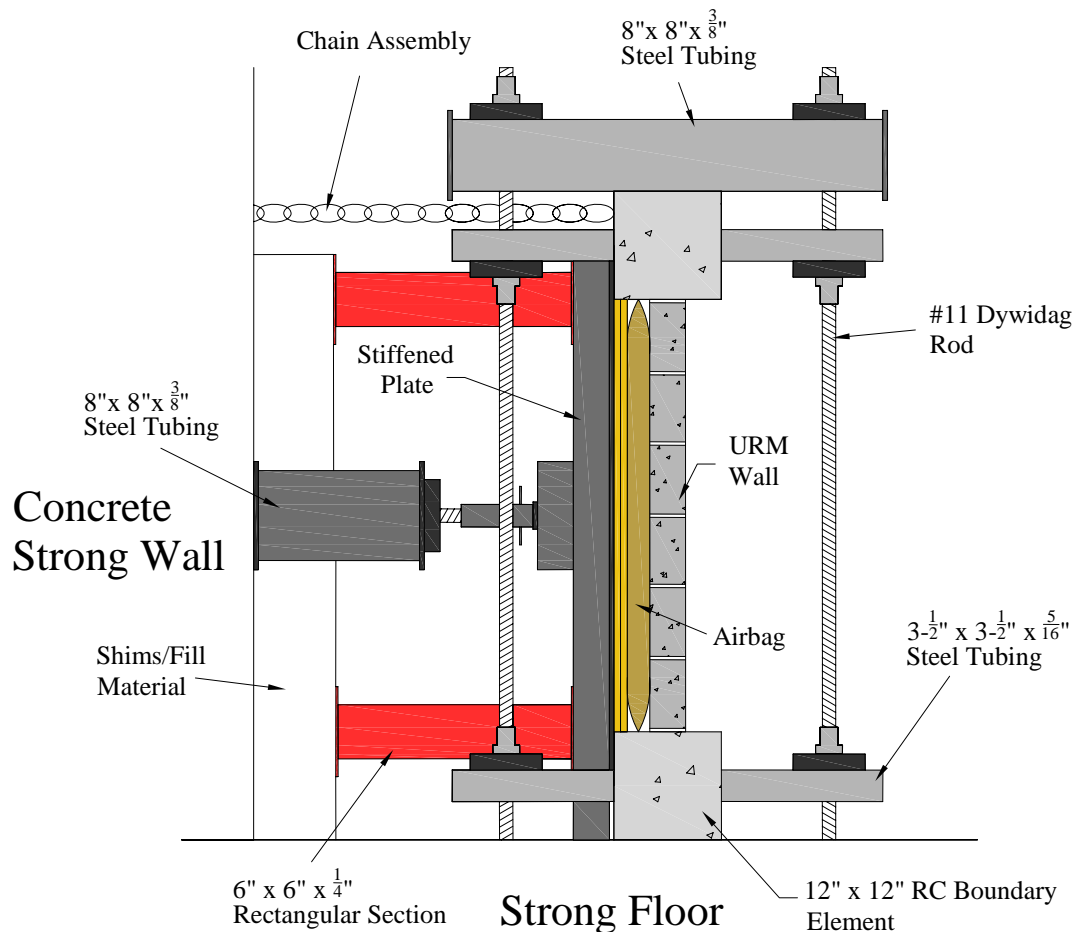
Conversion: 1 in. = 25.4mm

Figure 5.10. Schematic of Phase 1 Test Setup

For each of the Phase 1 walls, the deflection was measured at five locations along the vertical wall profile using a series of string transducers. The use of string transducers

Figure 5.11. Phase 1 Test Setup

allowed for the deflection to be accurately monitored throughout the full duration of the test. In addition to the string transducers, a single linear variable differential transformer (LVDT) was placed at the mid-height location in an attempt to observe and document the initial cracking of the walls. Although the system used to tighten the chains and restrain the upper boundary element was highly effective, it was not entirely capable of preventing horizontal translation from occurring. Therefore, a single LVDT was used to monitor the horizontal translation of the upper boundary element throughout the testing of the URM walls.

For each of the retrofitted walls, strain gage data were acquired along the vertical profile of the wall at five locations. For the walls strengthened with the GFRP-polyurea system, strain gages were applied directly to the FRP grids prior to embedding them within the polyurea. Walls retrofitted using only polyurea material had strain gages applied directly to the surface of the elastomeric coating. The locations of the string transducers, LVDTs, and the strain gages are presented in Figure 5.12.

The pressure in the airbag was monitored through the use of a 15psi (103kPa) pressure transducer as well as a standard 30psi (207kPa) dial pressure gage. Initially, both gages were used during the testing; however, in the event that the capacity of the strengthened URM walls exceeded 15psi (103kPa), the pressure transducer could be disconnected and pressure data recorded explicitly from the use of the dial pressure gage. Two hoses were connected to the inflation chuck of the airbag. One hose was used to supply air to the bag, and one hose was used to connect the pressure gages which monitored the pressure within the airbag. A pressure regulator was connected in-line with the hose that was supplying air to the bag, which allowed the rate of airbag inflation and deflation to be controlled.

    (a) Vertical Profile Instrumentation   (b) Boundary Element Translation

Figure 5.12. Phase 1 Instrumentation

The testing procedure used for each of the walls in this phase of the experimental program was rather simple because all of the data were recorded through the use of a data

acquisition system (DAS), and the testing was performed using a single cycle. The deflection data, strain data, and airbag pressure data were sampled at a rate of 2Hz. The airbag was initially inflated until the bag was in contact with the wall and was then allowed to inflate at a constant rate, which initially corresponded to a rate of 1.0psi/min (6.90kPa/min). However, as the walls underwent larger deflections the rate of inflation was kept constant, and the loading rate decreased significantly. For each of the walls, the testing was paused when the pressure in the airbag reached a value of 1.0psi (6.90kPa). At this point, the airbag coverage area was marked using spray paint, and the data acquired were checked to ensure that the data acquisition system and all of the instrumentation were functioning properly. After the initial marking of the airbag coverage area, load was applied until failure of the wall occurred. For walls that underwent extreme deflections, the airbag coverage area decreased significantly throughout the duration of the test, and it was necessary to mark the coverage area a second time immediately prior to failure.

5.2. TEST RESULTS

The following section presents the results from the testing of the Phase 1 walls. For each of the walls tested, a brief description of the behavior of the walls up to the point of failure, of the mode of failure, and of the fragmentation has been provided. In addition to the observed behavior of the walls, the load-deflection response for each wall has also been included in this section of the thesis to further illustrate the behavior of the walls. It should be noted that each of the plots presented in this section of the thesis presents two load-deflection relationships, a measured response, and an adjusted

response. Due to deficiencies in the airbag loading system and non-rigidity of the upper framing elements, it was necessary to adjust the measured response of the Phase 1 walls to allow for further comparison of the results. The methodology used to adjust the response is presented for clarification in Section 5.3. References to noted pressures and deflections observed during testing have been made with regard to the measured response values only. Additionally, plots of the load versus strain behavior and the deflected wall shapes can be found in Appendix A.

5.2.1. Wall P1-1. Wall P1-1 was the clay control specimen. At an applied pressure of 0.8psi (5.5kPa), the first crack was visible on the pressure applied face of the wall in the bed-joint at the lower boundary element location. At a pressure value of 1.9psi (13.1kPa), a major horizontal crack began developing one course above the mid-height location on the exposed face of the wall, and visible rigid body deformation was observed (see Figure 5.13). As the formation of the arch progressed, the mid-height crack grew along the full length of the bed-joint and continued to open. Wall P1-1 reached a peak airbag pressure value of 4.6psi (31.7kPa) at a deflection of 0.62in. (15.7mm) before the behavior of the wall became unstable and the pressure resistance began to drop, as shown in Figure 5.14. Ultimately, the pressure resistance decreased to a value of 3.6psi (24.8kPa), and the wall collapsed. The clay control wall achieved a maximum deflection value of 1.10in. (28.0mm). The debris scatter and poor resistance to fragmentation of the base masonry material can be seen in Figure 5.13b. In examining the masonry units of Wall P1-1, it was found that only minor crushing had occurred in the mortar of the bed-joints at the mid-height and boundary location. The wall ultimately failed due to instability.

(a) Horizontal Crack   (b) Wall Collapse

Figure 5.13. Wall P1-1 Failure
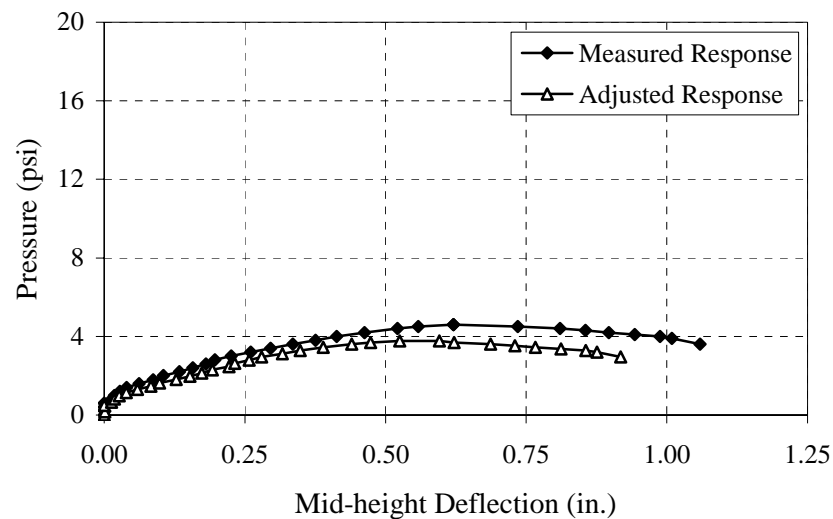
Conversions: 1 psi = 6.895 kPa; 1 in. = 25.4 mm

Figure 5.14. Load-Deflection Behavior – Wall P1-1

5.2.2. Wall P1-2. This wall was a clay wall specimen strengthened with the GFRP-polyurea retrofit. Due to the stiffness of the masonry and the high level of reinforcement of this specimen, the ultimate capacity of Wall P1-2 was not achievable using the airbag system. Therefore, the wall was initially loaded using an airbag, but upon reaching the capacity of this system, was loaded using a hydraulic jack. The first

cracks in Wall P1-2 occurred at an airbag pressure value of 1.2psi (8.3kPa) and were found to occur in the bed-joint at the location of the upper boundary element. Loading continued until a peak applied pressure value of 23.0psi (158.6kPa) and deflection of 0.55in. (14.0mm) was reached, and the airbag system failed. Up to this point of the test, significant wall sliding was found to occur, and only hair-line cracks at the mid-height location were observed. To load the wall to failure, a line-load across the width of the wall at the mid-height location was applied using a hydraulic jack. The load imposed on the wall from the jack has been expressed as an equivalent uniform face pressure, which would induce the same mid-height moment as that of the force value applied using the jack. The wall reached an equivalent airbag pressure value of 29.5psi (203.4kPa) at a deflection of 0.64in. (12.3mm). At this point, flexural-shear cracks began to form from the point of load application, and the load resistance of the wall began to decrease (see Figure 5.15). Ultimately, the wall failed at an equivalent uniform pressure value of 21.6psi (148.9kPa) and a deflection of 1.12in. (28.5mm). The load resistance behavior of Wall P1-2 expressed as an equivalent uniform pressure is presented in Figure 5.16.

(a) Modified Loading System   (b) Flexural-Shear Cracks

Figure 5.15. Wall P1-2 Failure

(c) Wall Failure

Figure 5.15 (continued). Wall P1-2 Failure
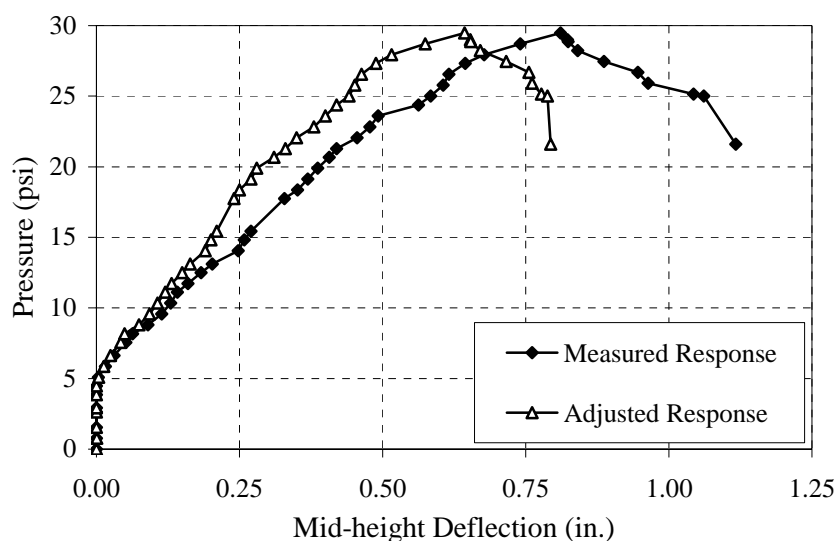
Conversions: 1 psi = 6.895 kPa; 1 in. = 25.4 mm

Figure 5.16. Load-Deflection Behavior – Wall P1-2

5.2.3. Wall P1-3. Wall P1-3 was the CMU control wall. This wall behaved similarly to Wall P1-1, the clay control wall. At a value of 0.8psi (5.5kPa), cracking in the bed-joints of both boundary elements was found to occur. As the applied pressure increased to a value of 2.1psi (14.5kPa), a horizontal crack began to develop in the bed-

joint one course above the mid-height location, as illustrated in Figure 5.17. Once the crack developed over the full-width of the bed-joint, the upper and lower segments of the wall began to rotate as rigid elements, and the cracks at the boundary locations and mid-height continued to grow in width. Wall P1-3 reached a peak pressure value of 5.9psi (40.7kPa) at a deflection of 0.75in. (19.1mm). Once reaching the peak pressure value, the mortar from the top bed-joint began to crush, and the load resistance began to decrease as shown in Figure 5.18. The wall collapsed at an applied pressure value of 4.0psi (27.6kPa) and a mid-height deflection value of 1.08in. (27.4mm). As illustrated in Figure 5.17c, the wall had little resistance to fragmentation.

(a) Horizontal Cracking   (b) Rigid-Body Behavior   (c) Debris Scatter
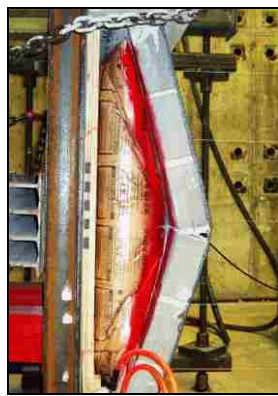
Figure 5.17. Wall P1-3 Failure

5.2.4. Wall P1-4. This wall was constructed from CMUs and was strengthened with the polyurea retrofit. The initial cracking of this wall occurred in the bed-joints at the boundary locations and was followed almost immediately by cracking at the mid-height location. The mid-height cracking occurred at a pressure value of 1.3psi (9.0kPa).
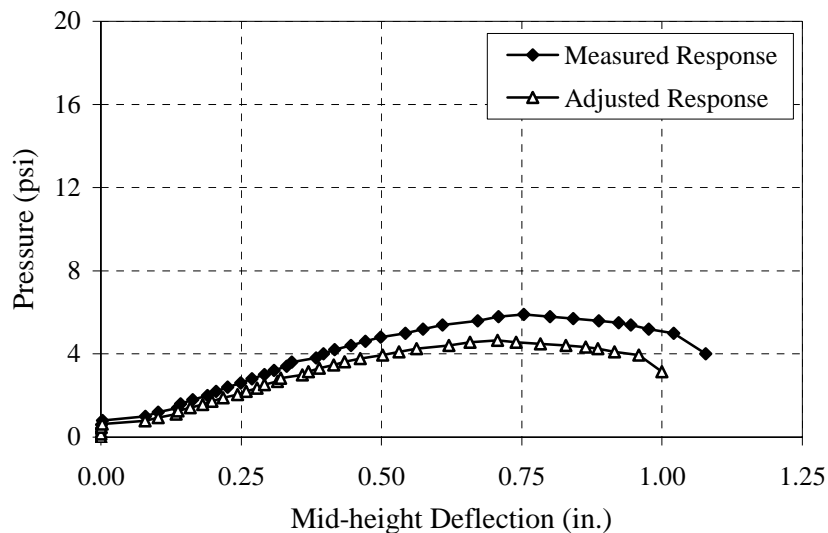
Conversions: 1 psi = 6.895 kPa; 1 in. = 25.4 mm

Figure 5.18. Load-Deflection Behavior – Wall P1-3

The peak pressure applied to this wall was 8.1psi (55.8kPa), which occurred at a deflection of 0.81in. (20.6mm). Beyond the peak, the load resistance began to decrease, and the upper and lower segments of the wall continued to deform as rigid bodies undergoing very large deflections as shown in Figure 5.19. The reduction in the pressure resistance slowly decreased until a resisting pressure of 1.07psi (7.4kPa) and a deflection of 4.03in. (96.5mm) were reached. The wall maintained this pressure until failure occurred due to rupture of the polyurea at mid-height, as shown in Figure 5.19b. The maximum mid-height deflection achieved by Wall P1-4 was 8.57in. (217.7mm). The load resistance behavior of this wall is presented in Figure 5.20. The failure behavior of the wall is presented in Figure 5.19c, and it can be seen that even after partial collapse of the URM wall, the polyurea remained bonded to the surrounding frame and prevented fragmentation of the base masonry material from occurring.
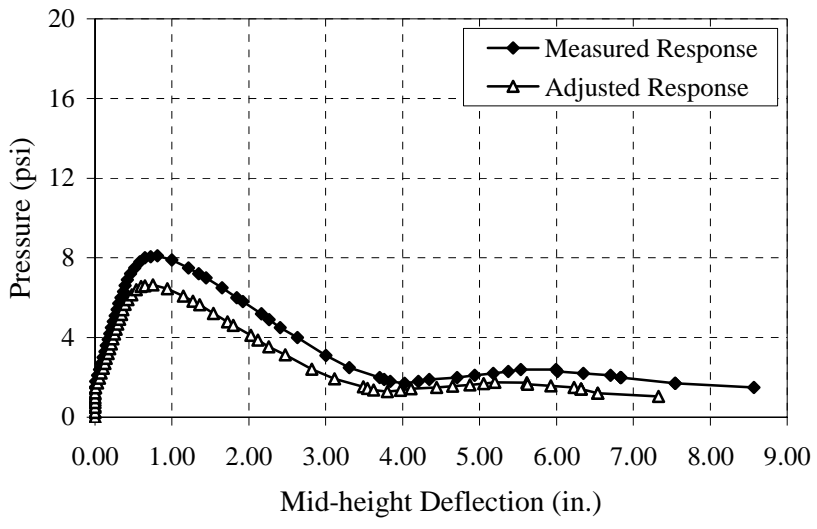
(a) Rigid-Body Deformation

(b) Rupture of Polyurea

(c) Wall Failure

Figure 5.19. Wall P1-4 Failure

Conversions: 1 psi = 6.895 kPa; 1 in. = 25.4 mm

Figure 5.20. Load-Deflection Behavior – Wall P1-4

5.2.5. Wall P1-5. This wall was constructed from concrete block and was strengthened using the GFRP-polyurea retrofit. Initially, cracks formed in the bed-joints of the upper and lower boundaries at a value of 1.4psi (9.7kPa). At 13.0psi (89.6kPa), the initiation of debonding of the polyurea material from the surrounding frame elements was observed. The debonding slowly progressed until the overlap of polyurea material fully debonded from the boundary elements on one side of the wall, forcing the wall into a form of negative bending about the vertical axis (see Figure 5.21). The wall failure occurred immediately after the polyurea debonded at an airbag pressure value of 14.3psi (98.6kPa) and a mid-height deflection value of 0.87in. (22.1mm). Prior to failure, no visible horizontal cracks were observed on the exposed face of the wall. Because the wall remained partially bonded to the surrounding frame elements, no fragmentation or debris from the substrate material resulted from the wall failure. Further investigation of the failed wall showed that no crushing had occurred in the CMUs, and only minimal crushing had occurred in the mortar of the bed-joints at the location of the boundary elements. The load-deflection behavior is illustrated in Figure 5.22.
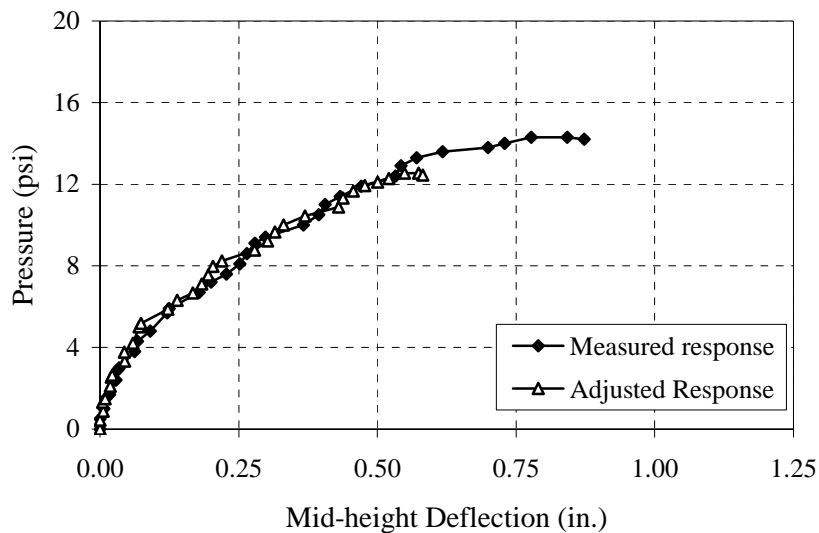

(a) Bending About Vertical Axis   (b) Debonding of Polyurea

Figure 5.21. Wall P1-5 Failure

Conversions: 1 psi = 6.895 kPa; 1 in. = 25.4 mm

Figure 5.22. Load-Deflection Behavior – Wall P1-5

5.2.6. Wall P1-6. Wall P1-6 was a control wall constructed from the WF-FA brick units. This wall cracked in the bed-joints at the boundary element locations almost immediately after loading was initiated. At an applied pressure of 1.6psi (11.0kPa), the first major horizontal crack began developing one course below the mid-height location, on the exposed face of the wall. At 3.5psi (24.1kPa), a second major horizontal crack formed in the bed-joint located one course above the mid-height location. As the test progressed, the horizontal crack below mid-height appeared to stop developing, and the width of the horizontal crack immediately above the mid-height location continued to grow as can be seen in Figure 5.23. The deflected shape of the wall was much less rigid than that of the clay and CMU control wall, and did not demonstrate the formation of a visible arching mechanism. This result can possibly be partially attributed to the poor bond behavior between the mortar and the smooth-faced WF-FA masonry units. Wall P1-6 reached a peak airbag pressure value of 5.2psi (35.9kPa) at a deflection of 0.96in.

(24.4mm). After reaching the peak pressure, the wall maintained this resistance value and continued to deform with little decrease in pressure resistance until immediately prior to collapse, as illustrated in Figure 5.24. The maximum value of mid-height deflection obtained by Wall P1-6 was found to be 1.22in. (31.0mm). It can be seen from Figure 5.23b that the wall had no resistance in preventing the debris scatter of the masonry upon failure. From examination of the WF-FA brick units after failure, it was found that crushing had occurred in the units at the mid-height location as well as at the location of the lower boundary element. The damage to the WF-FA brick units due to the crushing at the hinge locations is presented in Figure 5.23c.
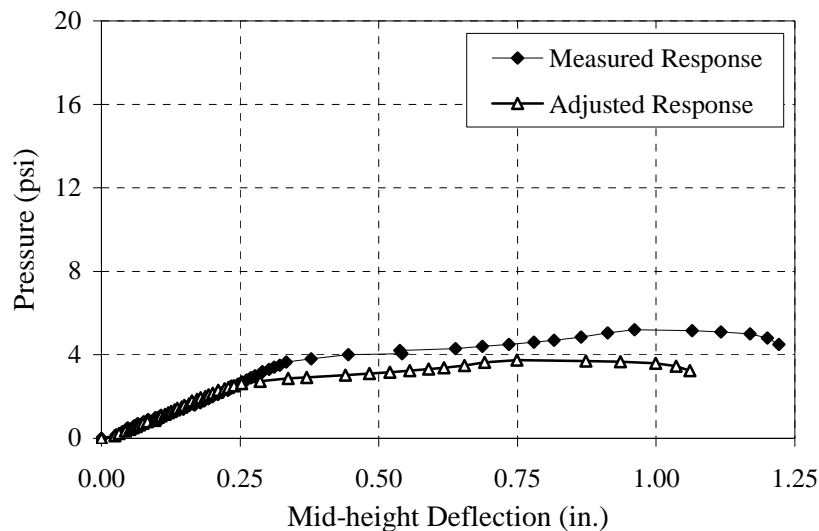

(a) Horizontal Cracking   (b) Scatter of Debris

(c) Crushing of WF-FA Brick Units
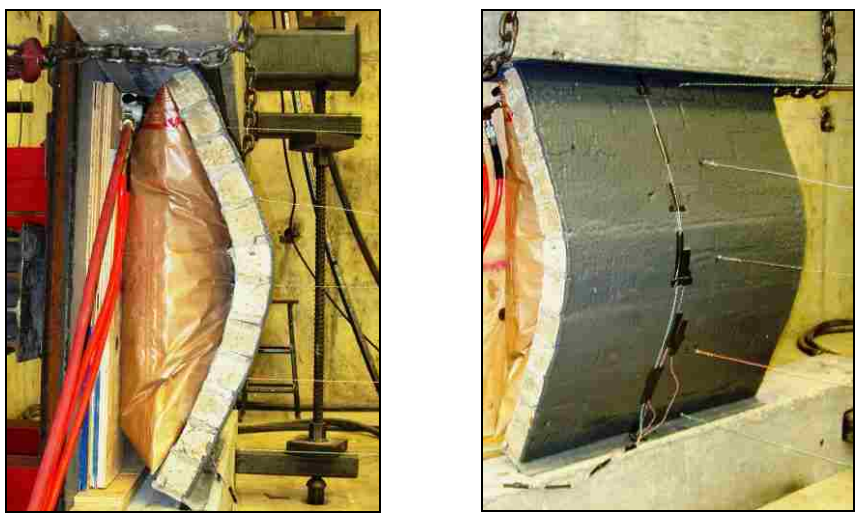
Figure 5.23. Wall P1-6 Failure

Conversions: 1 psi = 6.895 kPa; 1 in. = 25.4 mm

Figure 5.24. Load-Deflection Behavior – Wall P1-6

5.2.7. Wall P1-7. This wall was the second of two walls strengthened with the polyurea retrofit, and it was constructed from WF-FA brick units.   Wall P1-7 showed similar behavior to Wall P1-6 in that the wall did not appear to undergo rigid-body deformation, but rather deformed in more of a parabolic manner. At 3.8psi (26.2kPa), horizontal cracks formed in the bed-joint at the mid-height location, and at 4.5psi (31.0kPa), flexural cracks began developing in the WF-FA brick units at the mid-height location. The peak load resistance occurred at a measured pressure value equal to 5.7psi (39.3kPa) and a corresponding deflection of 0.69in. (17.5mm). Beyond the peak resistance, the behavior seemed to match that of Wall P1-4, the polyurea retrofitted CMU wall. The load resistance decreased at a fast rate, and the wall underwent very large deflections. The decrease in the pressure resistance stopped upon reaching a value of 2.5psi (17.2kPa) with a mid-height deflection of 2.85in. (72.4mm). As the wall continued to deform, large cracks formed at the mid-height location in the WF-FA units

as well as the bed-joints (see Figure 5.25). The load resistance remained relatively

constant until failure occurred in the polyurea at the location of the lower boundary

element. The failure of the wall has been presented in Figure 5.25c, and the load

resistance behavior is illustrated in Figure 5.26. The maximum measured mid-height

deflection achieved by the wall was 6.90in. (175.3mm).
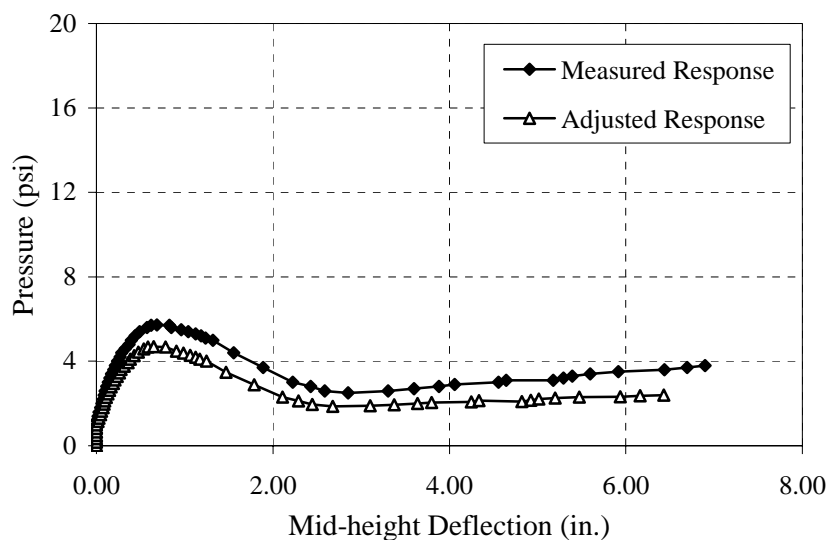

(a) Deformed Shape

(b) Flexural Cracks in WF-FA   (c) Failure

Figure 5.25. Wall P1-7 Failure

Conversions: 1 psi = 6.895 kPa; 1 in. = 25.4 mm

Figure 5.26. Load-Deflection Behavior – Wall P1-7

5.2.8. Wall P1-8. This wall was constructed from WF-FA brick units and was strengthened with the GFRP-polyurea retrofit. The behavior of this wall was similar to that of the previously discussed walls with the GFRP-polyurea retrofit (Walls P1-2 and P1-5). Initially, cracks formed in the bed-joints at the boundary locations, and only minor horizontal cracks at the mid-height location were observed prior to failure. Wall P1-8 reached a peak measured pressure of 18.1psi (124.8kPa), which corresponded to a mid-height deflection value of 0.70in. (17.8mm). Immediately after reaching these peak values, the bond between the polyurea and the upper boundary element failed, and the wall collapsed (see Figure 5.27). The maximum deflection achieved by Wall P1-8 prior to collapse was found to be 0.85in. (21.6mm). The sudden failure behavior is illustrated in Figure 5.28. Figure 5.27a shows that although the wall collapsed and did not remain suspended to the frame as the previously discussed retrofitted walls had, only minor separation between the polyurea and the base masonry material had occurred. Upon

further inspection, it was also found that the units at the boundary locations had sustained

damage due to a combination of shearing forces and membrane forces (see Figure 5.27b).
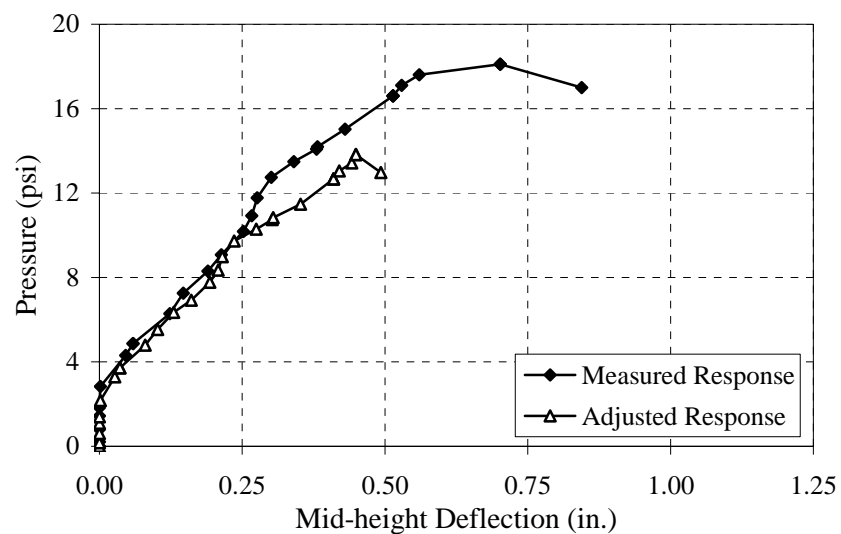

(a) Wall Collapse   (b) Damage Sustained to WF-FA Units

Figure 5.27. Wall P1-8 Failure

Conversions: 1 psi = 6.895 kPa; 1 in. = 25.4 mm

Figure 5.28. Load-Deflection Behavior – Wall P1-8

5.3. DISCUSSION

The following section provides discussion on the previously presented test results from Phase 1 of the research program. A brief discussion regarding the necessity and methodology of adjusting the laboratory measured response of the URM walls is addressed in this section of the thesis. Also, a detailed discussion of the influence of the strengthening systems and the influence of the base masonry material on the overall wall behavior has been provided.

5.3.1. Adjustment of Measured Response. As illustrated in the presentation of the Phase 1 test results, it was necessary to adjust the measured response of the URM walls to account for deficiencies in the airbag loading system and the lack of rigidity in the surrounding frame elements. The following outlines the methodology used to adjust the measured airbag pressures and the mid-height wall deflections.

5.3.1.1. Equivalent uniform pressures. The walls tested in Phase 1 of the experimental program were tested using an airbag system that was not capable of applying pressure to the entire face of the walls; therefore, it was necessary to determine an equivalent uniform pressure. The equivalent uniform pressure was developed from the theoretical mid-height moment applied to the walls, evaluated from the actual airbag coverage area and the pressure measured in the airbag system. Because the geometry as well as the behavior was unique for each of the walls tested, it was necessary to determine unique pressure adjustment factors for each of the walls in this phase of the testing program.

The coverage capability of the airbags was measured by spraying paint onto the exposed airbag surface throughout the testing of the walls. This method provided a

means of determining the change in the coverage area as the wall deformed. Using this method, it was determined that the use of a single pressure adjustment factor was suitable throughout the duration of the testing for both the FRP strengthened and the unstrengthened URM walls. However, for URM walls strengthened with the polyurea only, it was necessary to determine a variable pressure adjustment factor that would account for the large changes in airbag coverage that occurred over the course of the testing due to large wall deformation. The methodology used to calculate the pressure adjustment factors and the equivalent uniform pressure values are developed in the following section.

The shear force, V, acting on the wall has been expressed in terms of the partial uniformly distributed load, w, that is acting on the wall:

$$V = \left(\frac{h}{2} - \frac{(v_{g1} + v_{g2})}{2} \right) w = Dw \tag{7}$$

where v_{g1} and v_{g2} represent the areas at the top and bottom boundaries of the wall that the airbag was not capable of covering. For simplification, the values inside the parenthesis of Equation (7) have been set equal to the constant 'D'. From equilibrium, the mid-height moment acting on the wall can be determined using Equation (8):

$$M = V \left[\frac{h}{2} - \frac{1}{2} \left(\frac{h}{2} - \frac{v_{g1} + v_{g2}}{2} \right) \right] = \frac{Dw}{2} (h - D) \tag{8}$$

The total moment resulting from a perfectly uniformly distributed load acting on the entire face of the wall has been denoted as M_{udl} and is determined from the following:

$$M_{udl} = \frac{w_{udl}h^2}{8} \tag{9}$$

By setting Equations (8) and (9) equal to each other, a relationship between the partial uniformly distributed load and the perfectly uniformly distributed load can be established:

$$M = M_{udl} \Rightarrow \frac{Dw}{2}(h-D) = \frac{w_{udl}h^2}{8} \tag{10}$$

$$w_{udl} = \frac{8Dw}{2h^2}(h-D) \tag{11}$$

In addition to the gaps in airbag coverage at the top and bottom boundaries, it is also necessary to account for the sides of the URM walls that were left unloaded during the testing. The uniform distributed load that is acting on the wall can simply be determined by multiplying the applied pressure by the width of the wall that the airbag is effectively loading. This relationship is expressed in Equation (12):

$$w = \left[b_m - h_{g1} + h_{g2} \right] p_{applied} \tag{12}$$

where h_{g1} and h_{g2} are the coverage gaps on each side of the wall, and $p_{applied}$ is the pressure applied by the airbag system. The same relationship can be used to express the case of a perfectly uniform applied pressure over the entire face of the wall:

$$w_{udl} = b_m p_{uniform} \tag{13}$$

Using the established relationship in Equation (11) and substituting it into Equation (13), the following relationship between the uniformly distributed pressure, $p_{uniform}$, and the only partially applied line load acting on the wall can be developed:

$$p_{uniform} = \frac{w_{udl}}{b_m} = \frac{8Dw}{2b_m h^2}(h-D) \tag{14}$$

Equation (14) can be simplified further, so it is entirely in terms of airbag coverage, wall geometry, and applied pressure by replacing 'w' with the relationship defined in Equation (12). The final expression for the equivalent uniform pressure as a function of the applied pressure measured from the airbag system is expressed using Equation (15):

$$p_{uniform} = \frac{8Dp_{applied}}{2b_m h^2}(h-D)\left(b_m - h_{g1} - h_{g2}\right) \tag{15}$$

This expression can also be expressed in the following manner where (PAF) represents the pressure adjustment factor:

$$p_{uniform} = (PAF) p_{applied} \tag{16}$$

Finally, the PAF can be calculated independently of the applied pressure using Equation (17):

$$(PAF) = \frac{8D}{2b_m h^2}(h - D)(b_m - h_{g1} - h_{g2}) \tag{17}$$

Using Equation (17), it was then possible to determine unique pressure adjustment factors for each of the eight walls tested in Phase 1 of the experimental program. In the case of the walls strengthened with the polyurea retrofit, the airbag coverage area was marked at two points over the course of testing. An initial airbag coverage area was marked during the pre-peak loading branch, and this coverage area was assumed to remain constant until the peak pressure was reached. The second measurement was taken late in the test, as close to the point of failure as possible. Using the two markings on the airbag, it was assumed that the coverage area would decrease in a relatively linear trend between the point of the peak pressure and the point of failure. As a result, the PAF applied for the walls with the polyurea retrofit was constant up to the point of the peak pressure and decreased linearly to the point of failure. The relationship between the

pressure adjustment factor and the load resistance for one of the polyurea retrofitted walls
is shown in Figure 5.29.
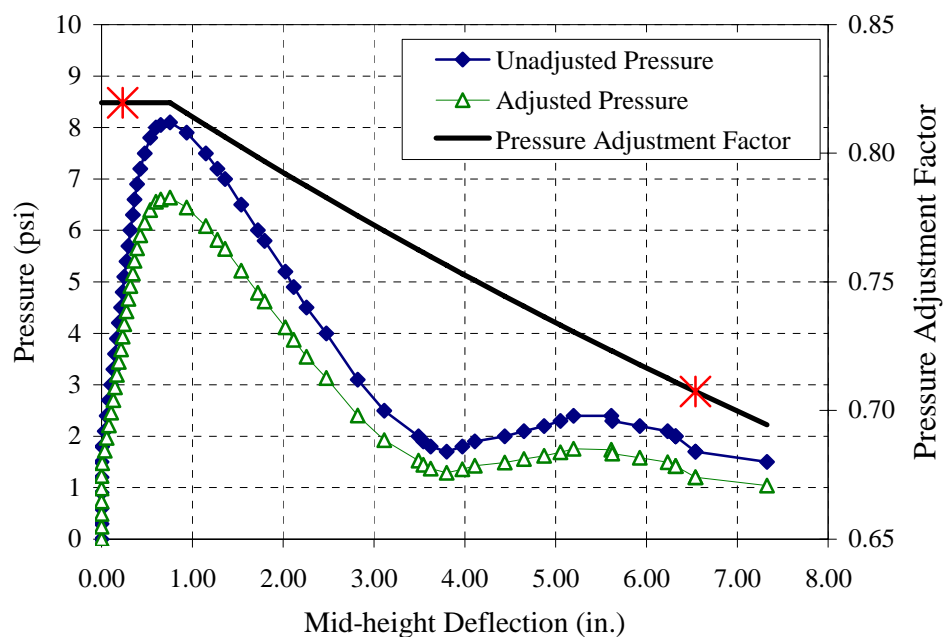
Note: X denotes the point at which the airbag coverage area was marked

Conversions: 1 psi = 6.895 kPa; 1 in. = 25.4 mm

Figure 5.29. Application of the Pressure Adjustment Factor (PAF)

5.3.1.2. Adjusted mid-height deflections. Due to translation of the upper
boundary element and horizontal wall sliding that occurred during the testing of the
Phase 1 walls, it was necessary to adjust the mid-height deflections. The purpose of this
adjustment is to prevent over estimation of the walls' ability to deform and absorb energy
that would be caused by the lack of rigidity in the surrounding frame elements. A simple
schematic has been provided in Figure 5.30 to illustrate the representation of the adjusted
mid-height deflection.

This method of adjusting the mid-height deflection values is applicable in
determining the energy absorption capabilities of the URM wall only. The adjusted
deflections do not account for any deformation or energy absorption from the interaction
of the wall and the surrounding frame.
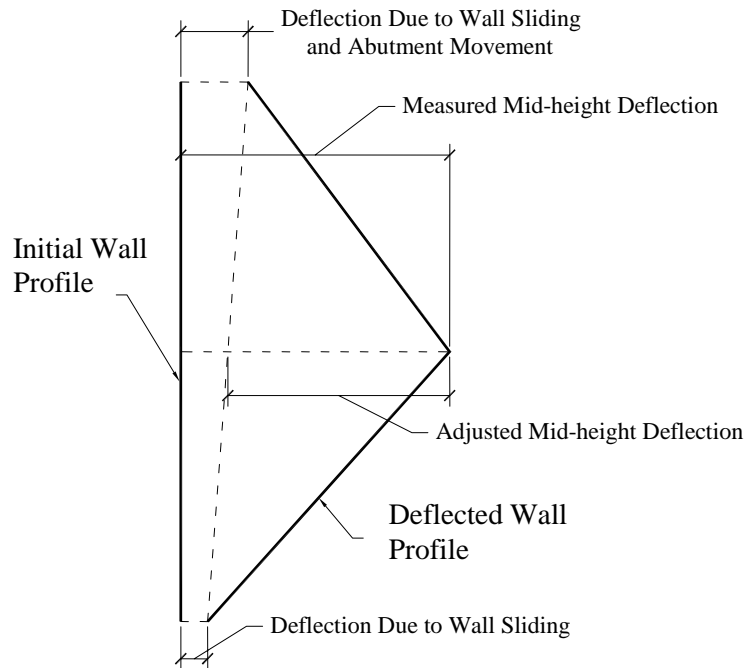
Figure 5.30. Adjusted Mid-height Deflection

A summary of the equivalent uniform peak pressures and the adjustments made to
the ultimate mid-height deflections have been presented in Table 5.2. It can be seen that
the pressure results for Wall P1-2 appear to be much larger than all other Phase 1 walls.
This is most likely due to the alternate testing method used to fail Wall P1-2. The
remainder of the discussion pertaining to the URM walls from Phase 1 of this study is
with reference to the adjusted load-deflection response.

Table 5.2. Adjusted Response Values – Phase 1 Walls

| Wall	Base Masonry (Retrofit Scheme)	Measured Peak Experimental Pressure psi (kPa)	Peak Equivalent Uniform Pressure psi (kPa)	Measured Ultimate Mid-height Deflection in. (mm)	Adjusted Ultimate Mid-height Deflection in. (mm)
P1-1	Clay (Control)	4.6 (31.7)	3.8 (26.2)	1.10 (28.0)	0.92 (23.4)
P1-2	Clay (GFRP-Polyurea)	*29.5 *(203.4)	29.5 (203.4)	1.12 (28.5)	0.80 (20.3)
P1-3	Concrete (Control)	5.9 (40.7)	4.7 (32.4)	1.08 (27.4)	1.00 (25.4)
P1-4	Concrete (Polyurea)	8.1 (55.8)	6.6 (45.5)	8.57 (217.7)	7.33 (186.2)
P1-5	Concrete (GFRP-Polyurea)	14.3 (98.6)	12.5 (86.2)	0.87 (22.1)	0.58 (14.7)
P1-6	WF-FA (Control)	5.2 (35.9)	3.7 (25.5)	1.22 (31.0)	1.06 (26.9)
P1-7	WF-FA (Polyurea)	5.7 (39.3)	4.7 (32.4)	6.90 (175.3)	6.43 (163.3)
P1-8	WF-FA (GFRP-Polyurea)	18.1 (124.8)	13.8 (95.1)	0.85 (21.6)	0.49 (12.5)

* Theoretical pressure from mid-height point load.

5.3.2. Influence of Retrofit Scheme. It can be seen from the presented test

results that both retrofit systems used in Phase 1 of the research program significantly

affected the behavior of the URM walls. For the purpose of comparing the two

strengthening methods, the load-deflection behavior for all walls in this phase of study

has been summarized with the use of three plots, shown in Figures 5.31 through 5.33.

Figure 5.31 pertains to the walls constructed from clay units, Figure 5.32 pertains to walls

constructed from the concrete block, and Figure 5.33 presents the load-deflection

behavior of the walls constructed from WF-FA masonry material.
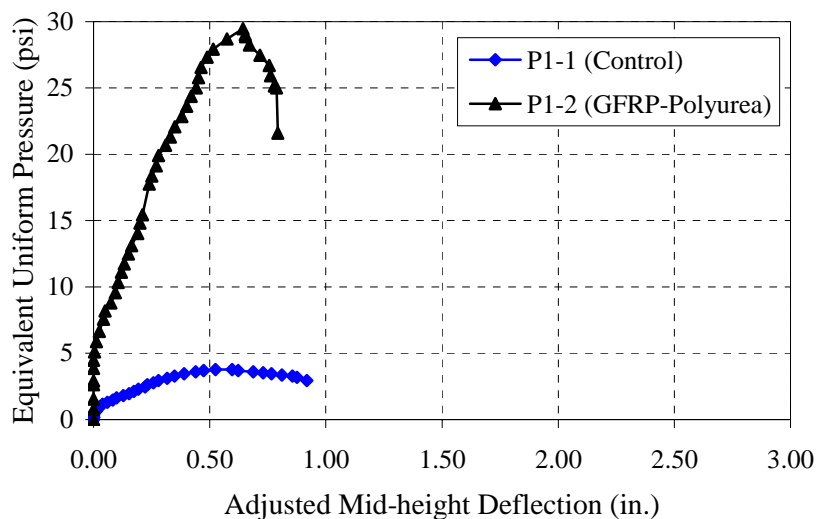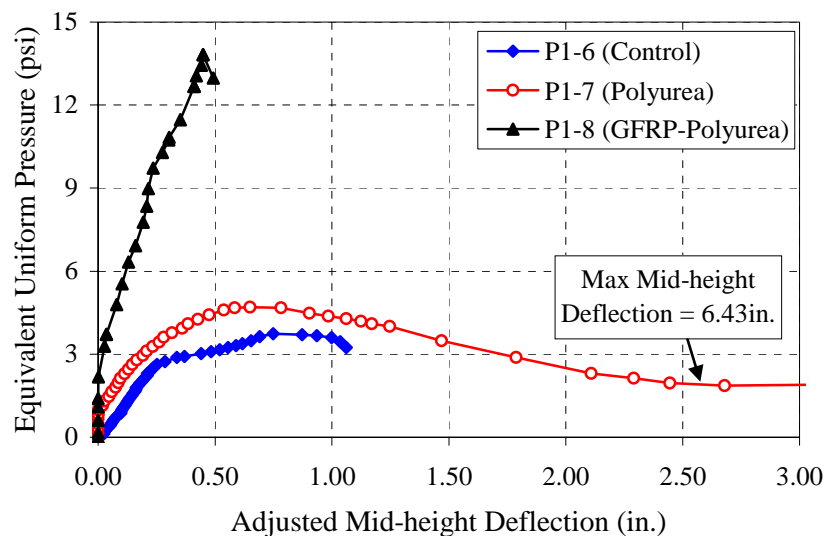

Conversions: 1 psi = 6.895 kPa; 1 in. = 25.4 mm

Figure 5.31. Load-Deflection: Clay Masonry Phase 1 Walls
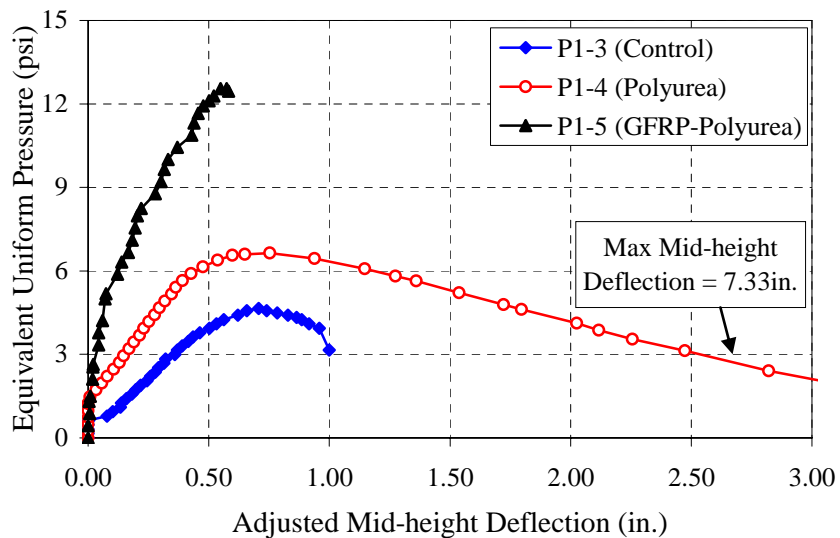
Conversions: 1 psi = 6.895 kPa; 1 in. = 25.4 mm

Figure 5.32. Load-Deflection: CMU Masonry Phase 1 Walls

Conversions: 1 psi = 6.895 kPa; 1 in. = 25.4 mm

Figure 5.33. Load-Deflection: WF-FA Masonry Phase 1 Walls

The retrofit system consisting of only spray-on polyurea material was

implemented for two of the walls in this phase of the study, Walls P1-4 and P1-7. This

retrofit method had little effect on the stiffness of the walls but was successful in adding

stability to the system, which aided in the formation of the arching mechanism. The

additional stability allowed the URM walls to further develop in-plane membrane forces

created as a result of the arching action, leading to modest increases in the out-of-plane

capacity. In comparison to the control walls, the use of the polyurea retrofit resulted in

an out-of-plane capacity increase of 40 percent for Wall P1-4 and 27 percent for Wall P1-

7. The most significant effect on wall behavior as a result of the polyurea retrofit was the

large increase in the energy absorption capability of the walls. It can be seen from the

load-deflection behaviors presented in Figures 5.32 and 5.33 that beyond the peak load

resistance, the resistance of the polyurea strengthened walls only moderately decreased as

the walls continued to undergo very large deformations. In comparison to the control

walls, which failed almost immediately after reaching the peak load resistance, the use of the polyurea greatly increased the energy absorption capability of the URM walls. The energy absorption has been quantified in Figure 5.34 through presentation of the external work. The external work done by each wall serves as a direct relation to the strain energy absorbed by the walls. From Figure 5.34, it can be seen that on the basis of energy absorption, the polyurea retrofitted walls greatly outperformed their counterparts constructed from the same base masonry material. The failure of the polyurea retrofitted walls was ultimately considered to be as a result of the rupture or debonding of the polyurea material. However, this failure only occurred after significant wall deformation and crushing of the masonry was observed. Additionally, at the ultimate limit state, the polyurea retrofit system almost entirely eliminated the occurrence of fragmentation or separation of the parent masonry material.

The GFRP-polyurea retrofit system was used on three of the URM walls and affected wall behavior in an entirely different manner than that of the polyurea retrofit. The use of the GFRP strengthening system resulted in a significant increase in both the stiffness and the capacity of the URM walls but also resulted in reduction of the wall deformation. When compared to the control walls, the GFRP-polyurea retrofit system resulted in capacity increases of 165 percent, 270 percent, and 675 percent, respectively, for Walls P1-5, P1-8, and P1-2. However, it should be noted that Wall P1-2 was tested using an alternate test method, and it is expected that the same capacity results may not have been achieved if Wall P1-2 had been tested to failure using the airbag system.

From Figure 5.34, it can be seen that the external work done by Walls P1-5 and P1-8 exhibited only slight increases over that of the control walls constructed from the
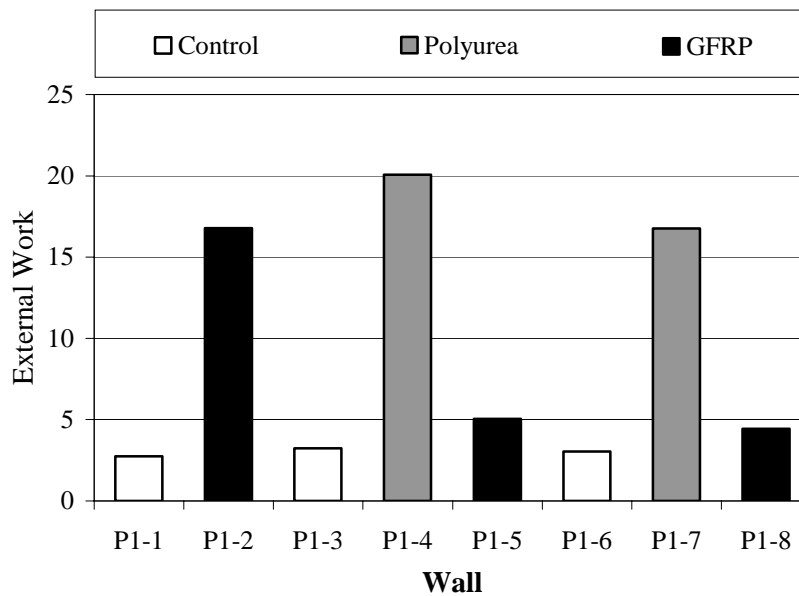
Figure 5.34. External Work Done by Phase 1 Walls

same base masonry material. Wall P1-2 showed a significant increase in the energy

absorption capability when compared to Wall P1-1, but again, it should be noted that

Walls P1-1 and P1-2 were loaded using two different testing methods. With the

exception of Wall P1-2, the GFRP strengthened walls were considered to fail prematurely

due to the debonding and shearing of the polyurea from the surrounding frame elements.

However, at the ultimate limit state, the use of the polyurea essentially reduced all debris

and fragmentation of the base masonry material. The failure modes of the Phase 1 walls

have been summarized in Table 5.3.

**5.3.3. Influence of Base Masonry Material.** In addition to the variable

strengthening methods used in this study, the influence of the base masonry material used

for wall construction has also been addressed to determine its effect on the resulting out-

of-plane behavior of the URM walls. To compare amongst the three base masonry

materials used in the construction of the Phase 1 URM walls, the load-deflection behavior

Table 5.3. Summary of Failure Modes for Phase 1 Walls

Wall	Failure Mode
P1-1	Crushing of mortar in bed joints; instability failure
P1-2	Flexural-shear cracking; followed by polyurea failure at boundary
P1-3	Crushing of mortar in bed joints; instability failure
P1-4	Slight masonry crushing at hinges; followed by polyurea rupture
P1-5	Slight masonry crushing at hinges; followed by polyurea failure at boundary
P1-6	Slight masonry crushing at hinges; instability failure
P1-7	Masonry crushing at hinges; followed by polyurea failure at boundary
P1-8	Masonry crushing at hinges; followed by polyurea failure at boundary

for all of the walls has been presented in three plots, shown in Figures 5.35 through 5.37.

Figure 5.35 pertains to the unstrengthened control walls, Figure 5.36 pertains to the

polyurea strengthened walls, and Figure 5.37 pertains to the GFRP-polyurea strengthened

walls. The deflection of the walls has been normalized with respect to the height of each

wall to account for the varying geometry of the walls in Phase 1 of the research program.

Figure 5.35 shows that on a normalized deflection basis, the wall constructed from the

WF-FA material, Wall P1-6, underwent the most lateral deformation at the mid-height

location with a normalized deflection value of approximately 3 percent of the wall height.

This figure also suggests that that the wall constructed from the CMUs, Wall P1-3,

deflected the least amount at the mid-height location with a normalized deflection value

of approximately 2 percent of the wall height. For all of the control walls tested in this

program, the formation of the central hinge as a result of rigid body deformation did not

occur exactly at the mid-height location, which led to a reduction in the maximum

measured deflection. The formation of the central hinge may have been influenced by weakness in the masonry bed-joints or by the centroid of applied pressure varying due to wall deformation.
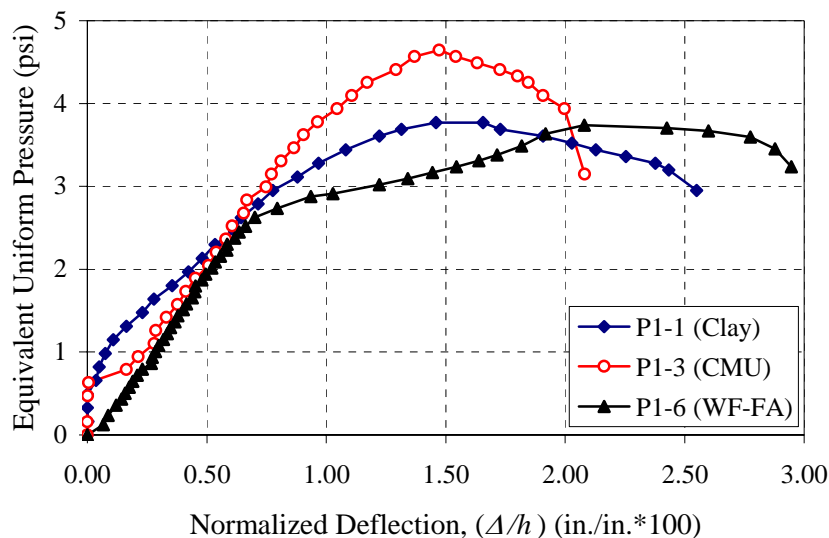
Conversions: 1 psi = 6.895 kPa; 1 in. = 25.4 mm

Figure 5.35. Load-Normalized Deflection: Phase 1 Control

In Figure 5.36, the comparison between the polyurea retrofitted walls, P1-4 and P1-7, is presented. This figure shows that the stiffness and the capacity of Wall P1-4 exceeded that of Wall P1-7. If one compares the peak load resistance of Wall P1-4 to the peak resistance of Wall P1-7, it results in a ratio of approximately 1.40. The same comparison can be performed on the compressive strength of the masonry units used to construct the two walls, which results in the masonry strength ratio of 1.48. This suggests that because neither of the walls failed due to instability, and because some form of masonry crushing was found to occur in both walls prior to failure, the out-of-plane load resistance can be directly related to the compressive strength of the masonry units.

Additionally, Figure 5.36 also shows that the wall constructed from the WF-FA masonry units, Wall P1-7, was able to maintain a higher load level while undergoing large lateral deflection, and achieved an ultimate normalized deflection of approximately 18 percent of the wall height. Wall P1-4 achieved a slightly smaller normalized deflection with a value of approximately 15 percent of the wall height.

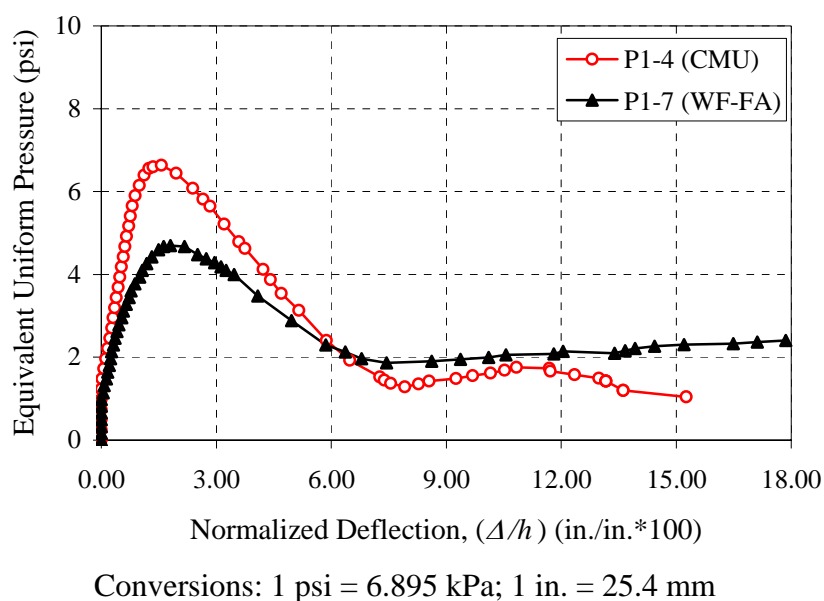Conversions: 1 psi = 6.895 kPa; 1 in. = 25.4 mm

Figure 5.36. Load-Normalized Deflection: Phase 1 Polyurea Retrofit

Lastly, the three GFRP-polyurea strengthened walls have been compared in Figure 5.37. The load-deflection behavior presented in this plot does not serve as a direct comparison of the three base masonry materials because the reinforcement index differs for each wall. However, the figure does present general trends in the out-of-plane behavior. Walls P1-5 and P1-8 appear to have similar stiffness characteristics even though the stiffness of the masonry used in the construction of the two walls varied significantly. The figure also shows the disparity between the behavior of the wall

constructed from the clay units, Wall P1-2, and the behavior of Walls P1-5 and P1-8. Although a high out-of-plane load capacity would be expected due to the high compressive strength of the clay units, Figure 5.37 may be misleading because Wall P1-2 was tested using a single point load applied at the mid-height location, and all other walls were tested using the airbag system.

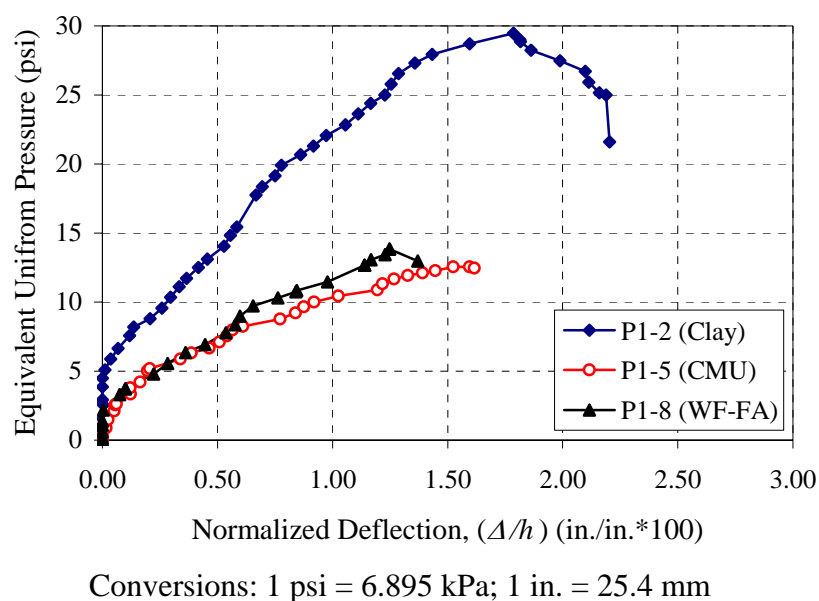

Conversions: 1 psi = 6.895 kPa; 1 in. = 25.4 mm

Figure 5.37. Load-Normalized Deflection: Phase 1 GFRP-Polyurea Retrofit

 Because the strength of the various types of masonry used in construction can vary significantly, the load-deflection behavior of the URM control walls has been presented in terms of a normalized pressure versus normalized mid-height deflection. This method of presenting the out-of-plane behavior may serve as a more general relationship between the three base masonry materials used. The pressure data has been normalized by dividing the equivalent uniform pressure by the compressive strength of

the parent masonry material. Figure 5.38 shows that the normalized pressure capacity of

the wall constructed from the WF-FA masonry material, Wall P1-6, greatly outperforms

the control wall constructed from the clay units and slightly outperforms the control wall

constructed from the CMU block. The performance of Wall P1-6 is believed to be

directly linked to the deformability of the wall. Unlike Walls P1-1 and P1-3, Wall P1-6

did not exhibit the pure rigid body behavior that is typically expected of non-slender

framed infills, but displayed some combination of bending and arching. It is believed

that this combination of bending and arching resulted in a greater depth of material being

subjected to compressive forces. It is also believed that the low stiffness of the WF-FA

material used to construct Wall P1-6 resulted in greater deformation at the hinge

locations, leading to larger depth of material being subjected to compressive forces at the

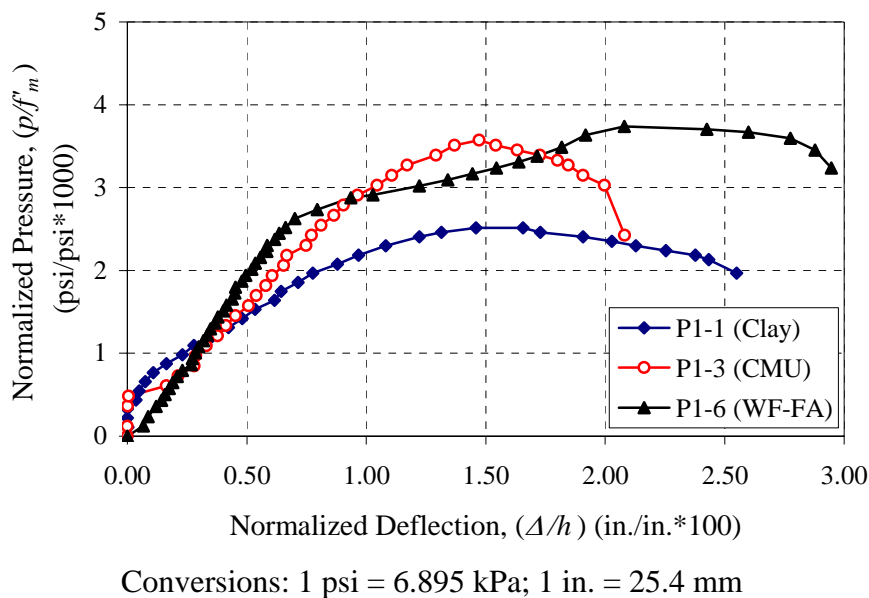hinge locations and increased wall stability.

Conversions: 1 psi = 6.895 kPa; 1 in. = 25.4 mm

Figure 5.38. Normalized Load-Normalized Deflection: Phase 1 Control

5.4. ANALYTICAL STUDY

The following section presents an analytical model for determining the out-of-plane load capacity for FRP strengthened non-slender URM walls. The model pertains to the ultimate limit state and is only applicable for non load-bearing URM walls undergoing one-way arching action.

5.4.1. Analytical Model Development. The development of the analytical model was based upon several different past works used to predict the out-of-plane load capacity for masonry walls, but the model was primarily developed from a previous model for predicting the behavior of unstrengthened URM arching walls (Anderson, 1984). Several different factors can be considered when attempting to model the behavior of URM arching walls. The model developed in this study considers the following:

1) Shrinkage and temperature strains, which are grouped together under the term ε_s.

2) Initial gaps, g_1 and g_2, between the ends of the walls and the abutments, other than that caused by 1).

3) Deformability/rigidity of the abutments in the direction of the span of the wall is addressed through use of their respective stiffnesses (load/unit deflection) K_1 and K_2 at the abutments. The stiffnesses are assessed from the mechanical properties of the beam/columns making up the surrounding frame.

4) Elastic shortening due to the arching thrust is calculated from a single modulus of elasticity, E_m, which incorporates the stiffness of the masonry units as well as the mortar joints (Anderson, 1984).

5) The eccentricity at which the arching thrust acts is referred to as *e* or *k·t* and is measured from the centerline of the cross-section. This term has been shown to be a function of the rotation of the ends of the walls, the stress level, and if desired could be made dependent on such factors (Anderson, 1984). However, since the purpose of this work is to produce limit state equations capable of predicting the load capacity at ultimate, the eccentricity has been taken as a constant proportion of the wall thickness.

6) The addition of FRP strengthening material will reduce the deformability of the wall and will reduce the arching thrust force (Galati, 2003). The stiffness contribution of the FRP has been defined using the variable K_3.

The ability to effectively develop an arching mechanism in a URM wall panel depends upon several different factors, including the interaction between the URM wall panel and its supports. Prior to loading, initial gaps between the surrounding frame abutments and the wall may exist. These gaps could have been created from fabrication or could possibly have developed due to shrinkage and temperature strains in the masonry. Ultimately, these initial gaps will affect the development of membrane forces, which are critical to the formation of the arching effect and therefore must be considered. Figure 5.39 presents the URM wall prior to loading. The variable *t* has been used to represent the thickness of the URM wall, and *h* represents the overall height of the wall. All other variables have been previously defined. It is assumed that the gaps at the boundaries of the wall are small and that under transverse load, will be closed due to wall deformation prior to reaching the cracking load. Once the cracking load is reached, the wall will develop into a three-hinged arch, with hinge locations at mid-height and the

upper and lower boundaries. Figure 5.40 shows the development of the three-hinged arch

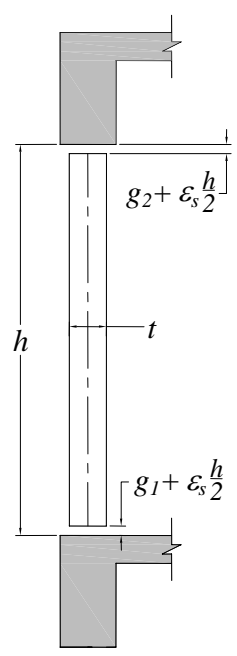for an end-restrained FRP strengthened wall.
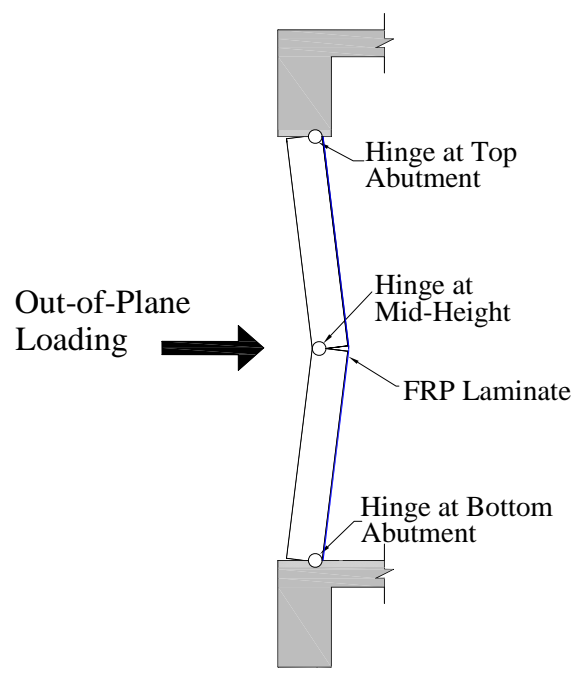

Figure 5.39. URM Wall Prior to Loading

Figure 5.40. Development of Three-Hinged Arch

Once the formation of the three-hinged arch occurs, it can be assumed that the upper and lower halves of the wall deform as rigid bodies. Analysis of only the bottom segment of the wall with the application of the resultant force from an out-of-plane uniformly distributed load results in the free-body diagram presented in Figure 5.41.
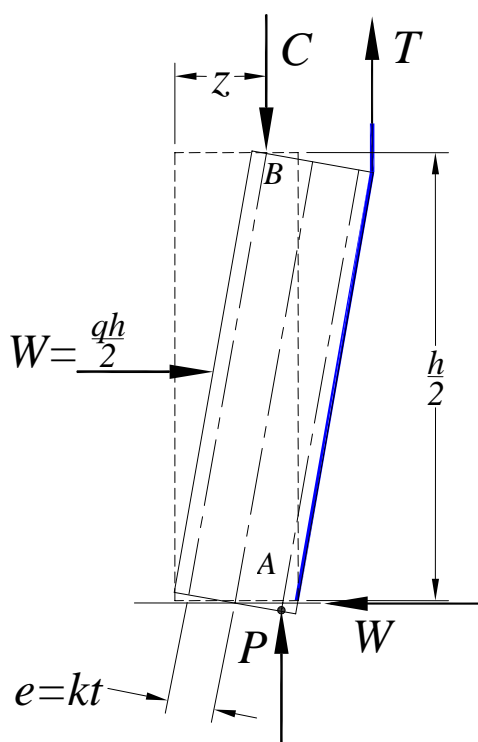

Figure 5.41. Free-Body Diagram of Bottom Wall Segment

The free-body diagram of the lower wall segment presented in Figure 5.41 represents the equilibrium of forces for a wall strengthened with an external FRP laminate and illustrates the location of the eccentric membrane forces. It should be noted that although the following equations have been developed from the basis of a uniformly distributed load, the methodology is applicable for any type of out-of-plane load that affects the upper and lower segments of the wall in a symmetric fashion.

The variables used in Figure 5.41 are defined as follows:

A = the location of the hinge at the wall boundary

B = the location of the hinge at mid-height

P = the developed arching membrane force, also referred to as the 'arch-thrust'

T = the tension force in the FRP

C = the compression force in the masonry at the mid-height hinge location

W = the resultant force from the uniform load applied to the lower wall segment

q = the uniform load applied to the lower wall segment

e = the eccentricity of the hinge location from the centerline of the wall ($e = kt$)

z = the lateral deflection at mid-height

From the internal equilibrium of forces, it has been shown that the compression force in the masonry at the mid-height hinge location can be expressed in terms of the arch-thrust force and the force in the FRP:

$$C = T + P \qquad (18)$$

To determine the location of these forces, it necessary to relate the lateral deformation of the wall to the system of forces presented in Figure 5.41. The lateral deflection of the wall depends upon multiple factors: the initial gaps at the support locations shown in Figure 5.39, the rigidity of the boundary supports, the stiffness of the masonry, and the stiffness of the FRP. Considering all of these factors, a series of expressions have been developed to determine the lateral deflection of the wall at mid-height.

The average movement of the abutments due to the membrane force P can be written as a function of the stiffnesses of the abutments, K_1 and K_2, as follows:

$$\delta_a = \frac{P}{2}\left(\frac{1}{K_1} + \frac{1}{K_2}\right) \tag{19}$$

Equation (19) implicitly assumes that the stiffness of the abutment is constant along the width of the wall. The movement of the wall accounting for the presence of gaps, shrinkage strains, and temperature strains is given by Equation (20):

$$\delta_i = \frac{\varepsilon_s h}{2} + \frac{g_1 + g_2}{2} \tag{20}$$

The shortening of the wall is based on the stiffness of the masonry as well as the arch-thrust force. Due to the nature of the arch formation, the arch-thrust force cannot be fully distributed throughout the entire cross-section of the wall. Therefore, it is assumed that the force is distributed through a compression core given by a parabolic thrust line (Anderson, 1984). The effective or mean width of this compression core can be calculated as follows:

$$t' = 0.61 \cdot t \tag{21}$$

Considering the effective width of the compression core defined in Equation (21), the shortening of the masonry due to the arch-thrust is defined as follows:

$$\delta_s = \frac{Ph}{2E_m t' b_m} \tag{22}$$

where E_m represents the modulus of elasticity for the masonry assemblage, and b_m represents the width of the wall.

Lastly, the deformation of the FRP can be determined using the tensile force, T, and the stiffness of the FRP, which has been defined as K_3:

$$\delta_{frp} = \frac{T}{K_3} \tag{23}$$

Previous studies have shown that due to the rigid body deformation experienced by FRP strengthened arching walls, much of the deformation in the strengthening material occurs locally at the location of the central hinge. Additionally, the full tensile force, T, does not act along the full height of the wall but only locally at the mid-height location. To account for these factors, it has been assumed that the deformation of the FRP at the ultimate limit state occurs over some unbonded length, l_b, which has been reflected in the stiffness of the FRP:

$$K_3 = \frac{A_{frp} E_{frp}}{l_b} \tag{24}$$

where A_{frp} represents the cross-sectional area of the FRP strengthening material, and E_{frp} is the modulus of elasticity of the FRP. From previous research studies, it has been determined that an appropriate value for the unbonded length, l_b, can be taken equal to 1.50in. (40mm) for URM arching walls strengthened with external laminates (Tumialan et al., 2003).

The developed expressions used to relate the deformation of the URM wall and surrounding frame to the internal forces can be related to the wall geometry as illustrated in Figure 5.42.

Using these expressions, the length of segment *AB* in Figure 5.42 is given by:

$$\overline{AB}^2 = \left(\frac{h'}{2}\right)^2 + (2e)^2 = \left[\frac{h}{2} + \frac{P}{2}\left(\frac{1}{K_1} + \frac{1}{K_2}\right) + \frac{T}{K_3}\right]^2 + (2e - z)^2 \tag{25}$$
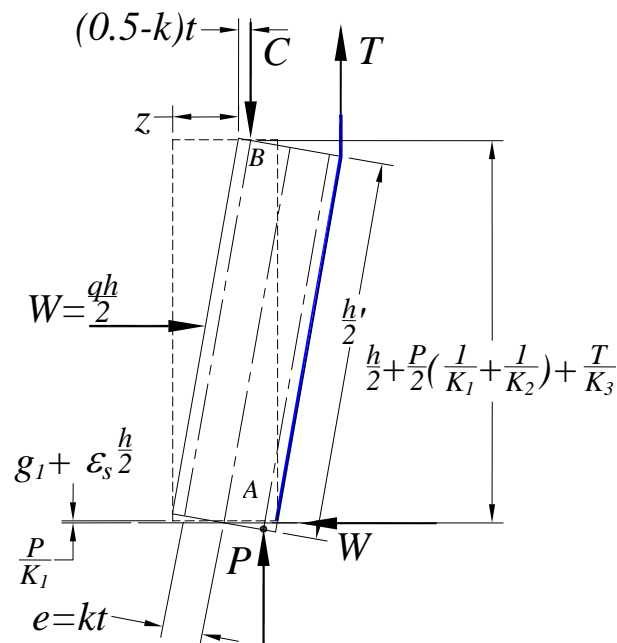

Figure 5.42. Geometrical Relationships for Bottom Wall Segment

Since $\dfrac{h'}{2} = \dfrac{h}{2}\left(1 - \dfrac{P}{E_m t' b_m} - \varepsilon_s - \dfrac{g_1 + g_2}{h}\right)$, Equation (25) can be written to represent the

overall mid-height deflection (Anderson, 1984):

$$z = 2kt - \sqrt{(2kt)^2 - m} \tag{26}$$

where

$$m = \left(\frac{h}{2} + \frac{P}{2}\left(\frac{1}{K_1} + \frac{1}{K_2}\right) + \frac{T}{K_3}\right)^2 - \left[\frac{h}{2}\left(1 - \frac{P}{E_m t' b_m} - \varepsilon_s - \frac{g_1 + g_2}{h}\right)\right]^2 \tag{27}$$

In determining the values of the forces imposed on the system, the following factors are considered:

1) The ultimate load that can be carried by the arching wall is governed by either the mid-height compressive load, C, or by the failure of the FRP (i.e., debonding or rupture). The stress-strain behavior of the FRP has been limited to effective values f_{fe} and ε_{fe}:

$$f_{fe} = k_m f_{fu} \tag{28}$$

$$\varepsilon_{fe} = k_m \varepsilon_{fu} \tag{29}$$

where f_{fu} and ε_{fu} correspond to the ultimate stress and ultimate strain of the FRP, respectively. The variable k_m is an efficiency factor that is implemented to account for premature failure modes. Table 5.4 summarizes values for k_m based on previous test results of URM walls strengthened with FRP grids, FRP laminates, and NSM FRP bars (Tumialan et al., 2003; Galati et al., 2006).

2) The limiting arch-thrust is considered to induce stress over a depth equal to *2t·(0.5-k)* (Anderson, 1984). The stress has been expressed as a uniform distribution through use of the rectangular stress-block factor *γ*.

Table 5.4. k_m Factors for Various Strengthening Systems

Strengthening System	Limitations	Resin Type	k_m
GGRP	-	Polyurea	0.65
FRP Laminates	If putty is used	Epoxy	0.65[1]
	If putty is not used	Epoxy	0.45[1]
NSM FRP Bars	FRP rectangular bars, Groove having the same height of the bar and width 1.5 times the one of the bar	Epoxy	0.65[2]
	FRP circular bars, Square groove 1.5 times the diameter of the Bar[4]	Epoxy	0.35[2]
	FRP circular bars, Square groove 2.25 times the diameter of the Bar	Epoxy / LMCG[3]	0.55[2]

[1] From Tumialan et al., 2003.

[2] From Galati et al., 2006.

[3] Latex Modified Cementitious Grout.

[4] Latex Modified Cementitious Grout can not be used with a standard square groove having dimensions 1.5 times the diameter of the bar.

3) The strain distribution at the mid-height location of the wall is assumed to vary linearly, and it is assumed that the neutral axis depth can be related to the depth of the uniform stress from 2) by way of the factor β_1.

4) The eccentricity of the ultimate arching thrust, $k \cdot t$, is considered to be the same at each of the three hinge locations.

Because masonry in compression exhibits a non-linear response, it is necessary to account for variable stress distributions that will occur due to differing modes of failure. For tensile failures, or failure of the FRP prior to crushing, the strain in the masonry will not reach its maximum value, and the distribution of stress must be adjusted to account for this. Therefore, when tensile failures govern (FRP rupture or FRP debonding), the following should be used to represent the distribution of the compressive stress in the masonry at the mid-height location (Garbin et al., 2005):

$$\beta_1 = 2 - \frac{4\left[\left(\frac{\varepsilon_{mu}}{\varepsilon'_m}\right) - \tan^{-1}\left(\frac{\varepsilon_{mu}}{\varepsilon'_m}\right)\right]}{\left(\frac{\varepsilon_{mu}}{\varepsilon'_m}\right)\ln\left(1+\left(\frac{\varepsilon_{mu}}{\varepsilon'_m}\right)^2\right)} \tag{30}$$

$$\gamma = 0.90\frac{\ln\left(1+\left(\frac{\varepsilon_{mu}}{\varepsilon'_m}\right)^2\right)}{\beta_1\left(\frac{\varepsilon_{mu}}{\varepsilon'_m}\right)} \tag{31}$$

To evaluate Equations (30) and (31), the following recommended values from the Building Code Requirements for Masonry Structures (ACI 530-02/ASCE 5-02/TMS 402-02) can be assumed for the strain in the masonry at the peak compressive stress:

$$\varepsilon'_m = 0.0024, \text{ for clay masonry} \tag{32a}$$

$$\varepsilon'_m = 0.0019, \text{ for concrete masonry} \tag{32b}$$

Additionally, the recommended maximum usable strain ε_{mu} at the extreme compression fibers can be taken as follows:

$$\varepsilon_{mu} = 0.0035, \text{ for clay masonry} \tag{33a}$$

$$\varepsilon_{mu} = 0.0025, \text{ for concrete masonry} \tag{33b}$$

When crushing of the masonry is the controlling mode of failure, the following values presented in Table 5.5 can be used directly for the values of γ and β_1:

Table 5.5. Equivalent Stress Block Factors (Garbin et al., 2005)

Parameter	Concrete	Clay
β_1	0.805	0.822
γ	0.853	0.855

From the equilibrium of moments with respect to point *B* in Figure 5.42, the ultimate out-of-plane load resistance, q_u, of the masonry wall is given by Equation (34):

$$q_u = \frac{8}{h^2}\left[P(2kt - z) + T(0.5 + k)t\right] \tag{34}$$

The tension force in the FRP at the ultimate limit state is governed by Equation (35):

$$T = \min\left\{A_{frp}f_{fe}, A_{frp}E_{frp}\varepsilon_{frp}\right\} \tag{35}$$

where ε_{frp} is the effective strain in the FRP and is determined through the use of Equation (36):

$$\varepsilon_{frp} = \min\left\{\varepsilon_{fe}, \varepsilon_m\left(\frac{t - \dfrac{2t(0.5 - k)}{\beta_1}}{\dfrac{2t(0.5 - k)}{\beta_1}}\right)\right\} \tag{36}$$

To simplify the problem, it is recommended to assume that the crushing of masonry will be the governing mode of failure. In the event that $\varepsilon_{frp} = \varepsilon_{fe}$ as the result of evaluating Equation (36), the ultimate limit state is that of tensile failure, and an iterative approach using Equations (30) and (36) must be performed to solve for the value of β_1.

The maximum compressive force at the mid-height of the wall is determined using the following:

$$C = 2t(0.5 - k)b_m(\gamma f'_m) \tag{37}$$

where f'_m is the gross compressive strength of the masonry.

Having determined the value of the compressive force, C, using Equation (37), the membrane force P can be solved directly from the equilibrium of forces:

$$P = C - T \tag{38}$$

Once values of T and P have been obtained, Equations (26) and (27) can be used to solve for the lateral deflection, z, and Equation (34) can be used to determine the ultimate out-of-plane load capacity q_u.

5.4.2. Model Calibration. To determine applicable values for the eccentricity of the compressive forces at the hinge locations, the model was calibrated with the use of experimental data from this study as well as other previous works (Carney and Myers, 2003; Galati, 2003). Previous research has shown that a k value of 0.45 is appropriate for unstrengthened URM walls (Anderson, 1984). Also, studies have shown that as the level of strengthening increases, the in-plane force due to arching action decreases (Galati, 2003). Therefore, it seemed appropriate to express the parameter k in terms of the reinforcement level and to limit k to a maximum value of 0.45.

For each wall used in the calibration, the value of k was selected such that the load capacity results from the analytical model matched that of the experimental data. Thirteen walls were used to calibrate the model with reinforcement indexes varying from 0.20 to 1.07. Figure 5.43 shows that the parameter k is dependent upon the reinforcement

level as well as the height-to-thickness ratio. The level of reinforcement has been

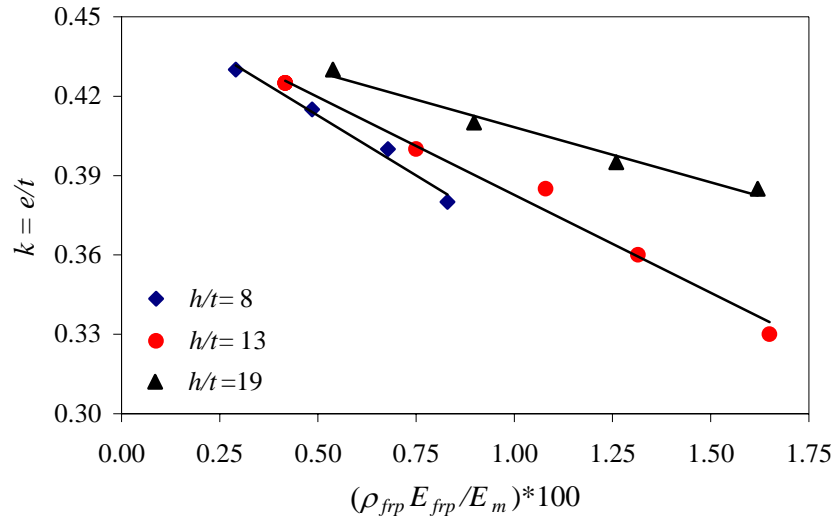expressed in terms of the normalized reinforcement ratio.

Figure 5.43. Correlation of Eccentricity Factor, *k*, and the Reinforcement Level

Figure 5.43 shows that the correlation between the parameter *k* and the level of

reinforcement is relatively linear. Additionally, the slopes of the trend lines plotted in

Figure 5.43 can be related to the height-to-thickness ratio through a linear relationship as

well. Therefore, the following empirical relationship, which considers the reinforcement

level as well as the height-to-thickness ratio of the URM wall, was established:

$$k = 0.45 + \frac{\rho_{frp}}{100} \frac{E_{frp}}{E_m} \left[\left(\frac{h}{t} \right)^2 - 780 \right] \tag{39a}$$

$$0.33 \le k \le 0.45 \tag{39b}$$

Equation (39) has been limited to a minimum value of 0.33 because the determined relationship is based on a limited data set, and further experimentation needs to be done to determine appropriate *k* values for large reinforcement levels.

5.4.3. Validity of the Analytical Model. To assess the validity of the presented analytical model, the experimental results from this study as well as other experimental studies have been compared with theoretical load capacity predictions computed using the analytical model. In all, experimental results from 24 FRP strengthened URM walls have been used to assess the validity of the analytical model. A matrix summarizing the URM walls used for comparison can be found in Appendix B. Additionally, the individual numerical load capacity predictions for each of the URM walls are presented in Appendix B.

The data used to assess the validity of the analytical model encompassed experimental testing of strengthened URM walls with height-to-thickness ratios ranging from 8.5 to 19.2. The reinforcement indexes of these walls ranged from values of 0.20 to 1.89.

Figure 5.44 shows that the majority of the analytical predictions were within approximately 20 percent of the ultimate state load capacity values obtained from laboratory testing. However, in the most extreme cases, the model over-predicted capacity by as much as 56 percent, and under-predicted capacity by 31 percent. Note that the two greatest instances of analytical over-predictions pertained to strengthened walls that were found to achieve lower capacities than their unstrengthened URM counterparts.

The variation in the accuracy of the model is most likely due to the method of calibration. The function developed to determine the eccentricity of the arch-thrust, *k*, is

not capable of accounting for the variations among the walls used to assess the validity. To further refine the model and improve the load-capacity predictions, a larger data-set consisting of strengthened URM arching walls with varied height-to-thickness ratios, varied reinforcement indexes, and varied base masonry materials is required. With use of such a data set, the methodology in determining an appropriate value for the eccentricity of the arch-thrust related through the parameter *k* could be improved.
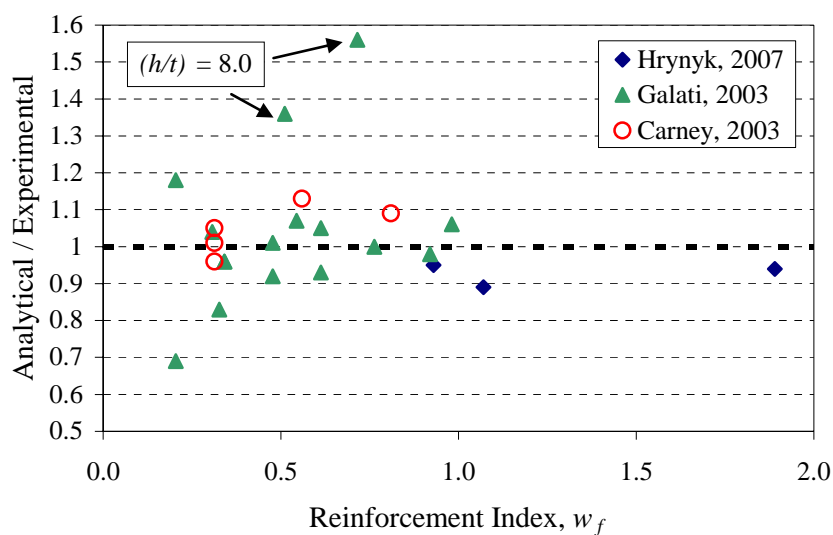

Figure 5.44. Analytical versus Experimental Ultimate Load

6. PHASE 2 – SLENDER INFILLS

The following section of the thesis presents the portion of the research study dedicated to URM walls that are classified as slender infills. Unlike the Phase 1 walls, the walls in this phase of the study were not impacted by the presence of surrounding structural elements, allowing freedom to move in the longitudinal direction. In this section, the experimental program and test results for the Phase 2 walls are presented. A detailed discussion of the results from the wall testing has been provided, and the test results have been compared with analytical predictions.

6.1. EXPERIMENTAL PROGRAM

6.1.1. Wall Construction. The Phase 2 walls were constructed by the same group of masons that built the walls presented in Phase 1 of this study, and they were constructed using techniques similar to those employed for the Phase 1 walls. The Phase 2 walls were built off of a flat concrete surface and were constructed using a running bond with all mortar joints finished flush with the surface of the masonry units. All of the walls had a uniform width of 24in. (610mm). Walls constructed from clay brick units consisted of 12 courses and were 36in. (914mm) in height, and walls constructed from the CMU blocks consisted of 6 courses and were 48in. (1219mm) in height. The construction of one of the Phase 2 clay walls is presented in Figure 6.1. After the completion of wall construction, the Phase 2 walls were allowed to cure for a minimum of 28 days prior to being moved or undergoing external retrofit.

6.1.2. Strengthening Procedure. With the exception of one wall, the Phase 2 walls were retrofitted explicitly by way of embedding either one or two layers of GFRP

(a) Quarter Wall

(b) Half-Wall

(c) Bed-Joint Construction

(d) Completed Wall

Figure 6.1. Construction of Phase 2 Walls

grid into the spray-on polyurea material. One of the URM walls constructed from CMU

masonry units was retrofitted using only polyurea. To investigate the effectiveness of the

bond between the polyurea retrofit material and the base masonry material of the URM

walls, the walls in this phase of the study were constructed with and without the use of a

simulated retrofit anchorage system. For walls strengthened using the simulated retrofit

anchor, the polyurea material was applied to the full face of the URM wall, so during

testing, the interaction between the support reactions and the strengthening material

would serve as a means of preventing or delaying the occurrence of debonding at the member-ends. Walls retrofitted without the simulated anchorage condition had polyurea applied to the free-span of the URM walls only to eliminate all interaction between the support reactions and the strengthening material.

Prior to the application of the strengthening materials, the mortar joints of the walls were ground smooth to the face of the masonry units using a mason's stone, and all dust and debris were removed from the surface of the walls. In the case of the URM walls utilizing the unanchored retrofit, the wall edges and support locations of the walls were taped off, so only the free-span of the URM wall was exposed during the spray-on application of the elastomeric polyurea material. For the anchored retrofit, only the edges of the URM walls were taped off. The taped off Phase 2 walls are shown in Figure 6.2.

Figure 6.2. Phase 2 URM Walls Prior to Strengthening

Prior to spraying the walls with the elastomer, an epoxy-based primer was applied to the exposed surface of the URM walls. The epoxy primer was used to prevent reactions from occurring between the spray-on polyurea material and free moisture

within the base masonry material. The application of the primer and the primed walls are shown in Figure 6.3.

(a) Application of Primer   (b) Primed URM Walls

Figure 6.3. Primer Application of Phase 2 Walls

The primer was allowed to cure for approximately one hour prior to spraying the URM walls with the elastomeric polyurea material. After the primer had properly cured, a thin initial layer of polyurea was sprayed onto the exposed surfaces of the walls. Immediately after the first layer of polyurea was sprayed onto the wall surface, the FRP grid was embedded into the soft polyurea material. The set-time for the polyurea was approximately 10 to 20 seconds; therefore, the application of the grids had to immediately follow the spray application of the polyurea. For the purpose of applying the FRP grids as quickly as possible, the grids were precut to match the width of the walls and were cut slightly shorter than the free-span length of the walls. After the FRP grid was correctly positioned and embedded within the base layer of polyurea, a second application of polyurea was sprayed over the FRP until the surface was free of voids, and the GFRP grid material was fully embedded. For walls with two layers of grid material,

the second grid was embedded within the second layer of polyurea, and a third polyurea layer was applied to the surface to fully embed the grid and close all voids. The combination of the FRP and polyurea material resulted in an overall retrofit thickness of approximately 3/8in. (9.5mm) for the walls strengthened with a single layer of GFRP, and approximately 1/2in. (12.7mm) for the walls strengthened with two layers of GFRP. The spraying of the polyurea and the application of the GFRP grid are presented in Figure 6.4. Additionally, a schematic illustrating the simulated anchored and non-anchored retrofit schemes used for the walls has peen provided in Figure 6.5.

| (a) Initial Polyurea Layer | (b) Embedding FRP Grid |

| (c) Secondary Polyurea Layer | (d) Retrofitted URM Walls |

Figure 6.4. Retrofit Application for Phase 2 Walls

(a) Simulated Retrofit Anchor   (b) Un-anchored Retrofit
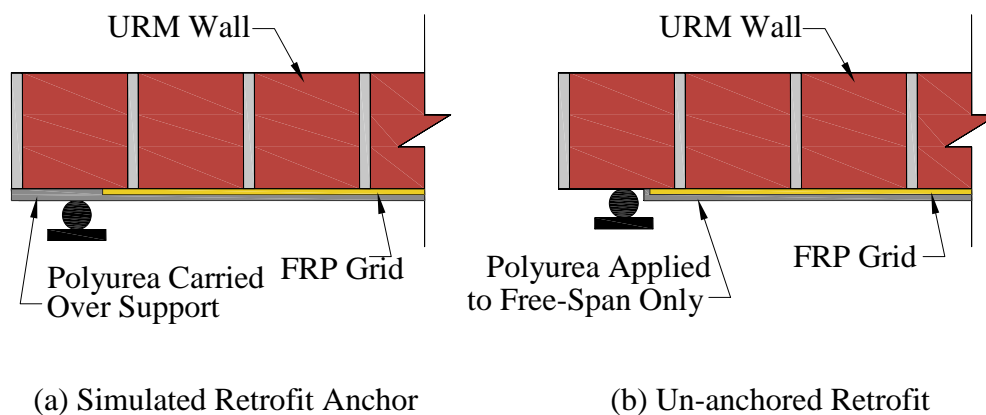
Figure 6.5. Retrofit Schemes for Phase 2 Walls

A test matrix for the Phase 2 walls has been provided in Table 6.1. The matrix provides a summary of the geometry and retrofit scheme used for each of the Phase 2 walls. The walls have been presented using the identification system established in Section 4.

Table 6.1. Test Matrix – Phase 2

Wall	Masonry	w_f	Free Span in. (mm)	Shear Span in. (mm)	Retrofit Anchor	Retrofit Scheme	
						Polyurea	GFRP
P2-1	Clay	1.14	33 (838)	13 (330)	√	√	√
P2-2	Clay	2.27	33 (838)	13 (330)	√	√	√
P2-3	Concrete	0.05	44 (1,118)	18 (457)		√	
P2-4	Concrete	1.01	44 (1,118)	18 (457)		√	√
P2-5	Concrete	1.01	44 (1,118)	18 (457)	√	√	√
P2-6	Concrete	2.02	44 (1,118)	18 (457)		√	√
P2-7	Concrete	2.02	44 (1,118)	18 (457)	√	√	√

6.1.3. Test Setup and Testing Procedure. The wall tests for Phase 2 of the research program were performed in the UMR's Engineering Research Laboratory (ERL). The walls in this phase of the study were loaded horizontally under four-point bending using a 400k (1780kN) capacity Baldwin Universal Testing Machine. The walls were constructed outside of the testing area and were later moved into place with the use of a standard pallet jack. To prevent any damage or cracking from occurring while moving the URM test specimens, the walls were braced using a metal banded wooden frame assembly. Once transported to the test-bed of the testing machine used to load the specimens, the wooden bracing system was removed from the URM walls. The wooden framing that was used to brace the URM walls is shown in Figure 6.6.

Figure 6.6. Braced URM Wall

The test setup for this phase of the study was rather simple. Because the Phase 2 walls were tested in the horizontal position under four-point bending, only minimal care

was needed to ensure that the walls would remain stable throughout the duration of the testing. Once the URM wall had been successfully transported to the bed of the testing machine, and all wooden bracing was removed, the walls were placed on end supports. The end supports were constructed from stiffened C-sections, which had an overall depth of 6in. (152mm). On the top of the end support beams, 1-1/2in. (38mm) diameter rollers and steel plates were welded in place, resulting in an overall support height of approximately 8in. (203mm). Due to the varying geometry between the walls constructed from the CMUs and the brick units, the walls were tested with different span lengths. The CMU walls had a free-span of 44in. (1,118mm), and the clay brick walls had a free-span of 33in. (838mm). Similarly, the points of load application also varied between the CMU and the clay walls. The CMU walls were tested with a shear-span of 18in. (457mm), and the clay brick walls were tested with a shear-span of 13in. (330mm). The load was applied across the full width of the walls at the load application points over a length of 2in. (51mm) to prevent local bearing failure from occurring in the masonry units. A W-section with a depth of 4in. (102mm) was used to spread the load from the testing machine to the two load application points. The full test setup for the Phase 2 walls is illustrated in Figure 6.7 and Figure 6.8.

The load applied to the URM walls was measured using a 50k (222kN) capacity Cooper Donut load cell, which was placed between the spreader beam and a steel ball-joint assembly anchored to the upper platen of the testing machine. Deflection and strain data were measured at the midspan location only. The vertical deflections were measured with the use of two LVDTs, which were placed on each side of the URM wall.
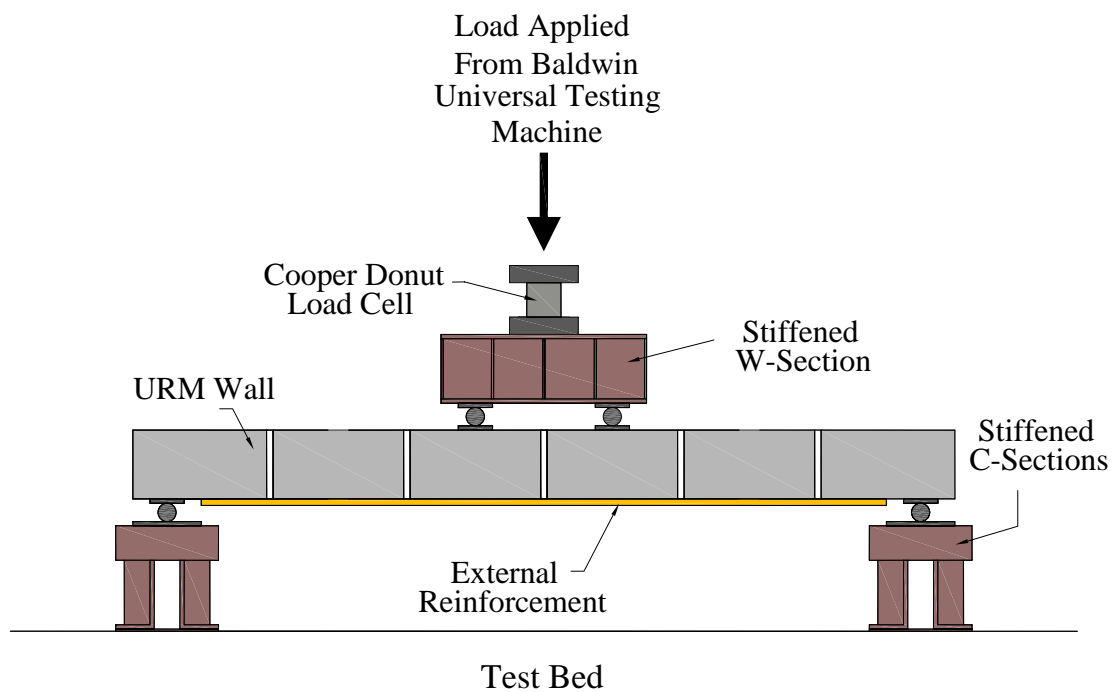
Figure 6.7. Schematic of Phase 2 Test Setup

Figure 6.8. Phase 2 Test Setup

Two strain gages were placed at the midspan location of the walls. The strain

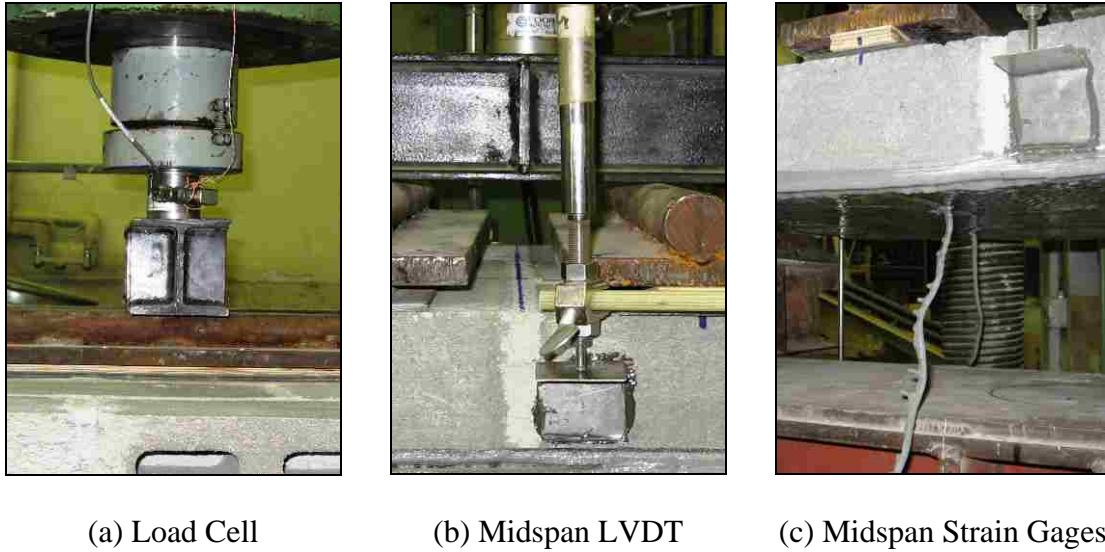gages were applied directly to the FRP grids prior to embedding them within the

(a) Load Cell   (b) Midspan LVDT   (c) Midspan Strain Gages

Figure 6.9. Phase 2 Instrumentation

polyurea. For the wall retrofitted using only the polyurea material, the strain gages were applied directly to the surface of the polyurea. The load cell, the locations of the LVDTs, and the locations of the strain gages are presented in Figure 6.9.

The test data were recorded through the use of a data acquisition system (DAS), and the test was performed using a single cycle. The deflection data, strain data, and applied load were sampled at a rate of 2Hz. The load was applied at a constant rate until a value of 1.0k (4.4kN) was achieved. At this point, the test was paused, and the data were checked to ensure that both the instrumentation as well as the DAS were functioning properly. After checking the data to ensure proper function of the instruments, the testing continued until URM wall failure was achieved. Throughout the testing, the location and initiation of cracks in both the mortar joints as well as the masonry units were noted. Additionally, observation of the bond behavior between the polyurea and the base masonry material was also documented and recorded throughout the URM wall testing.

6.2. TEST RESULTS

The following section presents the results from the testing of the Phase 2 walls. For each of the walls tested, a brief description of the behavior of the walls up to the point of failure, the mode of failure, and the fragmentation has been provided. In addition to the observed behavior of the walls, the load-deflection response for each wall has also been included in this section of the thesis. Additionally, plots of the midspan moment versus deflection and the midspan moment versus strain behavior can be found in Appendix C.

6.2.1. Wall P2-1. Wall P2-1 was the first of two clay walls tested in Phase 2 of the research program. The wall was retrofitted using the GFRP-polyurea retrofit with a single layer of grid material, and it was constructed using the simulated retrofit anchorage condition. Cracking in the interface between the masonry units and the midspan mortar joint was observed almost immediately after load was applied to the wall. As the applied load increased, flexural cracking in the bed-joints became visibly apparent in the middle third of the free-span of the wall. At an applied load of 10.1k (44.9kN) and a midspan deflection value of 0.94in. (23.9mm), the formation of the first major flexural-shear crack in the shear-span location was observed (see Figure 6.10). As the load resistance continued to increase, the development of the flexural-shear cracks was observed. Wall P2-1 reached a maximum load resistance value of 11.2k (49.8kN) at a midspan deflection value of 1.26in. (32.0mm). As loading continued beyond the peak resistance, the masonry began to split and deteriorate in the shear-span region in which the flexural-shear cracking initiated. The load resistance slowly decreased until the masonry had fully separated from the strengthening material, which occurred at an applied load of 5.6k
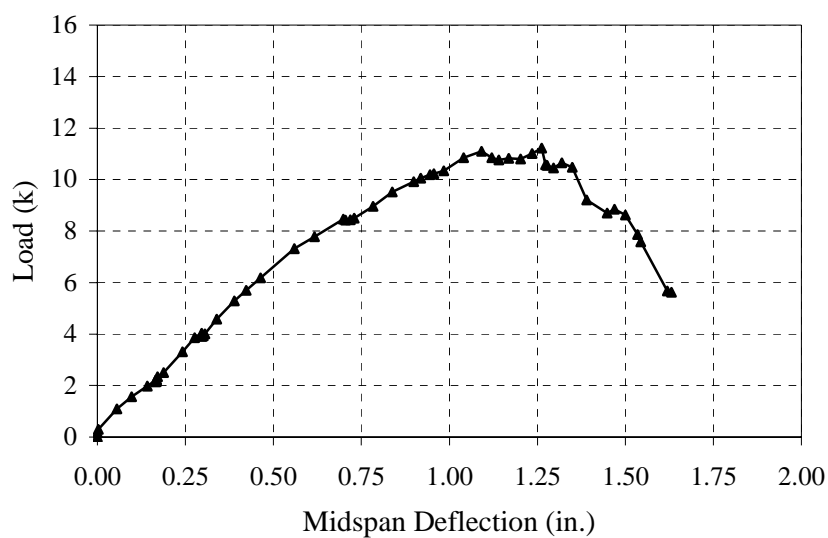
(24.9kN) and midspan deflection of 1.63in. (41.4mm). The separation and splitting of the

masonry is illustrated in Figure 6.10b. The load-deflection response for Wall P2-1 has

been provided in Figure 6.11.

(a) Flexural-Shear Cracking   (b) Ultimate Failure

Figure 6.10. Wall P2-1 Failure

Conversions: 1 k = 4.448 kN; 1 in. = 25.4 mm

Figure 6.11. Load-Deflection Behavior – Wall P2-1

6.2.2. Wall P2-2. This wall was the second of two strengthened URM walls constructed from clay brick units. Wall P2-2 was strengthened with two layers of grid material using the GFRP-polyurea retrofit system with polyurea applied to the entire face of the wall to simulate the presence of an anchored retrofit system. The wall behaved similarly to Wall P2-1 in that cracking occurred almost immediately at an applied load value of 0.7k (3.1kN). As testing progressed, flexural cracking was observed in the bed-joints throughout the constant moment region of the wall. At an applied load of 10.9k (48.5kN), the formation of flexural-shear cracks originating from the point of load application were observed. At 12.8k (56.9kN), a major longitudinal crack forming through the shear-span on the compression face of the wall originating from the applied load was observed (see Figure 6.12). The wall reached a peak load resistance value of 15.3k (68.1kN) at a midspan deflection of 0.75in. (19.1mm). The wall failed almost immediately after reaching the peak load resistance (see Figure 6.13) by way of masonry splitting due to the development of flexural-shear cracks as shown in Figure 6.12b.

(a) Longitudinal Cracking   (b) Flexural-Shear Cracking

Figure 6.12. Wall P2-2 Failure
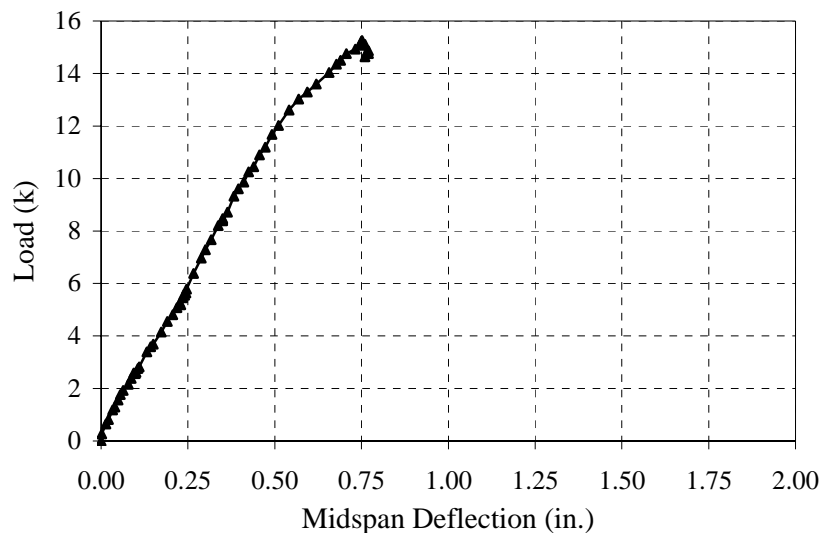
Conversions: 1 k = 4.448 kN; 1 in. = 25.4 mm

Figure 6.13. Load-Deflection Behavior – Wall P2-2

6.2.3. Wall P2-3. Wall P2-3 was constructed from concrete block and was the only Phase 2 wall retrofitted using the polyurea material exclusively. The polyurea was applied only to the free-span to avoid interaction between the strengthening material and the support reactions. The first cracks were observed in the midspan bed-joint at an approximate applied load of 0.4k (1.8kN). As testing progressed, the cracking at the midspan location continued to grow in width (see Figure 6.14), and minor flexural cracks were observed in the bed-joints outside of the constant moment region.   At an applied load of 1.5k (6.67kN), the polyurea strengthening material appeared to deform locally at the midspan region, and the midspan crack began to open very quickly. The wall maintained a relatively constant load resistance until reaching a midspan deflection of 4.20in. (106.7mm), where the first signs of rupture of the polyurea material were observed. As shown in Figure 6.14c, the polyurea began to rupture at midspan in several locations along the width of the wall. As the wall continued to undergo large deflections,

the wall began to separate into two segments and displayed rigid body deformation behavior. As the polyurea material continued to rupture, the load resistance of Wall P2-3 slowly decreased, as shown in Figure 6.15. Ultimately, the wall failed due to full rupture of the polyurea material, which occurred at a midspan deflection value of 7.01in. (178.1mm). Upon failure, the wall collapsed and separated into two half-wall segments (see Figure 6.14d).
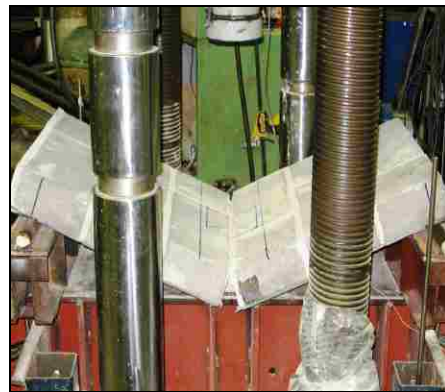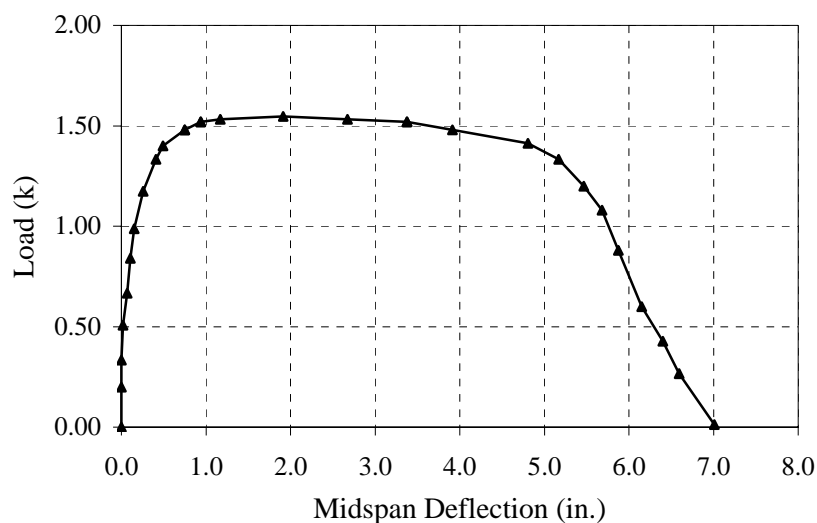

(a) Midspan Cracking   (b) Growth of Crack Width

(c) Rupture of Polyurea   (d) Wall Collapse

Figure 6.14. Wall P2-3 Failure

Conversions: 1 k = 4.448 kN; 1 in. = 25.4 mm

Figure 6.15. Load-Deflection Behavior – Wall P2-3

6.2.4. Wall P2-4. This wall was constructed from concrete block and was strengthened using the GFRP-polyurea retrofit system with one layer of grid material applied to the free-span of the wall. The first cracks occurred in the midspan bed-joint at an applied load of 0.9k (4.0kN). At a load of 3.9k (17.3kN), flexural cracks were observed in the CMU blocks throughout the constant moment region. As testing progressed, the formation of flexural cracking in the bed-joints of the shear-spans was observed. The first sign of flexural-shear cracking occurred at an applied load value of 6.4k (28.5kN) in the location of the shear-span and has been presented in Figure 6.16. The flexural-shear cracks originated from the points of load application and continued to grow until the masonry ruptured at an applied load of 10.1k (44.9kN) and a midspan deflection value of 0.87in. (22.1mm). After the masonry material had ruptured, the concrete masonry immediately debonded from the polyurea strengthening material, causing Wall P2-4 to collapse at the location of the support (see Figure 6.16b). The

maximum deflection achieved by Wall P2-4 was 0.96in. (24.4mm). The fracturing of the

masonry originating from the location of the applied load is presented in Figure 6.16c.

The load-deflection behavior for Wall P2-4 has been presented in Figure 6.17.
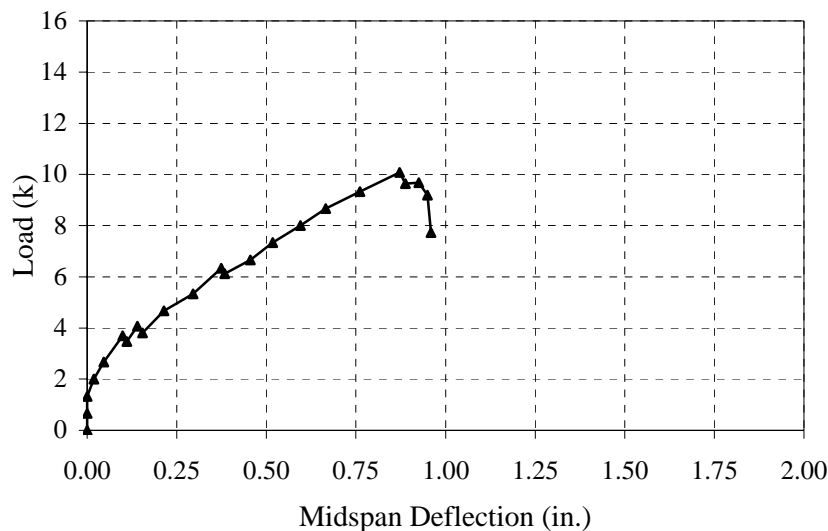

(a) Flexural-Shear Cracking   (b) Debonding of Masonry

(c) Fracturing of Masonry

Figure 6.16. Wall P2-4 Failure

Conversions: 1 k = 4.448 kN; 1 in. = 25.4 mm

Figure 6.17. Load-Deflection Behavior – Wall P2-4

6.2.5. Wall P2-5. Wall P2-5 was similar to Wall P2-4 in that this wall was constructed from concrete block and was strengthened with one layer of FRP grid material. However, the wall was also strengthened with the simulated retrofit anchorage condition. At an applied load of 3.4k (15.1kN), flexural cracks were observed throughout the constant moment region. Flexural-shear cracks were not observed until an approximate applied load of 8.0k (35.6kN) was reached. The flexural-shear cracks originated from the load application points and developed as the load increased. At an applied load value of 10.5k (46.7kN), rupture of the concrete masonry was observed in the shear-span as a result of flexural-shear cracking. However, unlike Wall P2-4, after the masonry ruptured, the load resistance continued to increase until the applied load of 11.3k (50.3kN) and a midspan deflection of 1.07in. (27.2mm) were achieved. At this point, the concrete masonry split through the shear-span causing the base masonry material to separate from the polyurea (see Figure 6.18). The ultimate deflection

achieved by Wall P2-5 was 1.16in. (29.5mm). The load-deflection behavior for the wall

has been presented in Figure 6.19.

(a) Separation from Polyurea   (b) Masonry Splitting

Figure 6.18. Wall P2-5 Failure
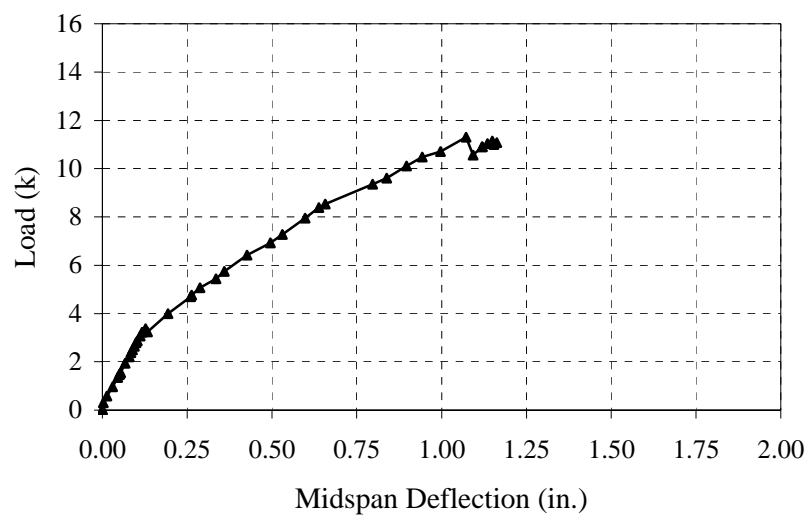
Conversions: 1 k = 4.448 kN; 1 in. = 25.4 mm

Figure 6.19. Load-Deflection Behavior – Wall P2-5

6.2.6. Wall P2-6. This wall was constructed from concrete block and was strengthened with the GFRP-polyurea retrofit using two layers of grid material embedded within the polyurea. The retrofit was applied to the free-span of the wall only to avoid interaction between the supports and the strengthening materials. The first flexural cracks were observed in the midspan bed-joint at an applied load of 0.7k (3.1kN). At a load of 4.0k (17.8kN), flexural cracks were observed in the concrete masonry units. As testing progressed, flexural cracks throughout the constant moment region as well as throughout both shear-spans were observed. At an applied load of 7.6k (33.8kN), the formation of the first major flexural-shear cracks were observed. Loading continued until reaching an applied load of 12.0k (53.4kN) and a midspan deflection of 0.54in. (13.7mm). At this point, the first sign of concrete rupture was observed in the masonry units immediately outside of the constant moment region originating from the applied load. The load resistance of the wall decreased significantly as the rupturing of the concrete masonry occurred. The rupturing of the masonry was the result of the flexural-shear cracking and is presented in Figure 6.20. As testing continued, the load resistance increased until the polyurea material debonded from the masonry at the support location (see Figure 6.20b), which occurred at a midspan deflection of 0.74in. (18.8mm). The sudden drop in the load resistance due to the initial rupturing of the masonry is illustrated by the load-deflection behavior presented in Figure 6.21. The figure also shows that the load resistance of Wall P2-6 continued to increase after the formation of the flexural-shear cracking until failure ultimately occurred by way of the debonding of the polyurea material from the base masonry material at the support location.

(a) Masonry Rupture

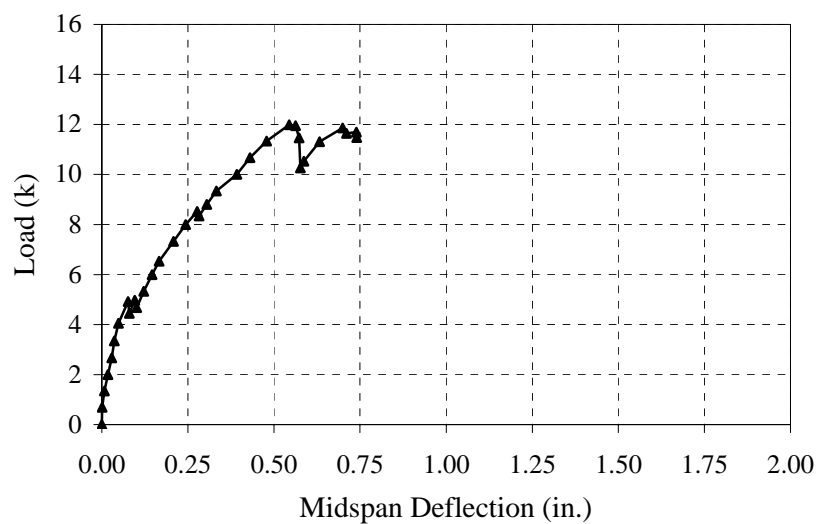(b) Debonding of Polyurea

(c) Separation of Masonry

(d) Wall Failure

Figure 6.20. Wall P2-6 Failure

Conversions: 1 k = 4.448 kN; 1 in. = 25.4 mm

Figure 6.21. Load-Deflection Behavior – Wall P2-6

6.2.7. Wall P2-7. Wall P2-7 utilized the same strengthening scheme as Wall P2-6, retrofitted with the GFRP-polyurea system using two layers of grid material embedded within the polyurea. Wall P2-7 was also constructed with the use of the simulated retrofit anchor. The behavior of Wall P2-7 was very similar to Wall P2-6. At an applied load of 4.3k (19.1kN), flexural cracks in the masonry units were observed. At an applied load of 7.0k (31.1kN), the first major flexural-shear cracks were observed in the shear-span of the wall. Almost immediately after the onset of flexural-shear cracking, the concrete masonry began to rupture as a result of the splitting action from the flexural-shear (see Figure 6.22a). In addition to the splitting action of the masonry, longitudinal cracking was observed in the shear-span location on the compression face of the wall. At 11.5k (51.2kN), the concrete began to split off from the surface, and the flexural-shear cracks had opened significantly, resulting in a slight decrease in the load resistance. As loading continued, the flexural-shear cracks continued to develop, and the masonry began to split and separate from the polyurea. At a midspan deflection of 0.82in. (20.8mm), the strengthened URM wall achieved its maximum load resistance of 14.1k (62.7kN). Beyond this point, the wall maintained significant resistance until the masonry split as a result of the flexural-shear cracking and ultimately separated away from the polyurea material in the shear-span (see Figure 6.22c). The maximum deflection achieved by Wall P2-7 was 0.94in. (23.9mm). The load-deflection behavior for Wall P2-7 has been presented in Figure 6.23. From the load-deflection behavior the ability of the wall to maintain load resistance even after the formation of the significant flexural-shear cracks can be seen.
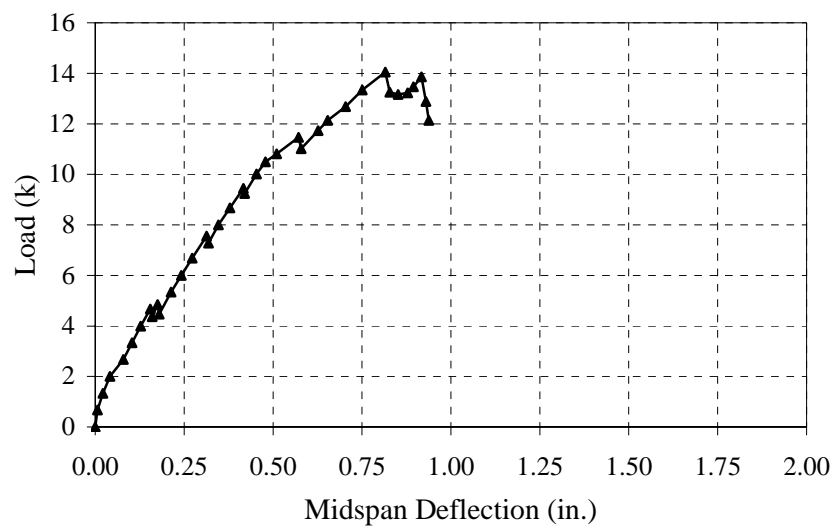
(a) Flexural-Shear Cracks

(b) Longitudinal Cracking

(c) Flexural-Shear Failure

Figure 6.22. Wall P2-7 Failure

Conversions: 1 k = 4.448 kN; 1 in. = 25.4 mm

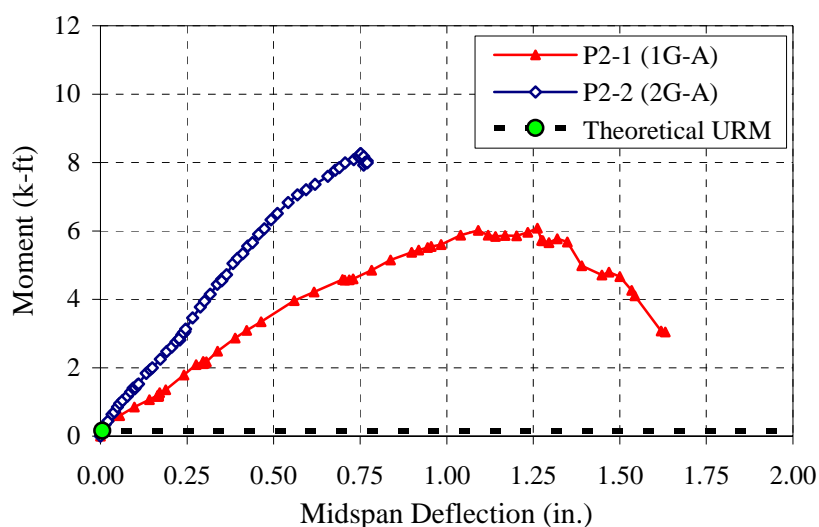Figure 6.23. Load-Deflection Behavior – Wall P2-7

6.3. DISCUSSION

The following section provides discussion on the presented test results from Phase 2 of the research program. A detailed analysis regarding the influence of the strengthening methods that were used to retrofit the URM walls has been provided. Additionally, the simulated retrofit anchorage condition and its affect on the governing mode of failure is addressed in this section of the thesis. The results have been compared to theoretical predictions.

6.3.1. Influence of Retrofit Scheme. From the Phase 2 test results, it can be seen that the GFRP-polyurea retrofit system was highly effective in improving the behavior of the slender URM walls in terms of capacity as well as deformation. For the purpose of quantifying the improvement of the strengthened URM walls, the results from the experimental testing have been compared to theoretical predictions of the load capacity and the ultimate deflection of non-retrofitted URM walls. The load resistance of the strengthened URM walls has been presented in terms of their respective moment resistances. The theoretical capacity and ultimate midspan deflection of the non-retrofitted URM walls is represented by the solid circular data-point included in the following figures presenting the moment-deflection behavior. For the purpose of clarification, in addition to the name of each wall, a unique set of descriptor characters provided in parentheses has been presented in the figures and illustrations provided in this section of the thesis. The first set of descriptor characters corresponds to the strengthening materials used to retrofit the walls. Characters '1G' corresponds to the use of one layer of GFRP material embedded within polyurea, '2G' corresponds to the use of two layers of GFRP material embedded within polyurea, and the character 'P'

corresponds to the use of the polyurea material exclusively. The second set of characters is used to indicate the retrofit anchorage condition. The character 'A' corresponds to the anchored retrofit, and the characters 'UA' correspond to the unanchored retrofit.
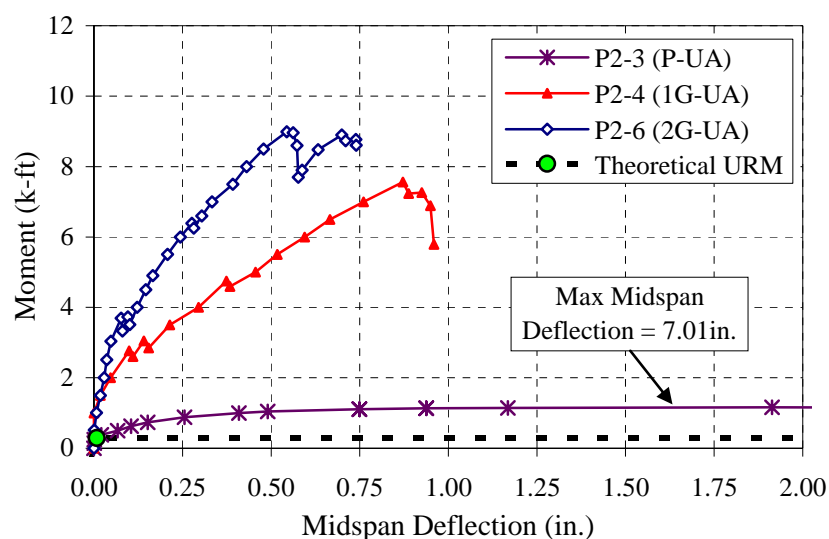
The moment-deflection behavior for the walls constructed from the clay base masonry, Walls P2-1 and P2-2, is presented in Figure 6.24. Walls P2-1 and P2-2 were strengthened using the anchored GFRP-polyurea retrofit with one and two layers of GFRP, respectively. In comparison to the negligible out-of-plane load resistance and deformation capability of the theoretical URM wall, the strengthened walls possessed superior capability in terms of load resistance as well as energy absorption. As a result of the external strengthening, the moment capacity of the clay masonry walls increased by factors of 38 times and 52 times that of the theoretical URM for Walls P2-1 and P2-2, respectively. Figure 6.24 also shows the increase in the wall stiffness and the reduction in deflection as the level of external reinforcement increased.
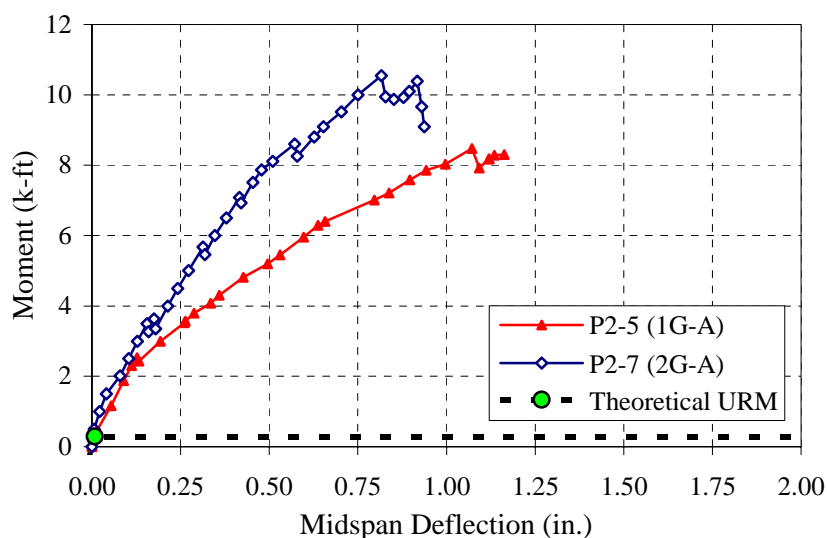

Conversions: 1 k-ft = 1.356 kN-m; 1 in. = 25.4 mm

Figure 6.24. Moment-Deflection Behavior: Clay (A) Phase 2 Walls

The behavior of the strengthened CMU walls without retrofit anchorage is presented in Figure 6.25. The figure highlights the difference in wall behavior due to the retrofit scheme. It can be seen that Wall P2-3, which was strengthened using polyurea exclusively, showed only marginal improvement in terms of load resistance, achieving a moment capacity of four times that of the theoretical URM. However, in terms of midspan deflection capability, Wall P2-3 showed a dramatic improvement over the unstrengthened theoretical wall capacity and showed potential in terms of energy absorption. Walls P2-4 and P2-6 were strengthened using the GFRP-polyurea retrofit. Their response behavior was similar to the response of the strengthened clay walls presented in Figure 6.24.

Conversions: 1 k-ft = 1.356 kN-m; 1 in. = 25.4 mm

Figure 6.25. Moment-Deflection Behavior: CMU (UA) Phase 2 Walls

Lastly, the behavior of the retrofit-anchored, strengthened CMU walls has been provided in Figure 6.26. The moment-deflection response shows similar behavior to the

previously presented results for the GFRP-polyurea strengthened walls. The external

reinforcement resulted in a dramatic increase in the capacity, with resulting capacities of

29 and 36 times that of the theoretical URM wall for Walls P2-5 and P2-7, respectively.
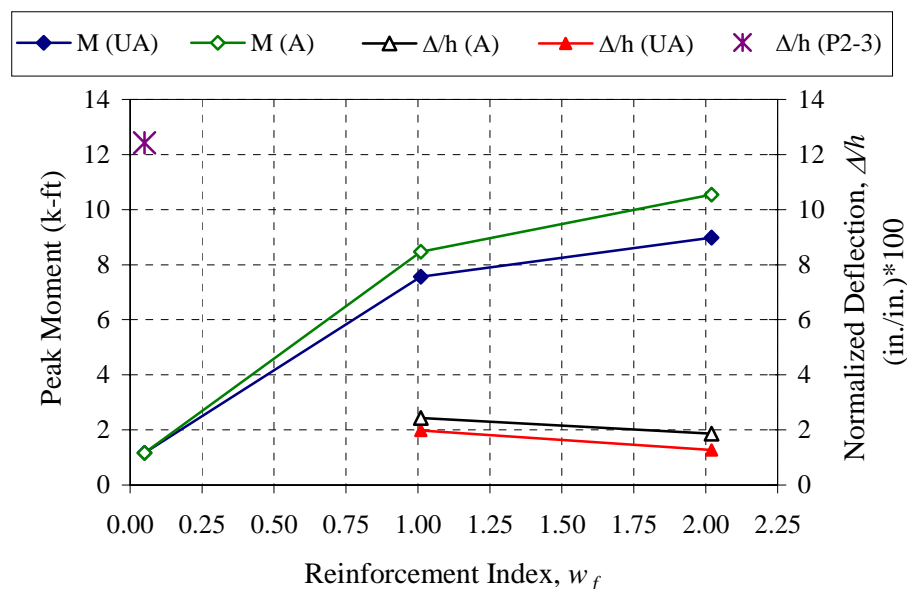

Conversions: 1 k-ft = 1.356 kN-m; 1 in. = 25.4 mm

Figure 6.26. Moment-Deflection Behavior: CMU (A) Phase 2 Walls

The relationship between the external reinforcement level and the resulting peak

moment capacity, as well as the relationship between the reinforcement level and the

normalized midspan deflection for the CMU walls has been provided in Figure 6.27. The

results from the anchored and unanchored retrofit methods have been presented

separately in the figure. It should be noted that in the case of the URM walls

strengthened using the GFRP-polyurea retrofit, the ultimate midspan deflection is

assumed to be that which corresponds to the peak moment resistance. In the case of the

Phase 2 polyurea strengthened URM wall, Wall P2-3, the ultimate deflection was taken

to be a value of 5.43in. (137.9mm). This point does not correspond to the peak moment

resistance, but rather to the point at which the moment-deflection behavior of Wall P2-3 becomes critically unstable. The reinforcement level of the URM walls has been expressed in terms of the reinforcement index, w_f, previously defined by Equation (5).

The relationship presented in Figure 6.27 shows slight adverse effects on the deformation ability of the strengthened URM walls as a result of increasing the level of reinforcement. Because Wall P2-3 was retrofitted using a different strengthening scheme than all other Phase 2 walls, the deformation relationship could not be established for walls strengthened with low levels of the GFRP-polyurea retrofit. For comparison purposes, the normalized deflection of Wall P2-3 is also included in Figure 6.27.

Conversions: 1 k-ft = 1.356 kN-m; 1 in./in. = 1 mm/mm

Figure 6.27. Influence of Reinforcement Level for CMU Walls

It can be seen that Wall P2-3 possessed high deformation capability in comparison to walls strengthened with higher levels of reinforcement. Although it is

expected that walls strengthened with the GFRP-polyurea retrofit at low reinforcement levels would possess an increased deflection capability over those presented, it is not expected that they would deform as illustrated by Wall P2-3 in Figure 6.27.

The effect of the retrofit anchorage is shown in the following two illustrations. Figure 6.28 presents the moment-deflection behavior of the strengthened CMU walls retrofitted with a single layer of GFRP, and Figure 6.29 presents the behavior of the strengthened CMU walls strengthened with two layers of GFRP. Both figures show that the use of the simulated retrofit anchor resulted in both an increase in the ultimate moment capacity as well as an increase in the ultimate deflection. In the case of the walls strengthened using the unanchored retrofit condition, debonding of the polyurea immediately followed the rupture of the masonry due to flexural-shear cracking. Walls strengthened using the anchored retrofit were capable of resisting load after the significant development of flexural-shear cracks.
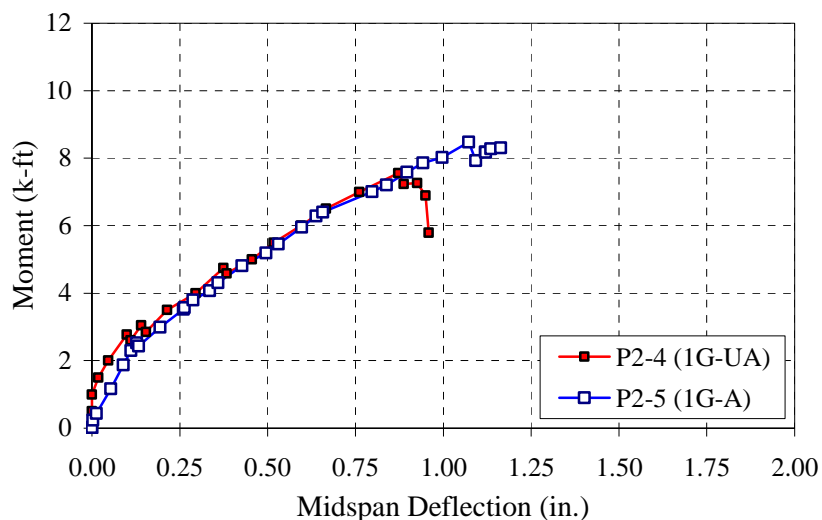
Conversions: 1 k-ft = 1.356 kN-m; 1 in. = 25.4 mm

Figure 6.28. Effect of Retrofit Anchorage: Single Layer of GFRP (1G)
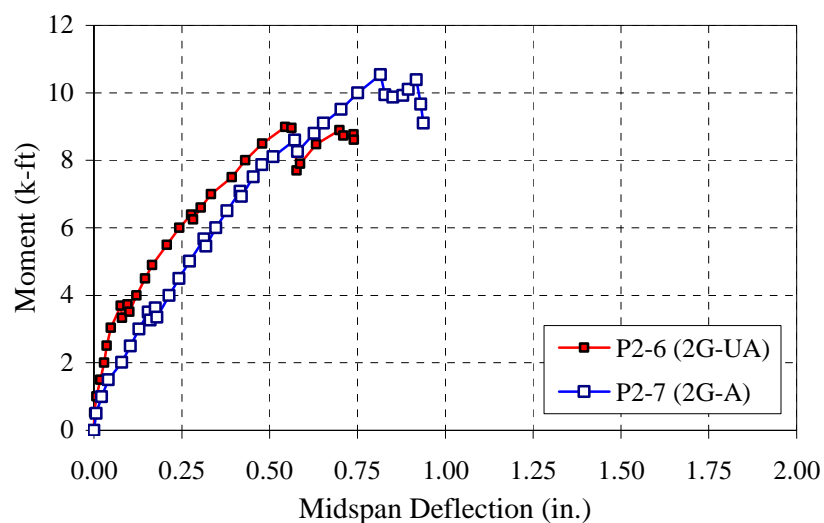
Conversions: 1 k-ft = 1.356 kN-m; 1 in. = 25.4 mm

Figure 6.29. Effect of Retrofit Anchorage: Two Layers of GFRP (2G)

With the exception of the Wall P2-3, which was retrofitted using polyurea only,

the failure of all the Phase 2 walls was attributed to some form of flexural-shear. The

failure modes from the testing of the Phase 2 walls have been summarized in Table 6.2.

Table 6.2. Summary of Failure Modes for Phase 2 Walls

Wall	Failure Mode
P2-1	Masonry rupture due to unit splitting; flexural-shear failure
P2-2	Masonry rupture due to unit splitting; flexural-shear failure
P2-3	Polyurea rupture; tensile failure
P2-4	Masonry rupture followed by debonding of polyurea; flexural-shear failure
P2-5	Masonry rupture due to unit splitting; flexural-shear failure
P2-6	Masonry rupture followed by debonding of polyurea; flexural-shear failure
P2-7	Masonry rupture due to unit splitting; flexural-shear failure

The energy absorption of the Phase 2 walls has been quantified by way of the external work done by each of the strengthened URM walls. The external work done by each wall serves as a direct relation to the strain energy absorbed by the strengthened walls. Portions of the load-deflection response demonstrating critically unstable behavior were not considered. Figure 6.30 shows that the external work done by the URM wall retrofitted with only polyurea, Wall P2-3, exhibited similar energy absorption characteristics to the other walls in this phase of the study strengthened using the GFRP-polyurea retrofit. Additionally, in the case of the CMU walls retrofitted with GFRP-polyurea, the increased level of external reinforcement had little or no effect on the external work done by the walls. However, the use of the simulated retrofit anchor resulted in significant improvement in the amount of external work done by the GFRP strengthened CMU walls.
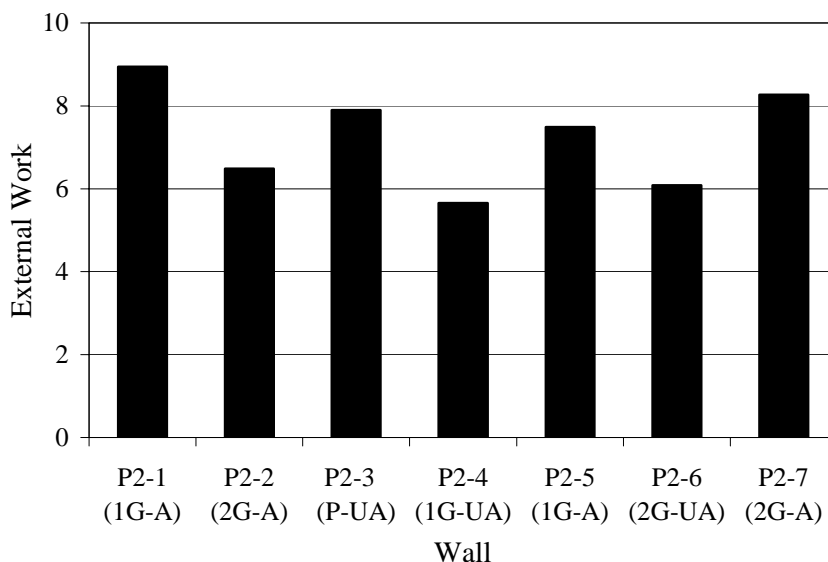
Figure 6.30. External Work Done by Phase 2 Walls

The peak moment resistances of the Phase 2 URM walls have been summarized in Figure 6.31. As the level of reinforcement increased, the capacity increased; the use of the retrofit anchorage system also resulted in an increase in capacity. Figure 6.31 also highlights the significant difference in load resistance capability among the polyurea retrofitted wall, Wall P2-3, and all other walls that were retrofitted using the GFRP-polyurea system.
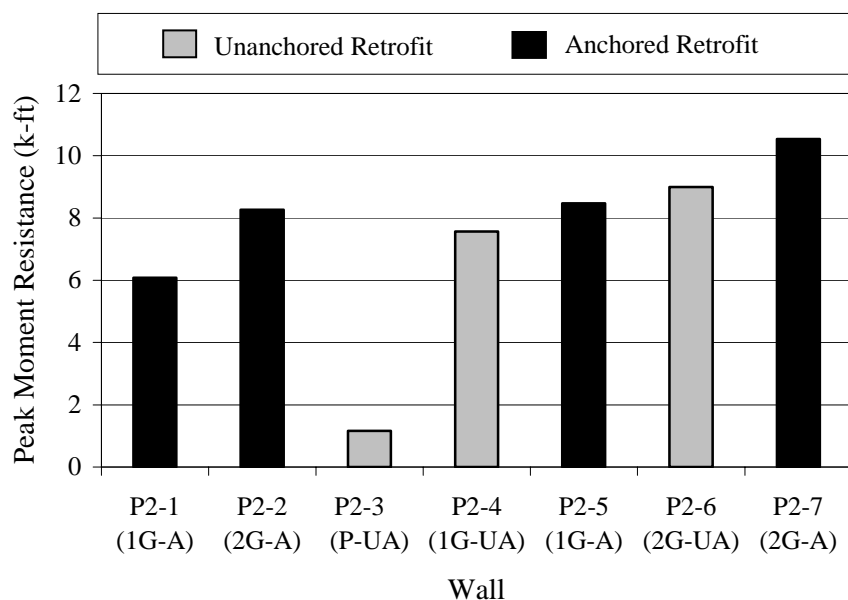
Conversions: 1 k-ft = 1.356 kN-m

Figure 6.31. Peak Moment Resistance for Phase 2 Walls

6.3.2. Analytical Predictions. To further assess the validity of the data obtained from testing, the experimental results for the GFRP-polyurea strengthened URM walls have been compared with theoretical analysis. The theoretical moment capacity was obtained using a moment-curvature approach for the cracking and the ultimate limit state. It was assumed that the distribution of stress in the masonry could be modeled using a

parabola and that at the ultimate limit state, the net compressive strength of the masonry was applicable due to the geometry of the masonry units used in the study.

The strain level in the masonry at the peak and ultimate response was assumed to be governed by the recommended values from the Building Code Requirements for Masonry Structures (ACI 530-02/ASCE 5-02/TMS 402-02), previously defined in Equations (32) and (33).

The theoretical midspan deflection was obtained using the conjugate beam method. When curvature is applied to the URM wall in the form of an external load, the midspan deflection of the URM wall at the state of masonry cracking can be determined using Equation (40):

$$\Delta_{cr} = \phi_{cr} \left(\frac{L^2}{8} - \frac{a^2}{6} \right) \tag{40}$$

where ϕ_{cr} represents the curvature in the URM wall at the cracking stage, and a represents the distance from the support to the applied load. Note that it was assumed that first cracking would occur in the interface of the mortar and masonry units, and the tensile resistance of the masonry at these locations was equal to that determined from the flexural bond test results previously presented in Section 3.

At the ultimate limit state, the midspan deflection can be determined using Equation (41):

$$\Delta_u = \frac{a(\phi_{cr} - \phi_u)}{6}(a + x_{uc}) + \frac{\phi_u}{6}\left(\frac{3 \cdot L^2}{4} - x_{uc}^{\ 2}\right) \tag{41}$$

where ϕ_u represents the curvature in the URM wall at the ultimate limit state, and

x_{uc} represents the theoretical uncracked length of the URM wall at the support location.

However, because the moment varies linearly between the support reaction and the

applied load, the uncracked length can be presented in terms of the cracking moment,

M_{cr}, and the ultimate moment, M_u, as follows:

$$\Delta_u = \frac{a^2(\phi_{cr} - \phi_u)}{6}\left(1 + \frac{M_{cr}}{M_u}\right) + \frac{\phi_u}{6}\left(\frac{3 \cdot L^2}{4} - \left(\frac{a \cdot M_{cr}}{M_u}\right)^2\right) \tag{42}$$

In addition to the flexural capacity, the nominal shear capacity of the masonry

walls was also calculated to determine the theoretical controlling mode of failure. The

nominal shear capacity, V_m, was obtained using Equation 3-21 from the Building Code

Requirements for Masonry Structures (ACI 530-02/ASCE 5-02/TMS 402-02):

$$V_m = \left[4.0 - 1.75\left(\frac{M_a}{V_a \cdot d_v}\right)\right]A_n\sqrt{f'_{m,n}} \tag{43}$$

where M_a represents the applied moment at the section under consideration, V_a represents

the applied shear force at the section under consideration, d_v represents the depth of the

masonry in the direction of the shear, A_n represents the net cross-sectional area of the

URM wall, and $f'_{m,n}$ represents the net compressive strength of the masonry. It should be noted that because the thickness of the implemented retrofits were quite significant, the net cross-sectional area includes the thickness of the strengthening materials.

The results from the moment-curvature analysis have been provided on the moment versus midspan deflection plot for each wall. Walls constructed from like-base masonry materials and strengthened with the same level of reinforcement have been presented together. The ultimate condition is based upon the assumed crushing strain of the masonry or the theoretical shear capacity; however, note that in all cases, the theoretical bending capacity was the controlling mode of failure. A single data-point has been provided beyond the theoretical crushing strain to illustrate the potential analytical behavior of masonry capable of reaching higher strain levels than those assumed.

Figure 6.32 shows that the theoretical analysis of the clay wall reinforced with a single layer of GFRP, Wall P2-1, appears to accurately predict the cracking behavior and the initial stiffness of the URM wall. However, the performed moment-curvature analysis does not account for the onset of flexural-shear cracking and the resulting degradation in wall stiffness. As a result, the theoretical analysis resulted in a grossly underestimated prediction of the ultimate midspan deflection. The theoretical prediction of the moment capacity of Wall P2-1 at the assumed point of theoretical crushing also resulted in underestimation of approximately 12 percent. The experimental capacity obtained for this wall actually falls between the theoretical bending moment-capacity and the moment-capacity determined from the theoretical shear resistance. Although the theoretical methodology used was not capable of accurately predicting experimental values for Wall P2-1, the predictions were comparable with the experimental values.
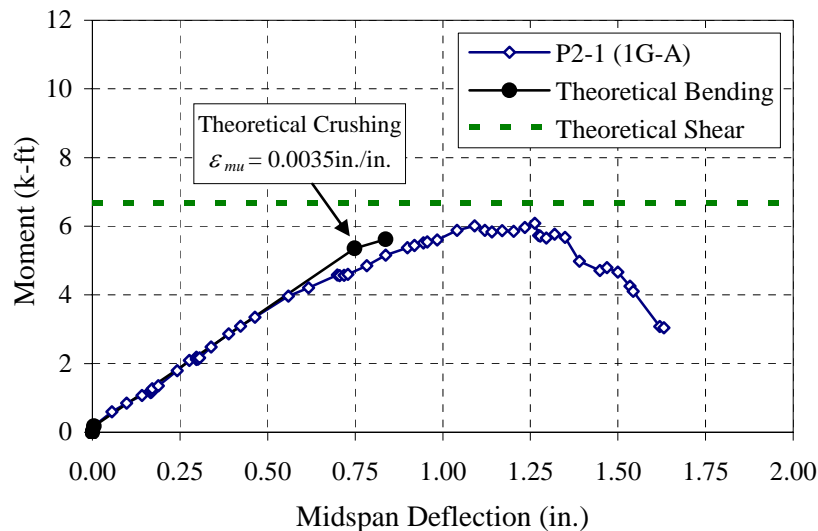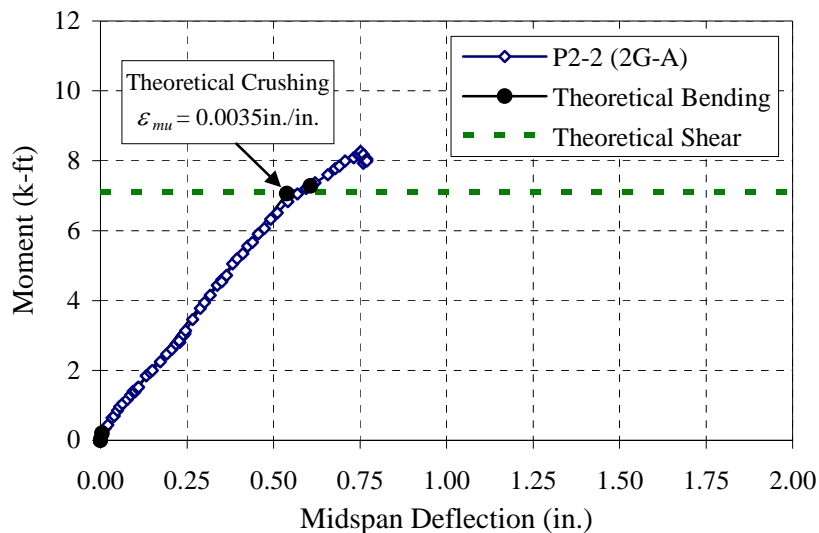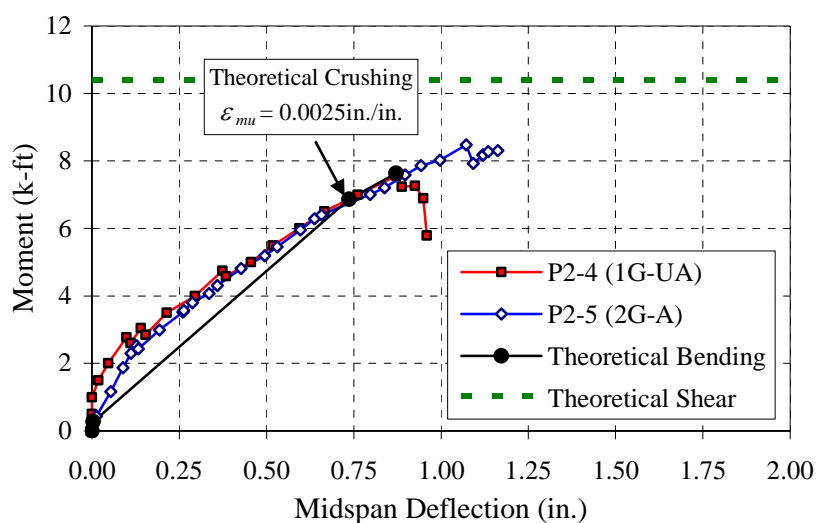
Conversions: 1 k-ft = 1.356 kN-m; 1 in. = 25.4 mm; 1 in./in. = 1 mm/mm

Figure 6.32. Analytical Prediction, Wall P2-1

The analytical behavior of the clay wall strengthened with two layers of GFRP, Wall P2-2, is presented in Figure 6.33. The analytical values match the wall behavior well in terms of initial cracking and wall stiffness. It appears as though the theoretical crushing value, as well as the theoretical shear capacity, matches with the point at which the onset of masonry rupture as a result of the flexural-shear behavior was observed. However, because the moment resistance of Wall P2-2 continued to increase after the occurrence of the flexural-shear induced rupture, the theoretical analysis at the assumed point of crushing resulted in underestimation of the moment capacity by approximately 14 percent, and underestimation of the ultimate midspan deflection by approximately 25 percent.

The experimental results from the two CMU walls strengthened with a single layer of GFRP, Walls P2-4 and P2-5, have been presented in Figure 6.34 and have been compared with analytical values. Note that the analytical values at the ultimate limit

Conversions: 1 k-ft = 1.356 kN-m; 1 in. = 25.4 mm; 1 in./in. = 1 mm/mm

Figure 6.33. Analytical Prediction, Wall P2-2

state coincide much better with Wall P2-4 than Wall P2-5. This result occurs because

Wall P2-4 failed immediately after the masonry ruptured as a result of flexural-shearing,

and the moment resistance of Wall P2-5 continued to increase after masonry rupture was

observed. Also, note that the predicted analytical stiffness of the strengthened CMU

walls is much lower than the measured response, which is most likely due to the

geometry of the CMU units and the overall geometry of the URM wall. Because the

walls constructed from the concrete block had much larger spacing between bed-joints,

cracking was not strictly limited to the location of the bed-joints as was observed in the

case of the clay URM walls, but it also occurred in the concrete block units. As a result,

the strengthened CMU walls were capable of maintaining much higher stiffnesses than

their clay wall counterparts. The secondary cracking behavior was not considered in the

analytical predictions, as the occurrence of such behavior will greatly vary depending

upon the overall geometry of the URM wall and the geometry of the masonry units.

Figure 6.34 shows that the analytical bending capacity predictions seem quite reasonable in comparison to Wall P2-4, but they grossly underestimate both the moment capacity and ultimate midspan deflection of Wall P2-5. The analytical prediction of the moment capacity of Walls P2-4 and P2-5 at the ultimate limit state based on the assumed theoretical crushing strain for concrete masonry underestimated the moment capacity by approximately 9 percent for Wall P2-4 and by approximately 19 percent for Wall P2-5.
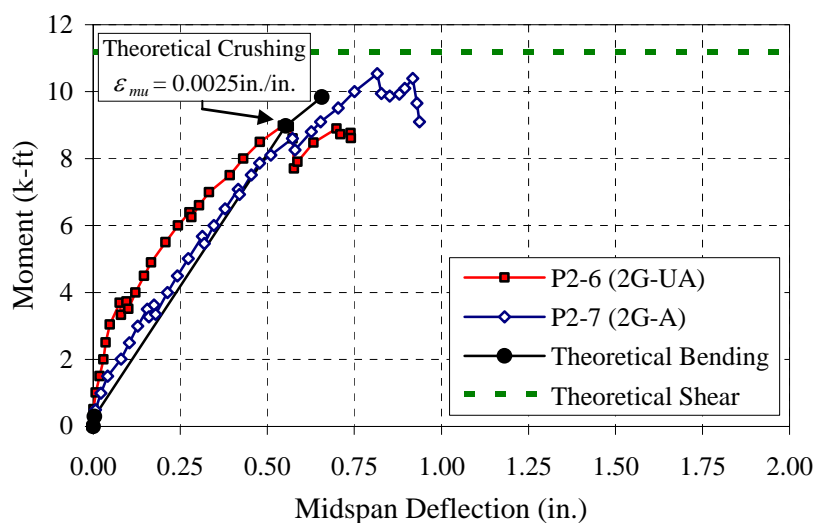

Conversions: 1 k-ft = 1.356 kN-m; 1 in. = 25.4 mm; 1 in./in. = 1 mm/mm

Figure 6.34. Analytical Prediction, Walls P2-4 and P2-5

The measured responses from the CMU walls strengthened with two layers of GFRP, Walls P2-6 and P2-7, are presented in Figure 6.35 and have been compared with analytical results. The theoretical behavior under-predicts the initial stiffness of the strengthened URM walls similarly to that presented in Figure 6.34. However, the analytical prediction at the ultimate limit state is very accurate when compared to the measured response of Wall P2-6, that resulted in theoretical values within 1 percent of the experimental values for both moment capacity and the ultimate midspan deflection.

When compared to Wall P2-7, the theoretical bending capacity at the ultimate limit state

under-predicts the moment capacity by 14 percent and under-predicts the ultimate

midspan deflection by more than 30 percent. However, the moment corresponding to the

ultimate shear capacity of the URM wall is very accurate in predicting the failure load of

Wall P2-7.

Conversions: 1 k-ft = 1.356 kN-m; 1 in. = 25.4 mm; 1 in./in. = 1 mm/mm

Figure 6.35. Analytical Prediction, Walls P2-6 and P2-7

The previously presented illustrations clearly show that the resulting theoretical

values produced using the moment-curvature analysis and assumed values for the

ultimate achievable strain in the masonry were relatively accurate for the walls

strengthened using the unanchored retrofit strategy. It was also shown that this

methodology was also shown to grossly underestimate the capacity as well as the

deformation capability of the strengthened URM walls utilizing the simulated anchored

retrofit condition. A numerical comparison between the analytical results and the

experimental results at the ultimate limit state for the GFRP strengthened URM walls has

been presented in Table 6.3.

Table 6.3. Comparison of Analytical Results – Phase 2 Walls

Wall	Experimental Moment Capacity k-ft (kN-m) (1)	Experiment Ultimate Deflection in. (mm) (2)	Analytical Moment Capacity k-ft (kN-m) (3)	Analytical Ultimate Deflection in. (mm) (4)	(3)/(1)	(4)/(2)
P2-1	6.08 (8.24)	1.26 (32.0)	5.35 (7.25)	0.75 (19.1)	0.88	0.60
P2-2	8.26 (11.20)	0.75 (19.1)	7.06 (9.57)	0.54 (13.7)	0.85	0.72
P2-4[*]	7.52 (10.20)	0.88 (22.4)	6.86 (9.30)	0.74 (18.8)	0.91	0.84
P2-5	8.47 (11.48)	1.07 (27.2)	6.86 (9.30)	0.74 (18.8)	0.81	0.69
P2-6[*]	8.99 (12.19)	0.54 (13.7)	8.97 (12.16)	0.55 (14.0)	1.00	1.02
P2-7	10.54 (14.29)	0.82 (20.8)	8.97 (12.16)	0.55 (14.0)	0.85	0.67

* Unanchored Retrofit Condition

7. GENERAL DISCUSSION AND CONSIDERATIONS

The following section has been provided to compare the results from both phases of study and provide more general discussion regarding the behavior of the URM walls tested. The influence of the arching effect and the limitations associated with strengthening URM walls has been addressed.

7.1. INFLUENCE OF ARCHING

From the results presented in Section 5 of this thesis, it is apparent that the formation of an arching mechanism had a significant effect on the behavior of the Phase 1 walls. As outlined previously in this thesis, literature suggests that the addition of in-plane membrane forces due to the deformation of non-slender framed infills can result in significant increases in the out-of-plane load capacity of both strengthened and unstrengthened URM infill walls. In an effort to assess the influence of the arching effect on the walls tested in this research program, results from the non-slender arching walls from Phase 1 have been compared with the results from the testing of the slender walls from Phase 2. The comparison has been limited to walls constructed from CMU masonry to avoid influence from the simulated retrofit anchor which was used for the Phase 2 clay walls. Because the walls from Phase 1 and Phase 2 of the research program were evaluated using different test methods, the results cannot be compared directly. For comparative purposes, the equivalent uniform pressure results from the Phase 1 walls have been presented in terms of their total static moments. Using the total static moment allows for direct comparison between the load-capacity results from the two phases of study. Additionally, the total static moment results from Phase 1 were reduced by a

multiplier of 0.67 to account for the difference in URM wall width between the two phases of study. The span length of the CMU walls varied slightly between the two phases with a length of 48in. (1,219mm) for the Phase 1 walls and a length of 44in. (1,118mm) for the Phase 2 walls. Presenting the load resistance in terms of the total moment will account for this variation in span length; however, note that no additional modification has been made to adjust the midspan deflections. For the purpose of clarification, in addition to the name of each wall, a unique set of descriptor characters provided in parentheses has been presented in the figures and illustrations provided in this section of the thesis. The first set of descriptor characters corresponds to the strengthening materials used to retrofit the walls. The characters '1G' correspond to one layer of FRP grid embedded within polyurea, and the character 'P' corresponds to the use of the polyurea material exclusively. The second set of characters is used to indicate the slenderness condition for each wall. The characters 'NS' correspond to framed non-slender walls, and the character 'S' corresponds to slender walls.

The total moment-deflection behavior for the CMU walls from both phases of study has been presented in Figure 7.1. The unstrengthened URM arching wall, Wall P1-3, greatly outperformed the theoretical behavior of a slender URM wall in terms of both moment capacity and deformation capability. Similarly, the Phase 1 wall strengthened using the polyurea retrofit, Wall P1-4, achieved a much larger moment capacity than its slender counterpart, Wall P2-3. However, both the slender and non-slender polyurea retrofitted walls possessed significant deflection capability. For the walls strengthened using the GFRP-polyurea retrofit, the slender wall slightly outperformed the non-slender wall in terms of both moment capacity and deflection. Figure 7.1 shows that Wall P1-5

exhibited a stiffer response than Wall P2-4, and it is believed that had Wall P1-5 not

failed prematurely due to lack of anchorage at the boundary connection, it would have

ultimately outperformed Wall P2-4 in terms of moment capacity due to the arching effect.

This is based on the fact that only minor damage had occurred to the mortar in the bed-

joints of Wall P1-5 and that essentially no damage had occurred to the masonry units

prior to the delamination of the polyurea from the surrounding frame elements.
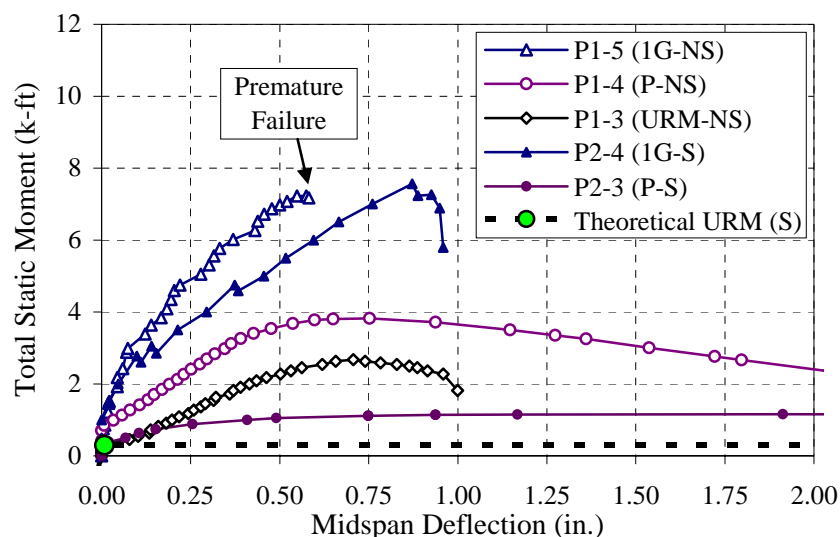
Conversions: 1 k-ft = 1.356 kN-m; 1 in. = 25.4 mm

Figure 7.1. Total Moment-Deflection Behavior, CMU Walls

The peak total static moment capacities are presented in Figure 7.2. The capacity

results have been presented separately for each retrofit scheme. The arching effect

resulted in significant increases in the total moment capacity for both the unstrengthened

URM walls and the URM walls retrofitted with polyurea exclusively. The peak total

moment resistances for the URM walls strengthened with the GFRP-polyurea retrofit

were comparable for slender and non-slender walls. However, as previously stated, it is

believed that the non-slender wall strengthened with the GFRP-polyurea retrofit would have ultimately outperformed its slender counterpart had it not failed prematurely from lack of anchorage at the boundary locations.

Conversions: 1 k-ft = 1.356 kN-m
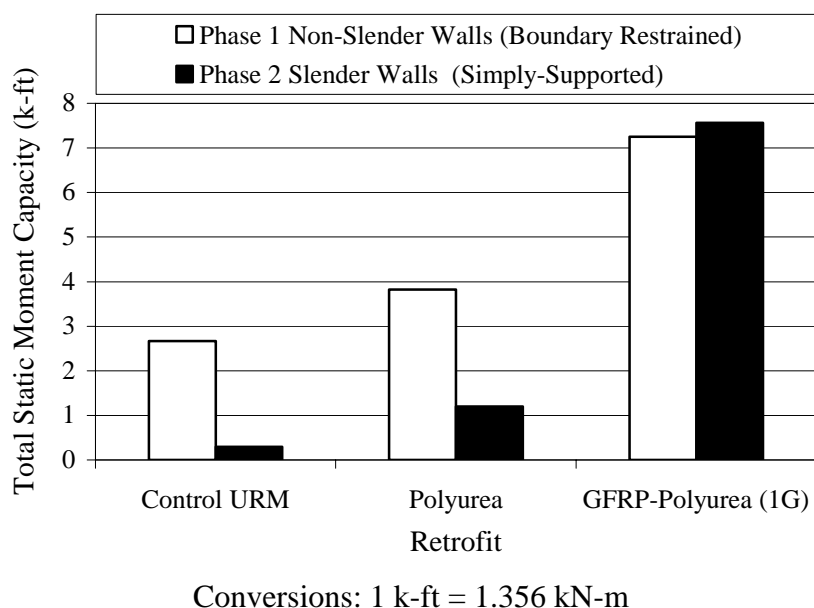
Figure 7.2. Peak Total Static Moment Capacity, CMU Walls

7.2. STRENGTHENING LIMITATIONS

The test results from this research program, as well as the results from previous studies, have shown that URM walls that exhibit arching behavior due to low height-to-thickness ratios and rigid boundary restraints can greatly outperform URM walls that do not exhibit an arching effect. However, because arching walls possess significant out-of-plane capacity prior to undergoing retrofit, the same level of capacity increase due to external strengthening that is realized by slender walls is not expected to be achieved by non-slender arching walls. To quantify the increase in the out-of-plane capacity of the URM walls due to the retrofits implemented in this study, the normalized capacities of

both the slender and non-slender URM walls have been provided in Figure 7.3. The

capacity results from both phases of study have been normalized with respect to the

unstrengthened URM walls from each phase of study.
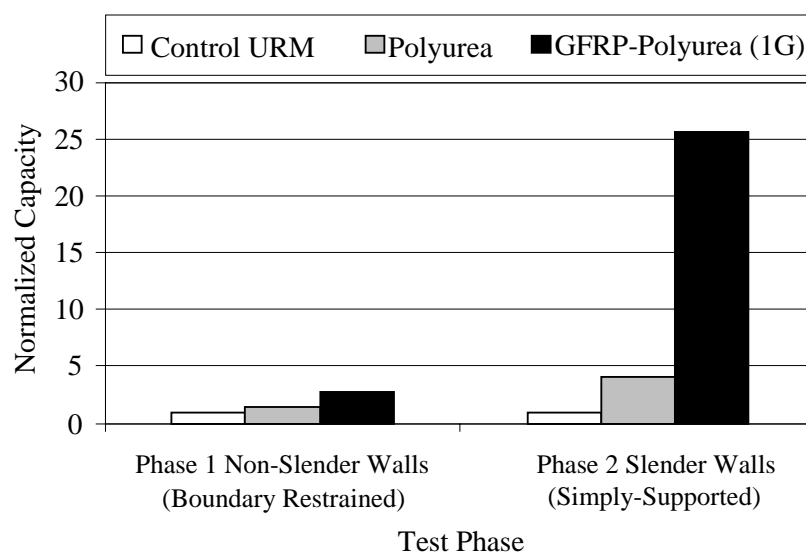
Figure 7.3. Normalized Total Static Moment, CMU Walls

Figure 7.3 shows that the additional capacity achieved by way of the URM wall

retrofits differs dramatically between the Phase 1 non-slender walls and the Phase 2

slender walls. For the Phase 1 walls, the employed retrofits resulted in relatively minor

increases in load resistance with normalized capacity values of 1.4 for the polyurea

retrofitted wall and 2.7 for the GFRP-polyurea retrofitted wall. In the case of the slender

URM walls, much greater increases in the load resistance resulted from the use of the

retrofits. The use of the polyurea retrofit for the slender CMU wall resulted in a

normalized capacity value of approximately 4.1, and the use of the GFRP-polyurea

retrofit resulted in a normalized capacity of approximately 25.6.

The effectiveness or the amount of improvement in capacity as a result of retrofitting URM walls has been shown to be highly dependent upon wall slenderness. The experimental results from this study showed that only marginal increases in capacity were achieved by non-slender walls exhibiting an arching condition as a result of the retrofit systems. To further explain this behavior, the analytical model presented in Section 5 was used to run several trial cases and establish a theoretical relationship between the developed in-plane membrane forces as a result of the arching effect and the force contribution from external reinforcement. The interaction between the compressive arch-thrust force and the tensile force in the reinforcement is presented in Figure 7.4.
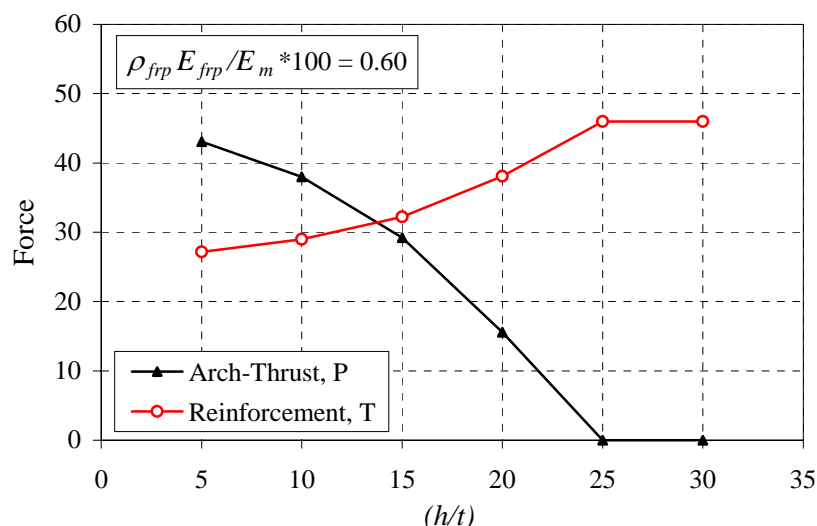
Figure 7.4. Arch-Thrust and Reinforcement Interaction

The relationship presented in Figure 7.4 suggests that the effect of arching decreases as the height-to-thickness ratio of a URM wall increases. Conversely, the figure also suggests that the force contribution from the external reinforcement increases as the height-to-thickness ratio of the URM wall increases. The interaction relationship

shown in Figure 7.4 will vary greatly depending upon the level of reinforcement and the material used in both the masonry construction as well as the URM wall retrofit. Note that because the relationship presented in Figure 7.4 was analytically generated, it is not intended to serve as true interaction behavior but only to illustrate a general trend as the figure does not consider premature failure modes and is only applicable for the level of reinforcement presented. The general interaction relationship presented in Figure 7.4 agrees well with the findings from the experimental study performed in this research program.

8. CONCLUSIONS AND RECOMMENDATIONS

This thesis has shown that external retrofit systems can be used to strengthen URM walls subjected to out-of-plane loading, and that the associated out-of-plane behavior of URM wall systems under quasi-static loading can potentially be improved as a result of external retrofit systems. The objective of this research was to investigate the use of modern materials to improve the overall behavior of URM infill walls and to mitigate the effects of blast. However, because the walls in this study were evaluated under quasi-static conditions exclusively, the findings from this thesis may serve only as a potential indicator of URM wall behavior due to actual blast events. Within this research program, the influence of retrofit scheme, base masonry material, and support conditions associated with strengthened infills have been investigated.

8.1. PHASE 1 – NON-SLENDER INFILLS

The following conclusions can be drawn from the Phase 1 investigation on non-slender infills:

- All of the strengthening techniques used in Phase 1 of the research program resulted in an increase in the out-of-plane load capacity, although the use of the polyurea retrofit resulted in only marginal capacity improvement by way of providing additional stability.

- The use of the spray-on polyurea material essentially eliminated all fragmentation and debris scatter upon the collapse and failure of the Phase 1 URM walls. This attribute is essential in reducing the amount of injuries and loss of human life

under actual blast events. However, it is uncertain as to whether the same level of debris scatter reduction would have occurred under actual impulsive blast events.

- All of the retrofit systems investigated in this study resulted in an increase in the energy absorption capability of the URM walls. Walls retrofitted exclusively with the spray-on polyurea greatly outperformed all other Phase 1 walls in terms of out-of-plane deformation capability.

- Although some crushing did occur in the masonry, the ultimate failure mode of the URM walls strengthened with the GFRP-polyurea retrofit was attributed to failure of anchorage between the polyruea and the surrounding frame elements.

- The use of the WF-FA base masonry material resulted in improvement in wall deformation capability when compared to traditional base masonry materials, and it also resulted in comparable load capacities.

- An analytical model used to determine the out-of-plane load capacity of externally strengthened URM arching walls has been presented. The following conclusions regarding the developed analytical model can be drawn:

    - The validity of the analytical model is dependent upon the developed empirical relationship used to evaluate the location of the compressive arching thrust, represented through the parameter k.

    - The model suggests that the out-of-plane load capacity and the development of the arching effect is highly dependent upon the stiffness of the surrounding framing members, the slenderness ratio, and the reinforcement level, which is consistent with findings from previous experimental studies.

8.2. PHASE 2 – SLENDER INFILLS

The following conclusions can be drawn from the Phase 2 investigation on slender infill walls:

- The use of the GFRP-polyurea retrofit resulted in capacity increases of more than 50 times that of the theoretical load resistance capabilities of non-strengthened URM walls.

- The use of the polyurea retrofit resulted in significant improvement in wall deflection and energy absorption capabilities. However, the polyurea retrofit resulted in only marginal increases in load capacity.

- The use of the simulated retrofit anchor resulted in increased deflections, increased load capacities, and increased energy absorption capabilities when compared to walls strengthened with no retrofit anchorage. This result suggests that although the unanchored GFRP-polyurea retrofit system was highly effective, the use of a retrofit anchorage system could potentially lead to further improvement in wall behavior.

8.3. GENERAL FINDINGS

The following general conclusions can be drawn from the consideration of the entire research program:

- The arching effect experienced by non-slender infills can result in significant increases in the out-of-plane load capacity for both strengthened and unstrengthened URM walls.

▪ The additional capacity achieved by way of the external retrofits was found to be much less for the non-slender arching infills than for the slender infills.

8.4. RECOMMENDATIONS FOR FUTURE WORK

The following presents recommendations for future studies investigating the behavior of strengthened URM infills subjected to out-of-plane loading:

▪ The use of the GFRP-polyurea retrofit should be investigated at the lower reinforcement levels. The ability of the polyurea material to control the URM wall failure upon rupture of the GFRP could potentially shed light on desirable behavioral traits that were not observed in this study.

▪ The use of a simple retrofit anchorage system for both slender and non-slender strengthened URM walls should be evaluated. It has been shown that such systems may lead to significant improvements in capacity, deformation capability, and overall wall behavior.

▪ All of the retrofit methods in this study should be evaluated under true blast loads. The results provided in this paper serve only as an indicator of potential behavior for URM infill walls subjected to actual blast events.

▪ The use of the WF-FA base masonry material should be further investigated. The material has shown promising characteristics in terms of deformation and energy absorption capability, which are attributes that may reinforce its use and applicability when designing URM walls for blast.

APPENDIX A.

TEST DATA – PHASE 1 WALLS

A.1. EQUIVALENT UNIFORM PRESSURE VERSUS STRAIN

Appendix A.1 presents the equivalent uniform pressure versus strain relationship for all of the strengthened Phase 1 walls. Each of the walls were instrumented with five strain gages along the vertical profile of the wall; however, in the case of Walls P1-2 and P1-7, one gage from each URM wall was damaged during the retrofit process. The location and naming system for the strain gages applied to the strengthened URM walls is shown in the schematic presented in Figure A.1-1.
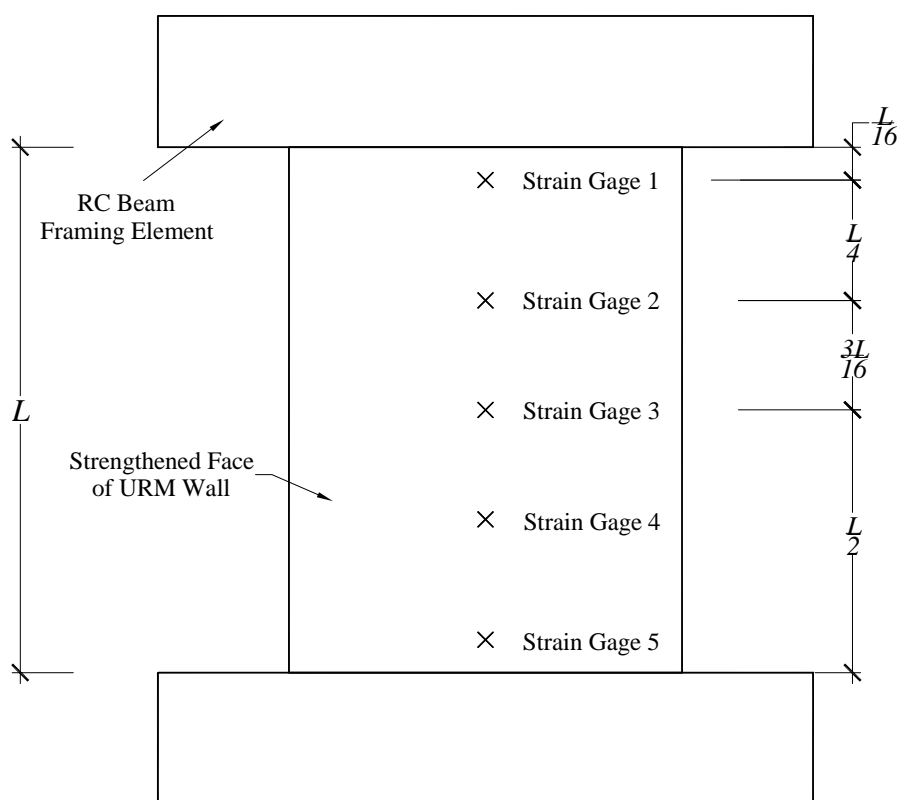
Figure A.1-1. Schematic of Strain Gage Locations
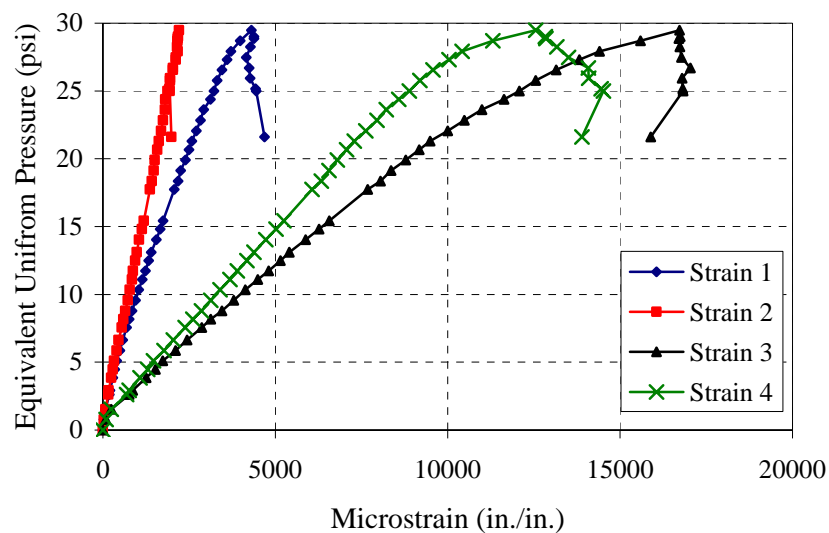
Conversions: 1 psi = 6.895 kPa, 1 in./in. = 1 mm/mm

Figure A.1-2. Equivalent Uniform Pressure versus Strain – Wall P1-2
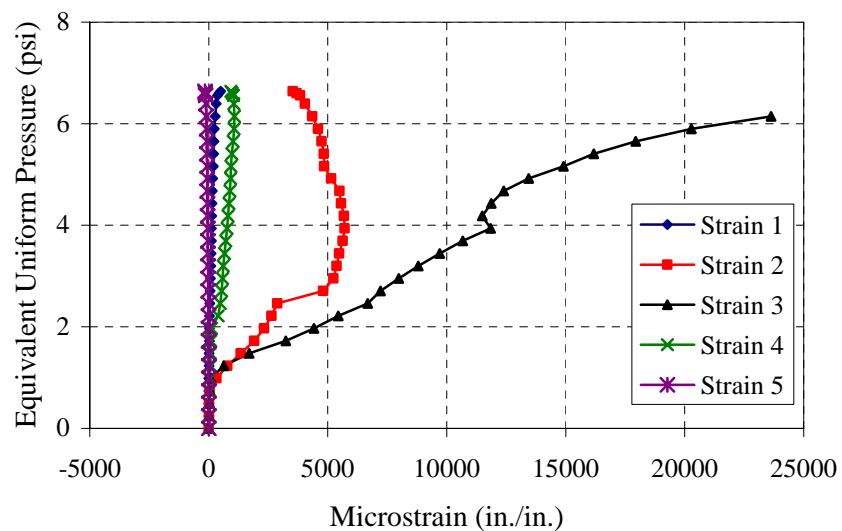
Conversions: 1 psi = 6.895 kPa, 1 in./in. = 1 mm/mm

Figure A.1-3. Equivalent Uniform Pressure versus Strain – Wall P1-4
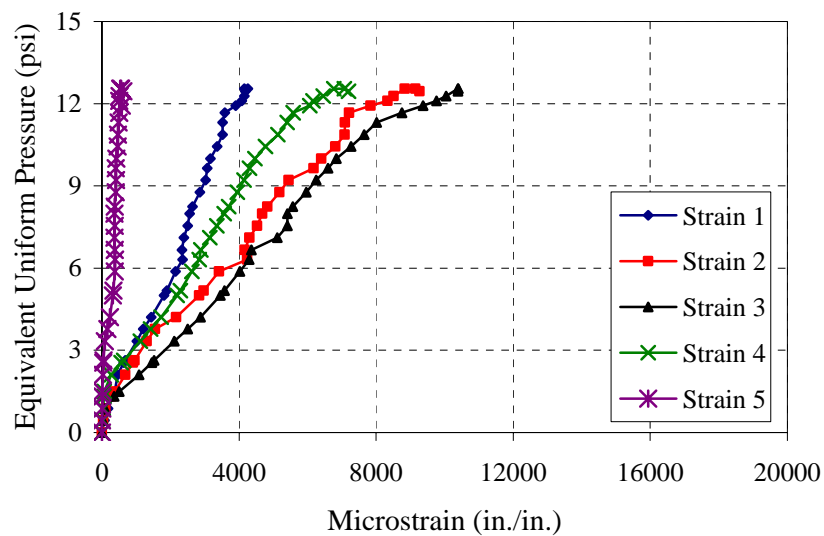
Conversions: 1 psi = 6.895 kPa, 1 in./in. = 1 mm/mm

Figure A.1-4. Equivalent Uniform Pressure versus Strain – Wall P1-5
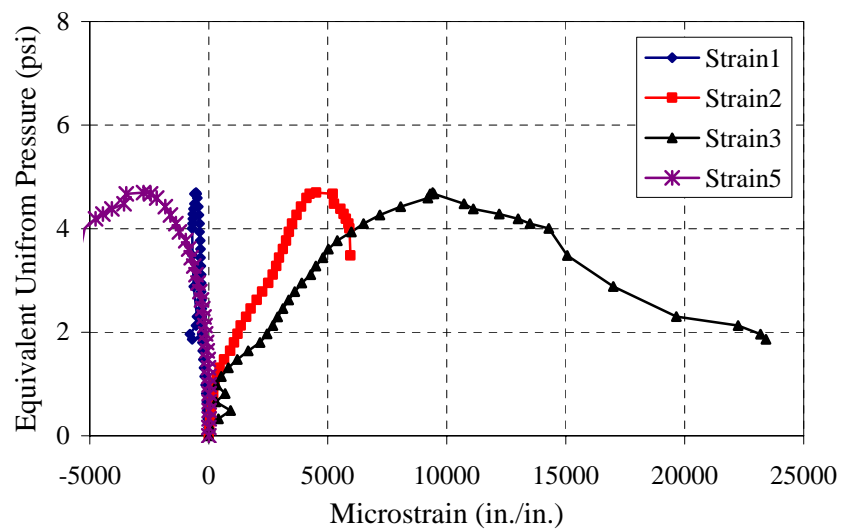
Conversions: 1 psi = 6.895 kPa, 1 in./in. = 1 mm/mm

Figure A.1-5. Equivalent Uniform Pressure versus Strain – Wall P1-7

Conversions: 1 psi = 6.895 kPa, 1 in./in. = 1 mm/mm
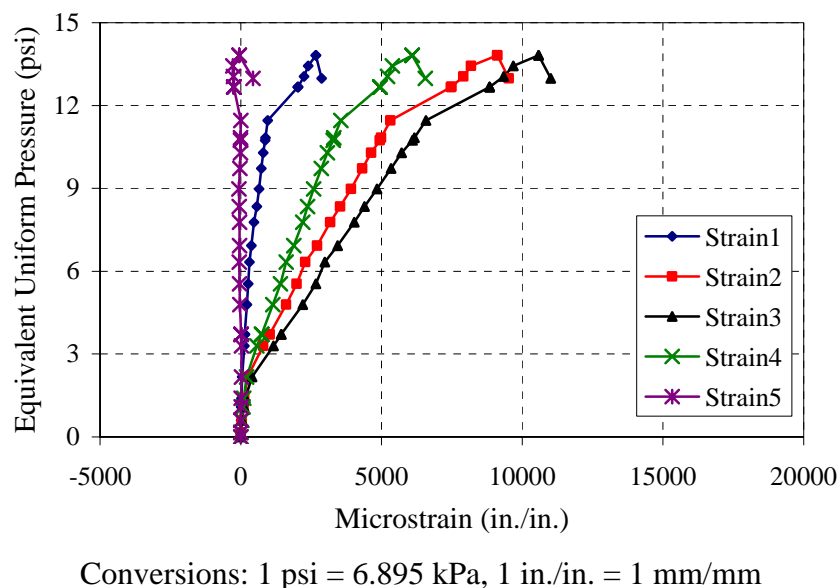
Figure A.1-6. Equivalent Uniform Pressure versus Strain – Wall P1-8

A.2. DEFLECTED SHAPE

Appendix A.2. presents the deflected shape for each of the URM walls tested within Phase 1 of the research program. Each of the walls were instrumented with five string transducers along the vertical profile of the wall, which were used to document the deflected shape throughout the full duration of the testing. However, in the case of Wall P1-6, only the midspan deflection was recorded at the ultimate condition as opposed to the entire deflected profile of the wall. Therefore, the deflected profile for Wall P1-6 is only presented up to an equivalent uniform pressure value of 3.5psi (24.1kPa). For all other walls, the deflected profile is presented incrementally in terms of the equivalent uniform pressure until failure occurs. The deflections presented in this section have been adjusted to account for the translation of the upper boundary element only.

168
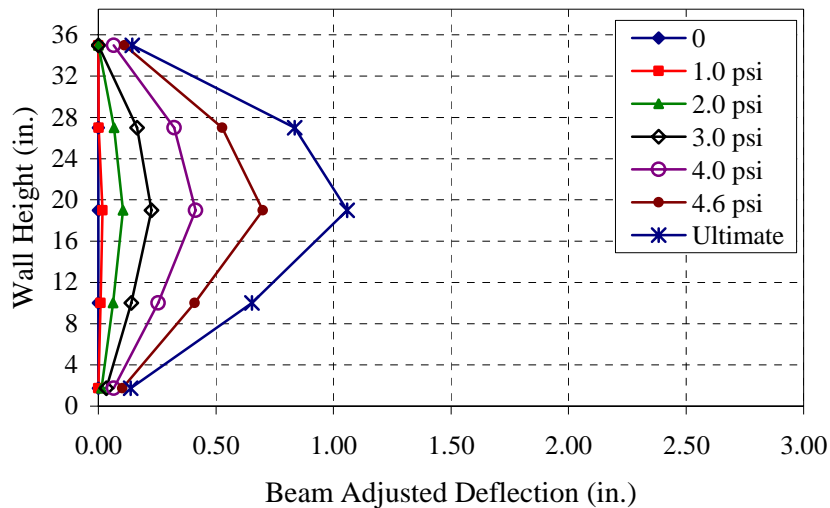
Conversions: 1 psi = 6.895 kPa, 1 in. = 25.4 mm

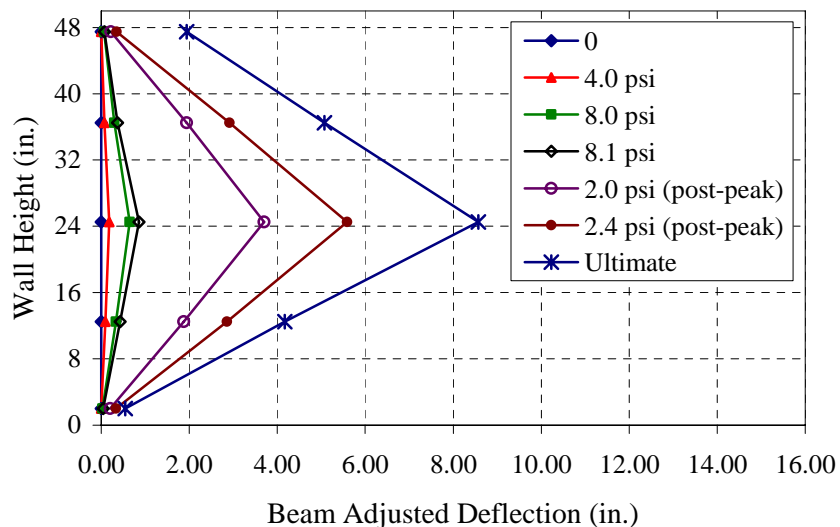Figure A.2-1. Deflected Shape – Wall P1-1
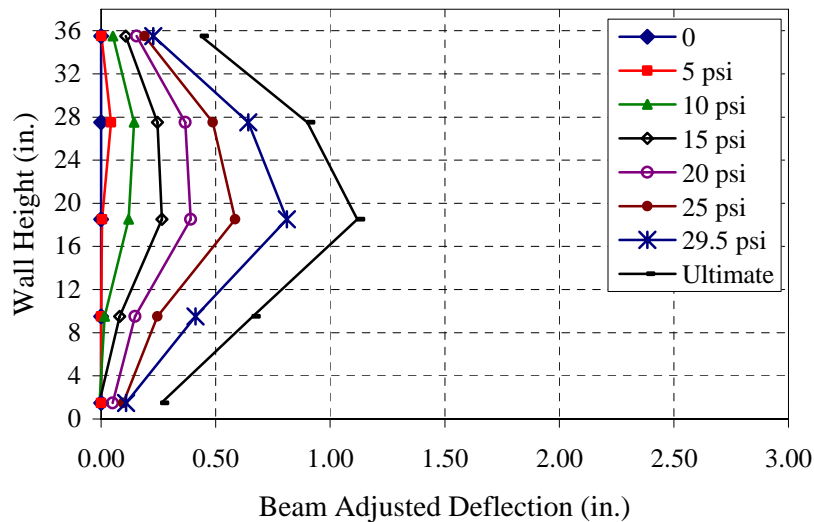
Conversions: 1 psi = 6.895 kPa, 1 in. = 25.4 mm
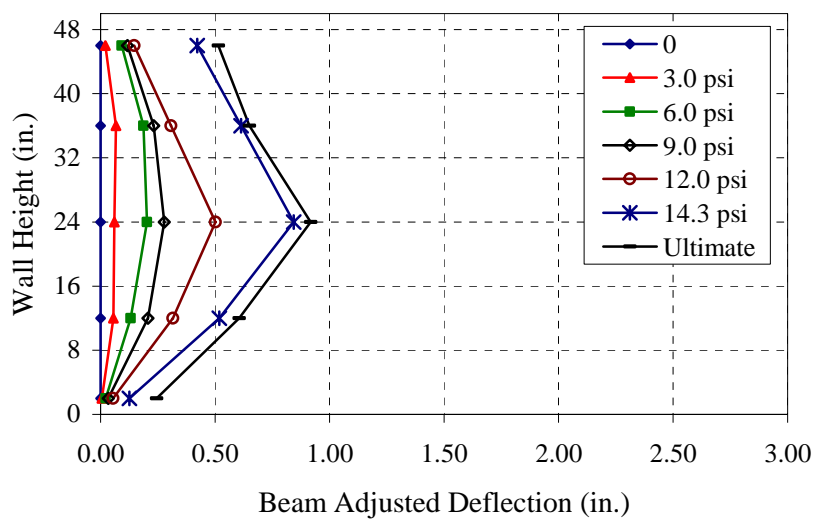
Figure A.2-2. Deflected Shape – Wall P1-2
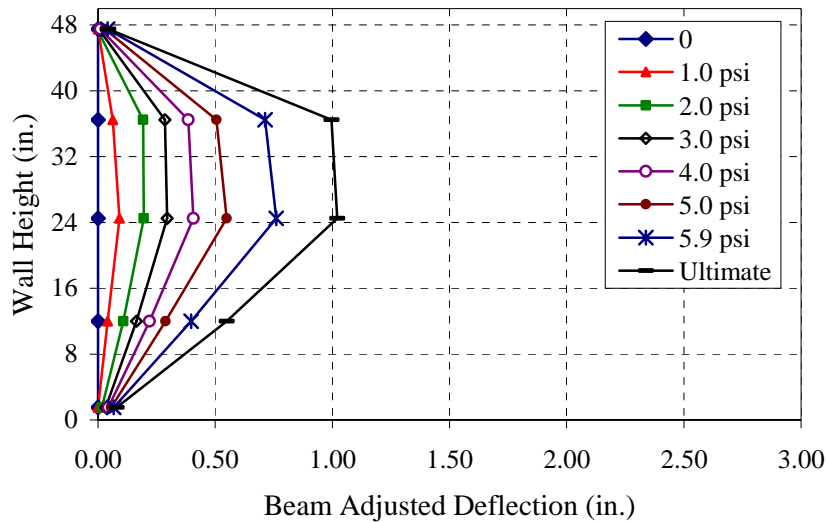
Conversions: 1 psi = 6.895 kPa, 1 in. = 25.4 mm
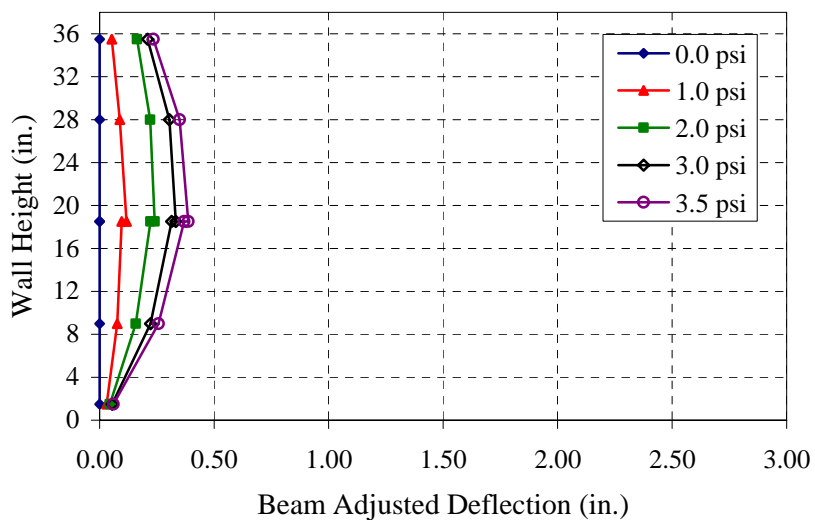
Figure A.2-3. Deflected Shape – Wall P1-3

Conversions: 1 psi = 6.895 kPa, 1 in. = 25.4 mm
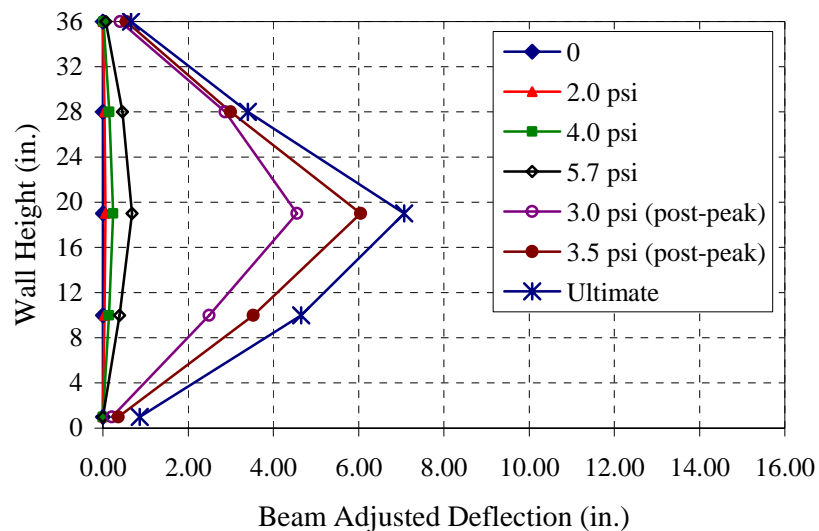
Figure A.2-4. Deflected Shape – Wall P1-4

Conversions: 1 psi = 6.895 kPa, 1 in. = 25.4 mm

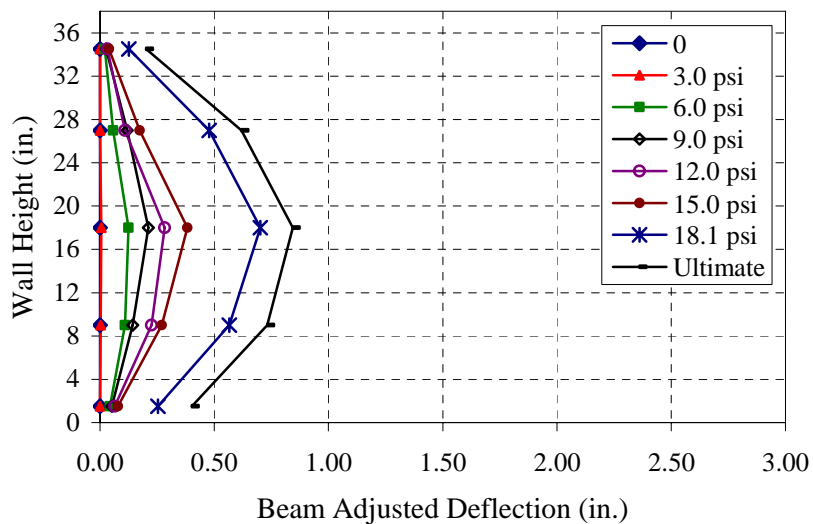Figure A.2-5. Deflected Shape – Wall P1-5

Conversions: 1 psi = 6.895 kPa, 1 in. = 25.4 mm

Figure A.2-6. Deflected Shape – Wall P1-6

Conversions: 1 psi = 6.895 kPa, 1 in. = 25.4 mm

Figure A.2-7. Deflected Shape – Wall P1-7

Conversions: 1 psi = 6.895 kPa, 1 in. = 25.4 mm

Figure A.2-8. Deflected Shape – Wall P1-8

APPENDIX B.

ANALYTICAL STUDY DATA – PHASE 1

Table B1. Matrix of Walls used in Analytical Study

Wall	(h/t)	w_f	f'_m, psi (MPa)	Masonry	Loading Method
P1-2	13.1	1.07	1500 (11.0)	Clay	Airbag
P1-5	13.2	0.93	1300 (9.0)	Concrete	Airbag
P1-8	13.1	1.89	900 (6.2)	WF-FA	Airbag
Galati, 2003	8.5	0.30	1650 (11.4)	Concrete	Concentrated Loads
Galati, 2003	8.5	0.50	1650 (11.4)	Concrete	Concentrated Loads
Galati, 2003	8.5	0.69	1650 (11.4)	Concrete	Concentrated Loads
Galati, 2003	8.5	0.89	1650 (11.4)	Concrete	Concentrated Loads
Galati, 2003	12.8	0.20	2500 (17.1)	Clay	Concentrated Loads
Galati, 2003	12.8	0.33	2500 (17.1)	Clay	Concentrated Loads
Galati, 2003	12.8	0.46	2500 (17.1)	Clay	Concentrated Loads
Galati, 2003	12.8	0.59	2500 (17.1)	Clay	Concentrated Loads
Galati, 2003	13.2	0.33	1500 (10.5)	Concrete	Concentrated Loads
Galati, 2003	13.2	0.55	1500 (10.5)	Concrete	Concentrated Loads
Galati, 2003	13.2	0.76	1500 (10.5)	Concrete	Concentrated Loads
Galati, 2003	13.2	0.98	1500 (10.5)	Concrete	Concentrated Loads
Galati, 2003	19.2	0.20	2550 (17.5)	Clay	Concentrated Loads
Galati, 2003	19.2	0.33	2550 (17.5)	Clay	Concentrated Loads
Galati, 2003	19.2	0.46	2550 (17.5)	Clay	Concentrated Loads
Galati, 2003	19.2	0.59	2550 (17.5)	Clay	Concentrated Loads
Carney, 2003	12.0	0.31	1350 (9.3)	Concrete	Airbag
Carney, 2003	12.0	0.31	1350 (9.3)	Concrete	Airbag
Carney, 2003	12.0	0.31	1350 (9.3)	Concrete	Airbag
Carney, 2003	12.0	0.56	1350 (9.3)	Concrete	Airbag
Carney, 2003	12.0	0.81	1350 (9.3)	Concrete	Airbag

Table B2. Numerical Comparison of Experimental and Analytical Results

Wall	Experimental Out-of-Plane load	Analytical Prediction	Analytical / Experimental
P1-2	21.6psi (148.9kPa)	19.2psi (132.7kPa)	0.89
P1-5	12.5psi (86.5kPa)	12.0psi (82.4kPa)	0.95
P1-8	13.8psi (95.3kPa)	13.0psi (89.6kPa)	0.94
Galati, 2003	10.9kip (48.3kN)	11.3kip (50.4kN)	1.04
Galati, 2003	9.8kip (43.5kN)	13.3kip (59.2kN)	1.36
Galati, 2003	9.61kip (42.8kN)	15.1kip (67.1kN)	1.56
Galati, 2003	12.5kip (75.5kN)	16.7kip (74.2kN)	0.98
Galati, 2003	11.7kip (52.2kN)	8.1kip (36.1kN)	0.69
Galati, 2003	10.3kip (45.6kN)	9.9kip (44.0kN)	0.96
Galati, 2003	12.3kip (54.9kN)	11.3kip (50.3kN)	0.92
Galati, 2003	11.9kip (53.1kN)	12.5kip (55.7kN)	1.05
Galati, 2003	6.5kip (29.0kN)	5.4kip (24.1kN)	0.83
Galati, 2003	6.1kip (27.1kN)	6.5kip (28.9kN)	1.07
Galati, 2003	7.4kip (33.1kN)	7.5kip (33.2kN)	1.00
Galati, 2003	7.8kip (34.7kN)	8.2kip (36.7kN)	1.06
Galati, 2003	2.6kip (11.6kN)	3.1kip (13.7kN)	1.18
Galati, 2003	4.5kip (19.8kN)	4.3kip (19.0kN)	0.96
Galati, 2003	4.9kip (21.9kN)	5.0kip (22.1kN)	1.01
Galati, 2003	5.9kip (26.3kN)	5.5kip (24.5kN)	0.93
Carney, 2003	8.0psi (55.2kPa)	8.0psi (52.9kPa)	0.96
Carney, 2003	7.6psi (52.4kPa)	8.0psi (52.9kPa)	1.01
Carney, 2003	7.3psi (50.3kPa)	8.0psi (52.9kPa)	1.05
Carney, 2003	8.4psi (57.9kPa)	9.5psi (65.4kPa)	1.13
Carney, 2003	10.1psi (69.6kPa)	11.0psi (75.7kPa)	1.09

APPENDIX C.

TEST DATA – PHASE 2 WALLS

C.1. MOMENT VERSUS MIDSPAN DEFLECTION.

Appendix C.1 presents the midspan moment versus the midspan deflection relationship for all of the URM walls tested in Phase 2 of the research program. The presented relationships are based upon the average midspan deflection determined from the data recorded using two LVDTs placed at midspan during testing.
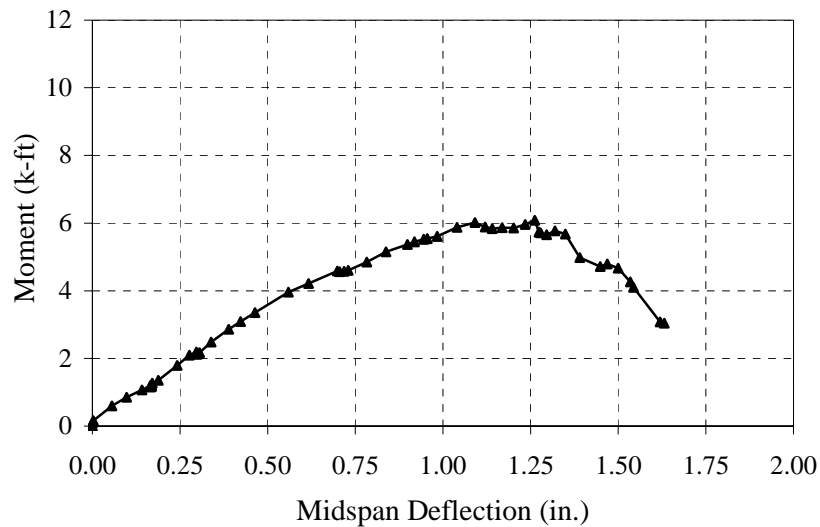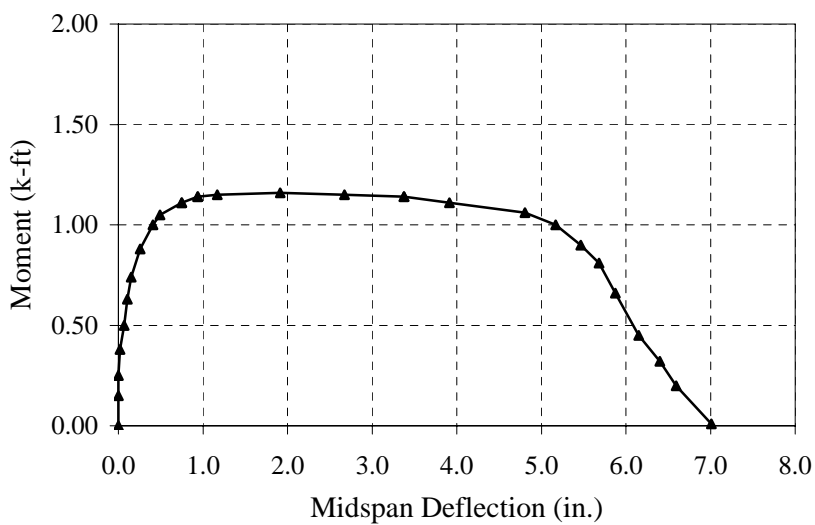

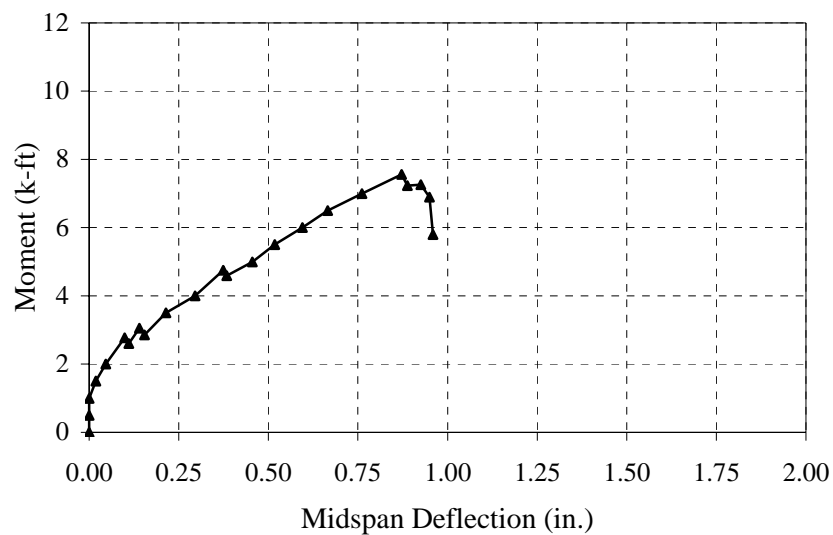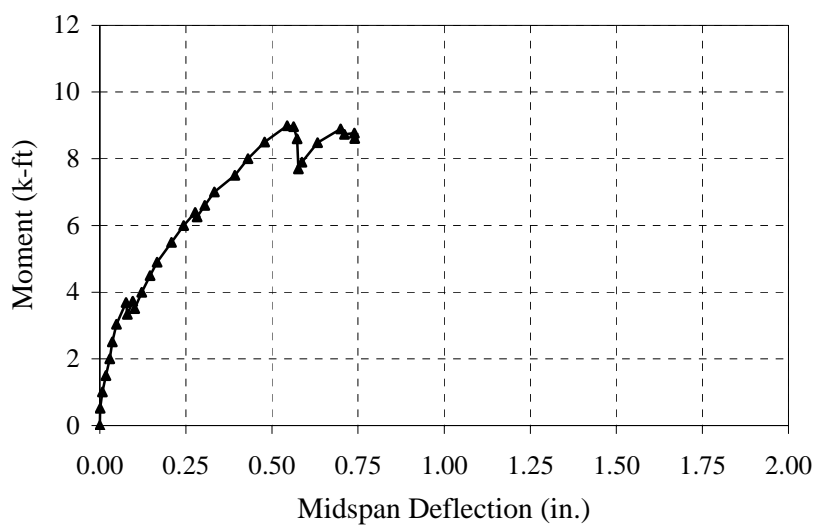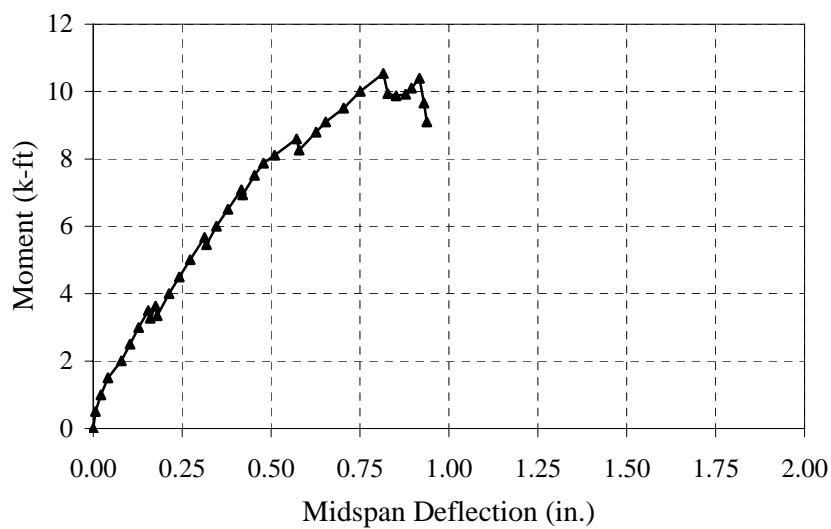Conversions: 1 k-ft = 1.356 kN-m; 1 in. = 25.4 mm

Figure C.1-1. Moment versus Midspan Deflection – P2-1
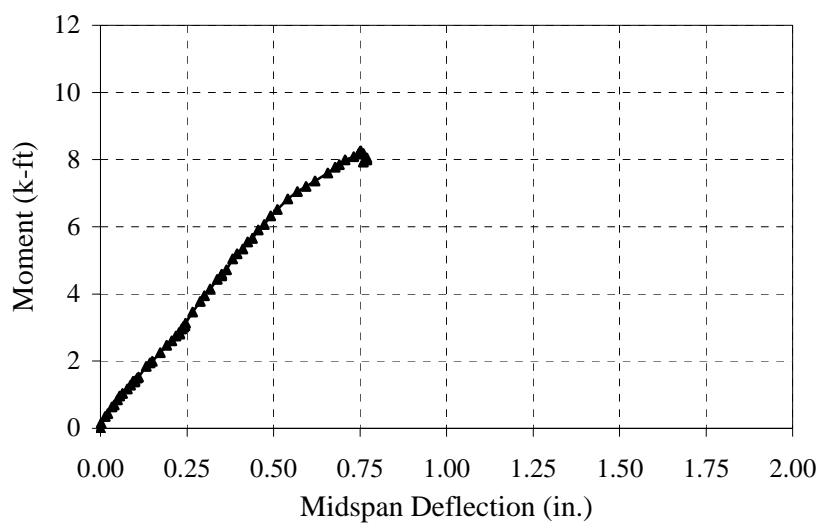
Conversions: 1 k-ft = 1.356 kN-m; 1 in. = 25.4 mm

Figure C.1-2. Moment versus Midspan Deflection – P2-2

Conversions: 1 k-ft = 1.356 kN-m; 1 in. = 25.4 mm

Figure C.1-3. Moment versus Midspan Deflection – P2-3

Conversions: 1 k-ft = 1.356 kN-m; 1 in. = 25.4 mm
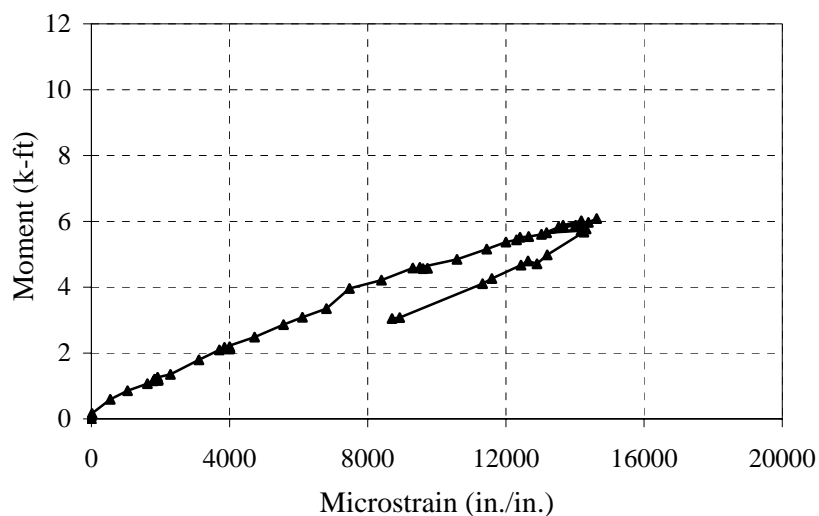
Figure C.1-4. Moment versus Midspan Deflection – P2-4
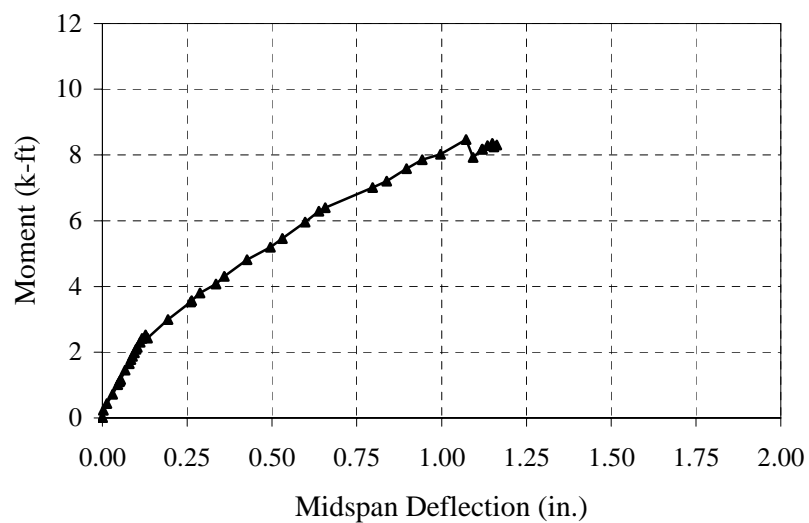
Conversions: 1 k-ft = 1.356 kN-m; 1 in. = 25.4 mm

Figure C.1-5. Moment versus Midspan Deflection – P2-5

Conversions: 1 k-ft = 1.356 kN-m; 1 in. = 25.4 mm

Figure C.1-6. Moment versus Midspan Deflection – P2-6

Conversions: 1 k-ft = 1.356 kN-m; 1 in. = 25.4 mm

Figure C.1-7. Moment versus Midspan Deflection – P2-7

C.2. MOMENT VERSUS MIDSPAN STRAIN

Appendix C.2 presents the midspan moment versus the midspan strain in the external strengthening material for all of the URM walls tested in Phase 2 of the research program. Two strain gages were used to record strain data at the midspan location, and the following figures present the average strain recorded. Note that the strain data has been presented in terms of microstrain. The strain gages on Wall P2-3 failed prior to reaching the ultimate limit state of the wall, and the instrumentation recording the strain data for Wall P2-5 also failed prior to reaching the ultimate limit state. The failure of the gages/instrumentation has been noted in the following figures where applicable.
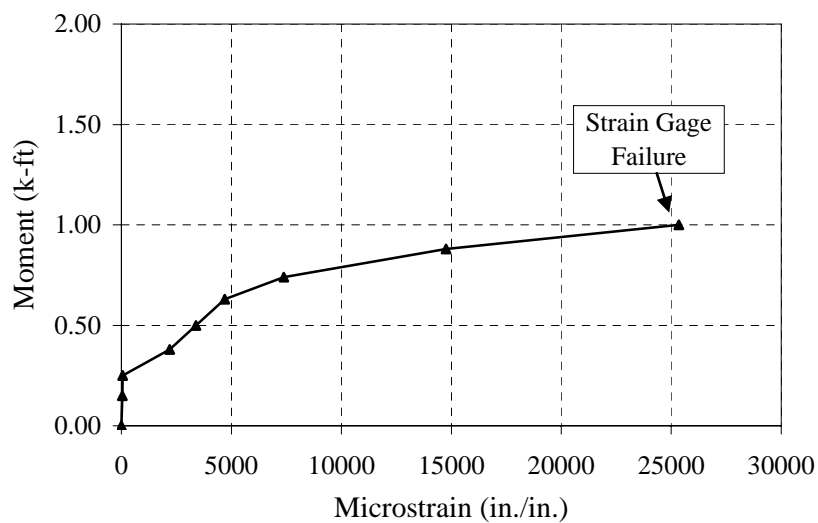

Conversions: 1 k-ft = 1.356 kN-m; 1 in./in. = 1 mm/mm

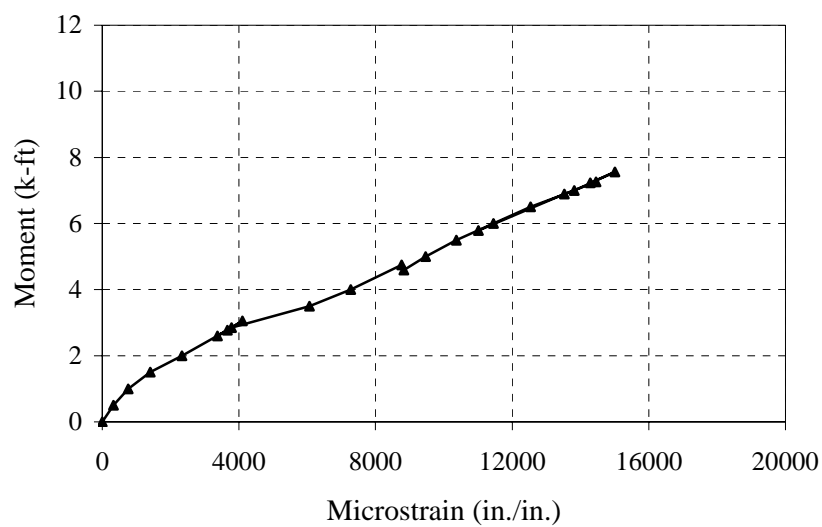Figure C.2-1. Moment versus Midspan Strain – Wall P2-1
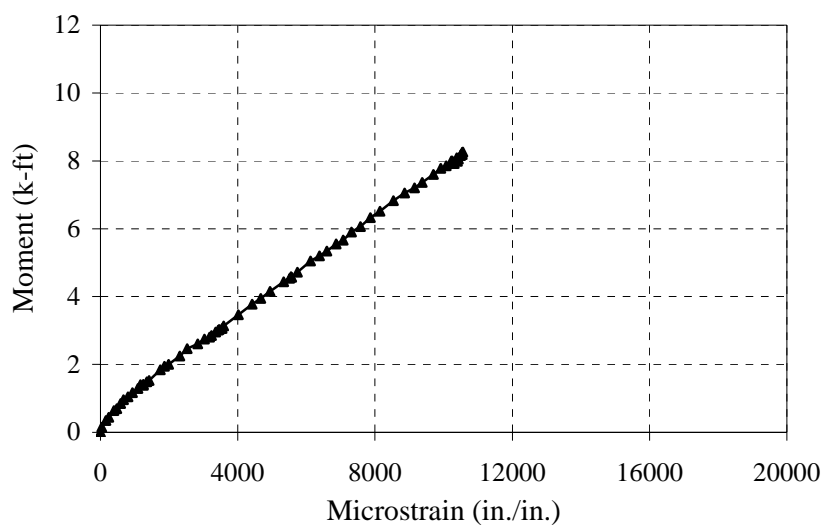
Conversions: 1 k-ft = 1.356 kN-m; 1 in./in. = 1 mm/mm

Figure C.2-2. Moment versus Midspan Strain – Wall P2-2

Conversions: 1 k-ft = 1.356 kN-m; 1 in./in. = 1 mm/mm

Figure C.2-3. Moment versus Midspan Strain – Wall P2-3

Conversions: 1 k-ft = 1.356 kN-m; 1 in./in. = 1 mm/mm

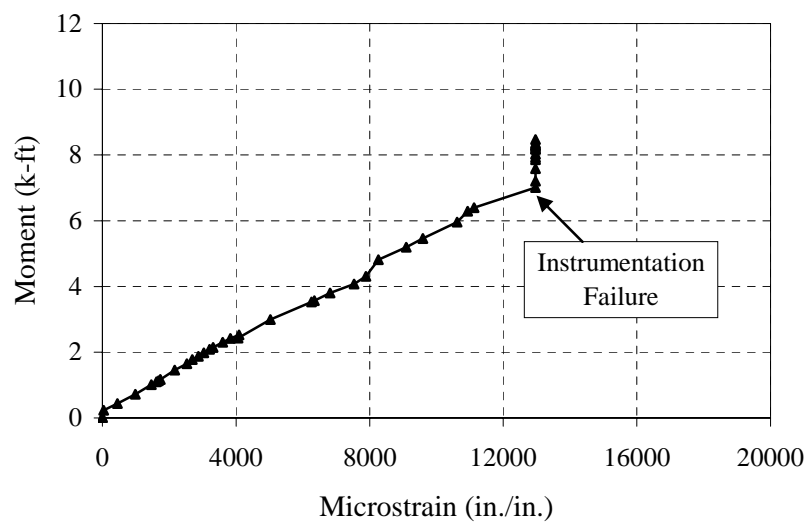Figure C.2-4. Moment versus Midspan Strain – Wall P2-4

Conversions: 1 k-ft = 1.356 kN-m; 1 in./in. = 1 mm/mm

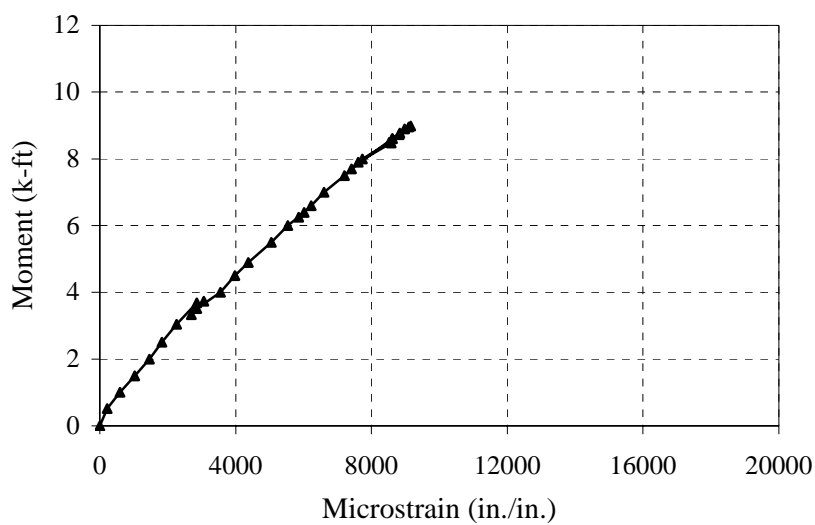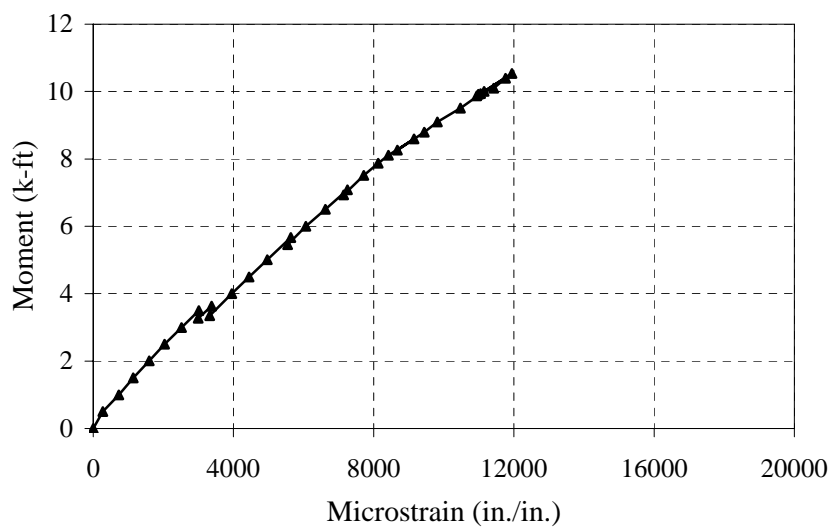Figure C.2-5. Moment versus Midspan Strain – Wall P2-5

Conversions: 1 k-ft = 1.356 kN-m; 1 in./in. = 1 mm/mm

Figure C.2-6. Moment versus Midspan Strain – Wall P2-6

Conversions: 1 k-ft = 1.356 kN-m; 1 in./in. = 1 mm/mm

Figure C.2-7. Moment versus Midspan Strain – Wall P2-7

BIBLIOGRAPHY

ACI Committee 440, Guide for the Design and Construction of Externally Bonded FRP Systems for Strengthening Concrete Structures (440.2R-02), American Concrete Institute, Farmington Hills, Michigan, 2002.

ACI Committee 440, Guide for the Design and Construction of Externally Bonded FRP Systems for Strengthening Concrete Structures (440.3R-04), American Concrete Institute, Farmington Hills, Michigan, 2004.

Anderson C., "Arching action in transverse laterally loaded masonry wall panels," *The Structural Engineer*, Volume 62B, Issue No.1, March 1984.

Angel R., Abrams D., Shapiro D., Uzarski J., and Webster M., "Behavior of Reinforced Concrete Frames with Masonry Infills," Report No. SRS 589, Department of Civil Engineering , University of Illinois at Urbana-Champaign, Urbana, IL, sponsored by the National Science Foundation, Arlington, VA, March 1994.

ASTM C 67 – 06, "Standard Test Methods for Sampling and Testing Brick and Structural Clay Tile," American Society of Testing and Materials, West Conshohocken, PA., 2006.

ASTM C 109/C 109M – 05, "Standard Test Method for Compressive Strength of Hydraulic Cement Mortars," American Society of Testing and Materials, West Conshohocken, PA., 2005.

ASTM C 270 – 05a, "Standard Specification for Mortar for Unit Masonry," American Society of Testing and Materials, West Conshohocken, PA., 2005.

ASTM C 469 – 02, "Standard Test Method for Static Modulus of Elasticity and Poisson's Ratio of Concrete in Compression," American Society of Testing and Materials, West Conshohocken, PA., 2002.

ASTM C 1072 – 05b, "Standard Test Method for Measurement of Flexural Bond Strength," American Society of Testing and Materials, West Conshohocken, PA., 2005.

ASTM C 1314 – 03b, "Standard Test Method for Compressive Strength of Masonry Prisms," American Society of Testing and Materials, West Conshohocken, PA., 2003.

Bogosian D.D. and Crawford J.E., "Energy Absorbing Retrofit Systems for Mitigating Blast Effects on Occupants of Conventional Buildings," *29th Explosives Safety Seminar*, New Orleans, LA, 2000.

Carney P. and Myers J.J., "Out-of-Plane Static and Blast Resistance of Unreinforced Masonry Wall Connections Strengthened with Fiber Reinforced Polymers," Center for Infrastructure Engineering Studies Report 03-46, University of Missouri-Rolla, Rolla, Missouri, 2003.

Connell J.D., "Evaluation of Elastomeric Polymers for Retrofit of Unreinforced Masonry Walls Subjected to Blast Loads," Master's Thesis, The University of Alabama at Birmingham, Birmingham, Ala, 2002.

Eurocode 6, "Design of Masonry structures – Part 1-1: General rules for reinforced and unreinforced masonry structures," CEN European Committee for Standardization, Ref. No. EN 1996-1-1, November, 2005.

Federal Emergency Management Agency (FEMA), "Risk Management Series, Primer for Design of Commercial Buildings to Mitigate Terrorist Attacks," FEMA 427, U.S. Department of Homeland Security, December 2003.

Galati N., "Out-of-Plane Behaviour of Masonry Walls Strengthened with FRP Materials," Ph.D. Dissertation, University of Lecce, Italy, 2003.

Galati N., Tumialan T., and A. Nanni, "Strengthening with FRP bars of URM walls subject to out-of-plane loads," *Journal of Construction and Building Materials*, Volume 20, Issues 1-2, February-March 2006.

Garbin E., Galati N., and A. Nanni, "Design Guidelines for the Strengthening of Unreinforced Masonry Structures Using Glass Grid Reinforced Polymers (GGRP) Systems," Technical Report Prepared for Bondo Inc. & TechFab LLC., University of Missouri-Rolla, Rolla, Missouri, March 2005.

Hendry A.W., Sinha B.P., and S.R. Davies, Design of Masonry Structures, 3rd Edition. Published by E & FN Spon, London, U.K., 1997.

Hu R., Liu H., and Y. Li, "High Pressure Compaction of Flyash into Building Materials," Master's Thesis, The University of Missouri-Columbia, Columbia, MO, 2001.

Joshi N. and Myers J.J., "Investigation of an Alternative Wood Fiber-Fly Ash Material for Infill Wall Systems," Center for Infrastructure Engineering Studies Report 06-60, University of Missouri-Rolla, Rolla, Missouri, 2006.

Mamlouk M.S. and Zaniewski J.P., Materials for Civil and Construction Engineers, Addison Wesley Longman Inc., Menlo Park, California, 1999.

Masonry Standards Joint Committee, Building Code Requirements for Masonry Structures. ACI 530-02/ASCE 5-02/TMS 402-02. American Concrete Institute, American Society of Civil Engineers, The Masonry Society, Detroit, New York, and Boulder; 2002.

Randall F.A. and Panarese W.C., <u>Concrete Masonry Handbook for Architects, Engineers, Builders</u>. Portland Cement Association (PCA), Skokie, Illinois, 1976.

TechFab, "MeC-Grid® Glass Fibre Grid for Strengthening Reinforcement, G15000-BX1," Technical Data and Use Guide, 2003.

Tumialan J. G., Galati N., and A. Nanni, 2003. "Field Assessment Of URM Walls Strengthened With FRP Laminates," Journal of Structural Engineering, Vol. 129, No. 8, pp. 1047-1056, 2003.

Tumialan J.G. and Nanni A., "In-Plane and Out-of-Plane Behavior of Masonry Walls Strengthened with FRP Systems," Center for Infrastructure Engineering Studies Report 01-24, University of Missouri-Rolla, Rolla, Missouri, 2001.

Velazquez-Dimas J.I., Ehsani M.R., and H. Saadatmanesh, "Out-of-Plane Behavior of Brick masonry Walls Strengthened with Fiber Composites," *ACI Structural Journal*, Volume 97, No. 3, May-June 2000.

Watson Bowman Acme Corporation, "Wabo®MBrace Primer, Viscosity Epoxy Primer," Document No. WBA5040_2-02, Amherst, NY, 2002.

Yu P., Silva P.F., and A. Nanni, "Application of Bondo Polyurea in Structural Strengthening of RC Beams and URM Walls," Center for Infrastructure Engineering Studies Report 04-49, University of Missouri-Rolla, Rolla, Missouri, August 2004.

VITA

Trevor Daniel Hrynyk was born in Sarnia, Ontario, Canada, on April 26, 1982. He received his post-secondary education in the United States, attending H.H. Dow High School in Midland, Michigan. In September of 2000, Trevor enrolled in the Department of Civil Engineering at the University of Waterloo, located in Waterloo, Ontario, Canada. He graduated with honors and distinction, receiving a Bachelor of Applied Science (B.A.Sc.) degree in the spring of 2005 with an emphasis in the area of concrete structures.

In September of 2005, Trevor began his graduate career, pursuing a Master's degree in the Department of Civil Engineering at the University of Missouri-Rolla (UMR). He studied under Dr. John Myers investigating the behavior of strengthened unreinforced masonry (URM) infill walls subjected to out-of-plane loadings, with a focused agenda on improving the behavior of URM walls subjected to blast loads. He received his Master of Science (M.S.) degree in Civil Engineering in August of 2007.